General Disclaimer

One or more of the Following Statements may affect this Document

- This document has been reproduced from the best copy furnished by the organizational source. It is being released in the interest of making available as much information as possible.

- This document may contain data, which exceeds the sheet parameters. It was furnished in this condition by the organizational source and is the best copy available.

- This document may contain tone-on-tone or color graphs, charts and/or pictures, which have been reproduced in black and white.

- This document is paginated as submitted by the original source.

- Portions of this document are not fully legible due to the historical nature of some of the material. However, it is the best reproduction available from the original submission.

research report

WYLE LABORATORIES
TESTING DIVISION, HUNTSVILLE FACILITY

WYLE LABORATORIES - RESEARCH STAFF

REPORT WR 69-7

AN EXPERIMENTAL INVESTIGATION OF PRESSURE FLUCTUATIONS CAUSED BY THE INTERACTION OF TURBULENCE WITH SHOCK AND EXPANSION WAVES

By

S. W. Radcliffe

Work Performed Under Contact No. NAS8-21100

March 1969

WYLE LABORATORIES
RESEARCH DIVISION, HUNTSVILLE FACILITY

COPY NO. _____

SUMMARY

This report describes an experiment to observe the acoustic waves generated in the interaction of turbulence with a shock wave. The wake of a flat plate mounted in the centerline of a supersonic wind tunnel acted as the turbulence environment, and the shock wave was caused by a wedge. Observations were primarily made by the traversing of a miniature microphone mounted in a movable instrument head. The most closely examined configurations involved flow Mach numbers of 1.99 and 3.14 and a wedge angle of 10 degrees. An increase in the fluctuating pressure level was observed within the region where it would be expected, although no positive identification of the acoustic nature of the fluctuations was possible. Fluctuating pressure levels which were measured were generally about 8 dB higher than those predicted on the basis of the recent paper by Ribner. An account of an unsuccessful attempt to measure increased fluctuating pressures due to the interaction between turbulence and an expansion fan is also given.

TABLE OF CONTENTS

TABLE OF CONTENTS (Continued)

LIST OF TABLES

LIST OF FIGURES

LIST OF FIGURES (Continued)

LIST OF FIGURES (Continued)

1.0 INTRODUCTION

Modern aerospace technology has led to the use of devices in which the high speed flows of gases are essential. Generally, the production of strong acoustic waves by such flows is regarded as an undesirable side effect. For example, community reaction to noise generated by jet aircraft in the vicinity of major airports makes the study of aerodynamic noise generating mechanisms a matter of current social importance. Also, in the early flight stages of rockets, the rocket structure is subjected to buffeting, some of which arises from an aerodynamic origin. One of the basic configurations in unsteady aerodynamics which can give rise to, or amplify, acoustic waves is that of a turbulent stream being convected supersonically into a shock front. The generation of acoustic waves in this way is possible both in supersonic exhausts from aircraft jet engines and in the flow over the surface of rockets in flight.

Theoretical studies which were begun by Ribner (References 1 and 2), Moore (Reference 3) and Chang (Reference 4) on the interaction of the vorticity, acoustic and entropy components, respectively, into which turbulence fields are normally analyzed, have been extended by the Research Staff at Wyle Laboratories in recent years under NASA-MSFC Contract Nos. NAS8-11038 and NAS8-21100 supporting aerodynamic noise research. Lowson (Reference 5) has extended the calculations presented in Reference 1 to include the predictions of acoustic amplitudes from vorticity interactions over a greater range of flow Mach numbers normal to the shock, as well as including near field effects. In the same report he has included calculations based on Moore's work on the amplification of acoustic disturbances by the shock wave. Cuadra (Reference 6), using Chang's theory, has calculated pressure fluctuations arising from the interaction of plane entropy waves of various orientations to the mean flow direction over a range of Mach numbers and flow deflections. An extension to the theory to allow estimation in the random case is put forward, and its implementation is the aim of a separate task of current work on the present contract. In this effort it is hoped to obtain estimates of the field resulting from simultaneous interaction involving contributions from all three components of the upstream turbulence, but at the time of writing no numerical results are available.

The objective of the series of experiments which are described in the present report is to demonstrate the generation of acoustic waves arising from the interaction of a turbulence environment with a shock wave. The initial approach to experimental problems was described in Reference 7. The experiments were carried out in a supersonic wind tunnel, the turbulence being the wake of a very thin wedge approximating a flat plate aligned with the flow, and the shock wave being that from a wedge inserted into the flow. The diagnostic equipment was primarily a miniature strain-gage microphone with diaphragm flush mounted on a movable instrument head. This report describes the behavior of this system and how the observations made with it can be interpreted.

Section 2.0 is devoted to assembling the relevant background data necessary to the understanding and interpretation of the experimental results. In Section 2.1 previous

direct observations on the generation of acoustic waves in shock interactions are summarized. The basis to the present experimental approach is described in Section 2.2, and Section 2.3 contains the pertinent parts of previous work which form the techniques for predicting and analyzing the experimental observations. In Section 3.0 the main parts of the physical setup and their behavior are described. This is followed in Section 4.0 by a detailed account of the experimental procedure and a record of events which occurred during the test series. Section 5.0 is a discussion of the experimental observations on the basis of the contents of Section 2.3, and extends to interpretation of mean flow, overall sound pressure levels and spectra.

A mechanism whereby rotation of a centered expansion fan due to the passage of a large eddy may give rise to an increase in fluctuating pressure on the surface downstream of a corner has been proposed by the author (Reference 8). An experiment to observe the effect was conducted at the end of the main experiments, and the results are described in Section 6.0.

Finally, in Section 7.0, conclusions are drawn and suggestions are made for improvement in experimental technique.

2.0 BACKGROUND INFORMATION

2.1 Previous Related Work

In discussing turbulent fields it is usual to follow Kovasznay's assumption of weak interaction (Reference 9) and regard the turbulence as being composed of fluctuating vorticity, entropy and acoustic modes. The interaction of any one of these with a shock wave will lead to the production of all three in the downstream flow. This may be intuitively expected. For example, suppose an entropy (or temperature) spot is incident upon a plane shock front. The element of shock front intercepting the entropy fluctuation will, for a short period, be propagating at a lower Mach number than a neighboring element if the entropy spot has a higher temperature than its surroundings. Consequently, the pressure and temperature ratios across the shock and the flow velocity induced by the shock will be different for each element, and acoustic and vorticity modes will have been introduced into the stream. Similar reasoning applies to pure vorticity and pure acoustic interactions with the shock wave. The present interest is in the generation of acoustic disturbances in the interactions.

The mechanisms of acoustic wave production from vorticity and entropy elements being convected into a shock wave have been observed experimentally. Kovasznay (Reference 10), in an experimental setup quite similar to the present one, detected large fluctuating hot wire responses when the wire was located outside, but close to, a turbulent wake of a 1 inch diameter rod in a Mach number 1.75 flow which had interacted with an oblique shock wave generated by a 10 degree flow deflection. These large fluctuations Kovasznay attributed to intense acoustic waves generated in the shock-turbulence interaction. These he estimated to be of the order 143 dB over a reference of 0.0002 dynes/cm^2. Traverses of the turbulent wake upstream and downstream of the interaction point revealed no observable change in the state of the turbulence. Vorticity and entropy modes were found to be of the order 4-6 percent and strongly anticorrelated; the traverses were made at about 5 and 8 body diameters along the wake axis. Schlieren investigation of the flow revealed an upstream displacement of the shock wave by the mean flow of the wake, an effect also observed in the present experiments. Kovasznay's findings were compatible with the predictions made by Ribner (Reference 2), although conclusive verification of the theory was not established.

Several investigators have experimented with normal shock interactions with the basic modes of vorticity and entropy. The first were Hollingsworth and Richards (Reference 11) who carried out a shock tube investigation on vorticity interaction. A starting vortex generated by the passage of the shocked flow over an airfoil mounted in the tube was traversed by the shock reflected off the blank end of the tube. Schlieren pictures revealed a circular (cylindrical, in three dimensions) density disturbance propagating outwards from the vortex center. The acoustic pulse represented by the density change was found to have a polar intensity distribution. Using the same type of experimental configuration, Dosanjh and Weeks (Reference 12) performed interferometric measurements on the density (and hence pressure) distribution around the

circumference of the wave. It was found that there were quantitative deviations from the alternate rarefaction-compression behavior predicted by Ribner. The behavior was better accounted for by a semiempirical relation expressing the source as a linear combination of monopole, dipole and quadrupole components. The decay of the acoustic pressure was observed to decrease monotonically with the inverse of the radius up to a distance of about 10 transmitted vortex core radii, and as the inverse root of the radius beyond this.

Werner (Reference 13) has also used a shock tube technique, employing grids to create the turbulence environment and hot wire and shadowgraph systems as diagnostics. However, it seems that positive identification of acoustic waves was not made. The work concentrated on a theoretical derivation of shock displacement by the turbulence and its correlation with shadowgraph pictures. In this case an order of magnitude agreement was found.

The interaction of an advancing shock front with a concentrated heat (entropy) source has been examined in another shock tube experiment by Dosanjh and Hamernick (Reference 14). Shock distortion, acoustic generation and the time behavior of the decelerated heated gaseous filament were observed by means of Schlieren and finite fringe interferograms.

In summary, the mechanisms for the generation of acoustic waves due to vorticity and entropy have been identified and examined quite closely both theoretically and experimentally. The interaction of a turbulent environment and a shock wave has also been seen to create acoustic waves, although the agreement between theory and experiment is not as well established.

2.2 Experimental Approach

Experimentally the problem of observing the interaction of an isotropic turbulence field with a shock wave may be approached in two ways. One is to use the shock and gas flow in a shock tube. However, the flow is of a transient nature, and unless a fairly large facility were available, the experiment would be geometrically confined to a space of, say, three inches. Further, as evidenced by Werner's work, the turbulence environment which would have to be created by a grid arrangement, would be unknown and would require special examination. One advantage would be that the acoustic sensor could be placed at rest with respect to the flow behind the shock wave. The other approach is to use the supersonic flow of a wind-tunnel, as did Kovasznay (Reference 10). In this case it is possible for the experiment to be continuous, although high frequency sensing devices are required due to the convection effect of the high speed flow.

It was decided to use the second approach. The turbulence was generated by the wake of an almost flat plate positioned on the center plane of a "two-dimensional" nozzle, and the shock wave was that arising from a wedge positioned in the test section, but

outside the turbulence. The sensing device was a miniature strain-gage type microphone (made by Kulite Semiconductors, Inc.) mounted on a movable instrument head. Although hot wire measurements to ascertain the nature of the turbulent wake were scheduled in the original approach (Reference 7), due to circumstances it was not possible to become involved in a necessarily long and painstaking experiment. It was decided instead to concentrate on finding the main effects, and to infer the nature of the turbulence from other sources (see Section 2.3). Note, however, that the turbulence environment is not isotropic; indeed, the convection velocity varies also and, as will be seen later (Section 2.3), both the turbulence intensity and the normal shock Mach number for the interaction have to be deduced with the help of References 15 and 16.

The general arrangement for the experiments is shown in Figure 1. Wedge AOB (usually 10-degree angle) generates the shock ODJEF in the M_1 flow, yielding a Mach number M_2 downstream. AC defines the leading expansion ray from the termination of the wedge. The flat plate is represented by GH, production of which intercepts the shock front at the interaction point, J; HJ is called the interaction distance. Obviously, the mean flow and turbulent level intercepting the shock will vary with interaction distance and this point is discussed in the next section. Acoustic sources may be located between D and E on the shock front, and since M_2 is held supersonic, the propagating radiation should be detectable within the wedge KDF. KD is inclined to the M_2 flow at the Mach angle, $\sin^{-1} 1/M_2$. In the experiments, traverses of the instrument head were performed along the dotted lines I and II, and will be referred to as the lower stream and upper stream traverses, respectively. Other arrangements of wedge, plate, and instrument head were used, but these subsidiary experiments will be described in Section 4.0.

The experiment differs from Kovasznay's in three respects. First, the turbulence is created without the addition of strong shock waves, which themselves may give rise to acoustic waves, and expansion waves. Second, the arrangement is "two-dimensional" so that the acoustic "source" is the line of interaction between the plane shock and the flat turbulence layer. The pressure sensor is also different, being a microphone rather than a hot wire. The microphone will respond to fluctuations in dynamic head as well as pressure waves. To reduce this effect, measurements were carried out mainly outside the turbulence. In the instances where it was not possible to align the instrument head with the local flow, and further minimize fluctuating dynamic head effects, the influence of instrument head orientation was examined. It was felt that the use of a diaphragm-type pressure transducer flush mounted on a flat surface would yield results which would be characteristic of those observed on the surface of rockets and launch vehicles.

Static pressure and shadowgraph systems were used to aid in the interpretation of the mean flow field.

2.3 Prediction Techniques

In order that predictions of the acoustic intensities may be made, a knowledge of the turbulent stream and a developed model relating the transfer of turbulent energy to acoustic energy by the shock wave must both be available. The description of each of these is contained in the present section.

2.3.1 Mean Flow and Turbulence Properties

Recently Demetriades (References 15 and 16) has performed a series of careful measurements using hot wires on the mean flow and turbulent properties of the axisymmetric wake of a rod positioned with its axis in the direction of a Mach 3 flow. The reservoir conditions were controlled so that the wake near the end of the rod was laminar. The turbulence developed several diameters downstream and was not influenced by trailing shock and expansion patterns. The mean velocity, density and temperature wake fields are given in Reference 15 as a function of η, a nondimensionalized radius, and $\bar{x}$, a nondimensionalized axial distance. In Figure 2 the axial velocity, u(0), and temperature, T(0), plots are reproduced from this reference; infinity subscripts refer to free stream conditions. $\bar{x}$ is defined as

$$\frac{(x - x_0)}{(C_D A)^{\frac{1}{2}}}$$

in which $(x - x_0)$ is distance of an axial point from the apparent origin of the self-similar developed part of the wake and $(C_D A)^{\frac{1}{2}}$ is an effective wake "drag" diameter; both x_0 and $(C_D A)^{\frac{1}{2}}$ are determined by experiment. Demetriades found that the radial variations in the self-preserving region were of the form $\exp(-k\eta^2)$ where k is 0.43 for velocity and 0.34 for temperature. η is based on L, a transverse length scale, which, again for axisymmetry, is plotted as a function of $\bar{x}$ in Figure 8 of Reference 15. At $\bar{x} \sim 50$, L is equal to $(C_D A)^{\frac{1}{2}}$; at $\bar{x} \sim 20$, $L \sim 0.7 (C_D A)^{\frac{1}{2}}$. Experimentally the self-preserving region was found to start at about $\bar{x} = 40$.

In Reference 16, Demetriades reports measurements on the turbulence of the same wake. He finds that the turbulence properties relax to a self-preserving form again at $\bar{x} \sim 40$. The variation of velocity fluctuations on the wave axis, $\Delta u(0)$, is shown in Figure 3. For large eddies there is found to be a strong anticorrelation between the velocity and temperature fluctuations, indicating that the strong Reynolds analogy (i.e., small fluctuations in total temperature) holds. The velocity autocorrelation macroscale is found to equal L, and remains fairly constant with radius. The radii of maximum rms velocity fluctuations occur near the radius of maximum shear, and reach about 20 percent higher than the axis value.

Demetriades has also performed spectral analyses on velocity and temperature fluctuations. Approximately it may be said that rms velocity fluctuations in a particular frequency interval are constant up to a nondimensionalized frequency, $n_s = 0.1$, where

$$n_s = f\Lambda_s/u,$$

f being the frequency, Λ_s, the longitudinal velocity autocorrelation macroscale (again approximately equal to L), and u the local velocity. At $n_s > 0.1$ the spectral content falls rapidly until at $n_s = 1.0$ it is less than 1 percent of its low frequency value. This behavior persists approximately for variation of both η and $\bar{x}$, although some effects are noticed which are not important to the present report. In the self-preserving region normalized spectral plots of velocity and temperature fluctuations are almost identical and uniform with radius.

The application of Demetriades' results to the present turbulence is not direct for two reasons. One is that the geometries of the turbulence generators are different; $(C_D A)^{\frac{1}{2}}$ cannot be calculated from geometrical cross-section for the flat plate in the manner possible for the rod. To circumvent this problem it will be assumed that the wake mixing is more characteristic of a typical length at right angles to the plane of the plate, than it is to any parameter involving its width. Secondly, the turbulence in the present case is originated within the boundary layers covering the flat plate, and without measurements it is difficult to define a virtual origin, x_0, for the wake. Further discussion of these problems is kept until Section 5.2, where experimental evidence will be available. There, an application of the axisymmetric results will be made, which is consistent with the observations of the present experiment. It should be mentioned that, for the present purposes, only an approximate estimate of the turbulence properties is required in view of uncertainties associated with other parts of the investigation.

2.3.2 Shock-Turbulence Interaction Theories

Since they have been well documented in other reports associated with the present contract it is not considered necessary here to repeat the detailed findings of Ribner (References 1 and 2), Moore (Reference 3), Chang (Reference 4), Lowson (Reference 5) and Cuadra (Reference 6) concerning the interaction of shock waves and turbulence. However, the results which are required for interpreting the present experimental data will be given.

Figure 4, taken from Reference 5, shows the calculated values of rms pressure fluctuations in the near and far fields as a function of Mach number normal to the shock wave. The pressure fluctuations are given in terms of those arising from unit turbulence intensity. It is seen that for Mach numbers normal to the shock of greater than about 1.1, near field rms pressure fluctuations of about 0.25 times the mean dynamic

pressure, q, of the flow are predicted for 10 percent turbulence. However, since the pressure and velocity disturbances of this wave are out of phase, this is not an energy propagation. To realize these pressure fluctuations some type of interaction boundary must exist close to the shock front. In the far field, pressure fluctuations are predicted to be around 0.08 q, again for 10 percent turbulence.

In a recent report Ribner (Reference 17) has extended his own calculations (References 1 and 2) to provide the flux of acoustic energy radiating downstream from unit area of the shock front as a function of turbulent energy flux into the shock. The efficiency of the turbulent energy to acoustic energy transfer process is found to vary almost linearly with the density ratio across the shock front, reaching a maximum of 0.062 at infinite Mach number. Figure 5, which is taken from Reference 17, shows the efficiency as a function of Mach number of the normal shock wave.

The turbulent energy flux, J_t, over each unit area of shock front, may be calculated from (see Reference 17)

$$J_t = \frac{5}{2} \rho u^3 \left(\frac{\Delta u}{u}\right)^2 \quad ,$$

u and Δu denoting mean and average fluctuating velocity components of the turbulence respectively.

The acoustic energy flux may be related to the acoustic pressure, p_{rms} at any point in a convecting field in the following way. For an acoustic field, the energy density is $p^2_{rms}/(\rho a^2)$ ergs/cm^3 (Reference 18), where a is the speed of sound, and ρ is the density of the propagating medium. In the present case the propagating acoustic field, originating at 0, is being convected with the flow velocity, u_2, behind the shock wave (see Figure 6). Thus, the flux of acoustic energy across a surface normal to $\overline{OP}$ has contributions corresponding to velocity vectors $\overline{OP}$ and $\overline{OQ}$. Assuming the acoustic wave is uniform in intensity along its circumference and has an effective pressure of p'_{rms}, the energy flux at the observation point equals

$$\frac{p'^2_{rms}}{\rho_2 a_2^2} (\overline{OP} + \overline{OQ}) \qquad \text{erg/cm}^2\text{/sec}$$

(This assumption is not strictly correct, as demonstrated in Reference 12, but it will serve to yield an estimate of p_{rms} sufficiently accurate for the present purposes. Note also that when it reaches the observer the $\overline{OQ}$ wave element is part of an acoustic front

of larger diameter than the $\overline{OP}$ element, and hence will have a smaller amplitude. However, this effect will be neglected at present in view of the previous assumption.) It is further assumed that the acoustic energy flux is uniform over the surface APB, whose area is A. Thus, the total flow of energy across APB is

$$\frac{p'^2_{rms}}{\rho_2 a_2^2} (\overline{OP} + \overline{OQ}) \cdot A \qquad \text{erg/sec}$$

which, when equated with the acoustic energy calculated from the turbulence intensity and Figure 5, yields a value of p'_{rms} at the observation point. The wave elements from the $\overline{OP}$ and $\overline{OQ}$ elements will be uncorrelated in phase, the turbulence being assumed random, so that the fluctuating pressure, p_{rms}, actually observed will be 3 dB higher than the estimate of p'_{rms}, since intensities of uncorrelated signals are added.

It can be mentioned that the observed acoustic field may be different from the predicted one if there is a relationship between the velocity and temperature fluctuations, for a given density. The strong anticorrelation which is indicated both by Kovasznay's (Reference 10) and Demetriades' (Reference 16) measurements would suggest that the acoustic disturbances may be stronger than those calculated neglecting entropy disturbances. Cuadra's report (Reference 6) contains a discussion of typical entropy fluctuation magnitudes in jets, wakes and boundary layers. Referenced to total temperature, it appears that 5 percent is a reasonable upper limit to temperature fluctuations generated in wakes and boundary layers at the present Mach numbers. Thus, for a Mach 3 stream and flow deflection of 20 degrees, the maximum pressure fluctuation generated would be (from Reference 6, Figure 29) 0.3q. Although this number represents the accumulation of high values for turbulence, flow inclination, etc., and an average value would probably be much smaller, nevertheless it does stress that entropy interaction could be quite significant. In the present investigation, however, prediction of the acoustic field will be mainly from the vorticity-shock wave interaction, but the entropy effect will be kept in mind.

3.0 APPARATUS

3.1 Wind Tunnel Facility

The experiments to be described were conducted in the 7-in. by 7-in. supersonic wind tunnel located at NASA Marshall Space Flight Center. A general view of the wind tunnel is shown in Figure 7. This is an atmospheric to vacuum blowdown tunnel whose supersonic Mach numbers are obtained with fixed, inter-changeable nozzle blocks. Atmospheric air is dried and stored in a tank provided with a rubber diaphragm to maintain constant supply pressure during blowdown. During the test series the pressure control mechanism failed and it was necessary, in order to maintain the time schedule, to run the tunnel without the drier and using atmospheric air. No water vapor condensation was observed in the test section when operating in this manner, except during the transients at opening and closing of the gate valve. The data obtained with undried air were considered satisfactory.

Three nozzle blocks were used during the experiments. These gave flow of nominal Mach numbers 1.99, 2.89, and 3.87 respectively. The addition of the turbulence generating plate (see Section 3.2.2) in the upstream position caused a change in throat area and modified the flow Mach number observed using the Mach number 1.99 and 2.89 nozzles. In the first case, the change was small enough to be neglected, but in the second case static pressure and shadowgraph data indicated a flow of Mach number 3.14, which is consistent with the change in throat area (see Section 5.1). For the Mach number 3.87 nozzle block the throat was well upstream (at least 10-1/2 in.) of the leading edge of the turbulence plate in both its upstream and downstream configurations. Table I gives a summary of some characteristics of the nozzles which were used.

A run time of at least 30 seconds was required for the purposes of the test, and this was always easily achieved. Maximum model blockage in the test section was 2 sq.in. (4 percent). Further tunnel blockage was introduced by the turbulence plate (approximately 0.5 sq.in. or 1 percent) and the model support strut mounted on the movable plate (1-1/4 sq.in. or 2.5 percent). In the worst condition, tunnel blockage occurred after about 1 minute run time with the Mach number 1.99 nozzle.

3.2 Model Components

The following models were designed by Wyle Laboratories and fabricated for the test by NASA-MSFC:

Instrument head
Turbulence generating plate
Shock generating wedges
Turbulence-Expansion wedges
Support struts and booms.

An instrumented shock generating wedge was also fabricated but was not required during the experiments.

A typical arrangement of the models in the tunnel is shown in Figure 8, and a view of the model assembly is shown in Figure 9.

3.2.1 Instrument Head

A diagram of the instrument head, which supports the Kulite Type CPL 070-4-Ultra-miniature microphone and a static pressure orifice, is shown in Figure 10(a). The sensors were located sufficiently near to the sharp leading edge so that the boundary layer which developed on the head was laminar. Reynolds number based on distance from the leading edge to the microphone was always less than 2.3×10^5, this figure occurring with the Mach number 1.99 nozzle. However, the sensors were sufficiently far downstream that the aerodynamic disturbances created by the underside supports and leads did not interfere with events on the upper surface. Shadowgraphs of the flow over the instrument head (e.g., Figure 28) verify that both these conditions were achieved; in fact, it may be observed that the sensors could have been located at least 1/4 in. further upstream without the risk of interference.

Figure 10(b) shows details of the static pressure orifice and Kulite microphone locating hole. The microphone was held in place by red wax, its sensitive surface flush with the upper surface of the head. Leads to both sensors were taped to the support boom.

It was possible to pivot the instrument head on an axis normal to the flow, and, with a flexibly designed support boom, it was, therefore, easy to locate the instrument at any point in the field of interest with any desired orientation.

3.2.2 Turbulence Generating Plate

Figure 11 is a diagram giving the dimensions of the turbulence generating plate. Its function was to produce a layer of turbulence extending across the test section with which to interact shock waves of various strengths. The turbulence environment in the stream was formed by the joining of the two turbulent boundary layers developed on the upper and lower surfaces of the plate. Reynolds numbers based on plate length are 5.2×10^6, 3.4×10^6, 3.0×10^6 and 2×10^6 for Mach 1.99, 2.89, 3.14, and 3.87 flows respectively. As will be seen later (Section 4.0) a turbulent layer whose thickness from shadowgraphs appeared to be about 0.5 in. was formed. On the shadowgraphs there was also evidence of trailing shock waves, although these were weak and not troublesome to the performance of the experiments.

The plate extended completely across the tunnel in its centerplane and was fixed to the tunnel walls by two No. 8 bolts on each side. The width of the plate was reduced slightly on the downstream side so that it would not damage the optical windows of the wind tunnel. During manufacture care was exercised to keep waviness in the plate

surface to a minimum. However, due to the effects of machining the light aluminum alloy it was found difficult to prevent curling of the plate material at the end of the long trailing taper section. The curvature introduced a projection of about 1/6-in. when viewed along the trailing edge; this was considered satisfactory. When the tunnel was operating no flutter or vibration of the plate was observed, except upon opening and closing of the gate valve when a transient was induced.

The plate could be mounted in either of two configurations, referred to as upstream and downstream positions. In the upstream position its leading edge was 0.5 in. downstream of the throat of the Mach number 1.99 nozzle and 1.5 in. upstream of the Mach number 2.89 nozzle throat. In both these cases no shock diamond pattern could be observed in the test section. For the Mach number 3.87 nozzle the leading edge was 10.5 in. downstream of the throat and a shock diamond was observed. The downstream configuration was 2 in. downstream in each of these cases, and in each instance a shock diamond was observed.

3.2.3 Shock Generating Wedges

Three shock generating wedges were constructed for the purpose of creating the oblique shock wave which interacted with the turbulent layer. The wedges had angles of 10 degrees, 20 degrees, and 30 degrees, and their dimensions are given in Figure 12. In the tunnel they were mounted on a support boom which, in turn, was fixed to the support strut (see Figure 9).

In the design stage it was decided to make three wedges, rather than to orientate the 10-degree wedge, because of the possibility of tunnel blockage. For the same reason the width of the wedge was restricted to 3 in. It was felt that this would provide a sufficiently two-dimensional interaction; however, as will be seen later (Section 5.1), the effects of three-dimensional flow, while not troublesome, are observable in the static pressure readings.

3.2.4 Turbulence-Expansion Wedges

These wedges were fabricated for the purpose of examining any increase in fluctuating pressure at the surface when a large scale turbulence passes over an expansion shoulder. (Section 6.0.) Dimensions of the 10 degree, 20 degree, and 30 degree expansion wedges are given in Figure 13. The wedges could be arranged in the flow so that either the first or second upper surfaces could be set tangentially to the flow. The upstream and downstream microphones were located at 3/8 in. from the corner on each wedge.

3.2.5 Support Strut and Booms

The dimensions of the supporting equipment which had to be fabricated are shown in Figure 14. The strut was fixed to the removable plate downstream of the nozzle block. The slots in the strut and support booms provided flexibility in locating and orientating the instrument head and wedges.

3.3 Shadowgraph System

For the shadowgraph work the direct shadowgraph system represented in Figure 15 was used. The source was a point discharge of a high voltage charged capacitor, the discharge being extinguished after about 1 microsecond. The Kodak 136 Safety Film measuring 20- by 8-in. was mounted in a lightproof holder and covered the whole aperture of the tunnel windows. Because of the geometry the shadows cast on the film were a slight magnification of their parent objects, the magnification depending upon the object's position in the tunnel and the position of the spark source. For the shadowgraphs in these experiments the spark source was located either on the line of the downstream edge of the turbulence plate, or along the line normal to the estimated point of interaction between the oblique shock wave and the centerline of the turbulence layer; the appropriate configuration is usually obvious from inspection of the shadow of the turbulence plate. On some of the shadowgraph pictures bright areas are observed; these are reflections from the surface of the models.

Although the shadowgraphs obtained in these experiments are most useful in drawing qualitative information about the flow field, it is not usually possible to calculate with any accuracy values of flow Mach number from the inclination of shock fronts and Mach lines. The reason for this is now described. In Figure 16, suppose the shock front created by, say, the shock generating wedge is the surface OPRCE. The section OPR is curved, and the section ORCE planar and tilted at the angle ROT (equal to angle CEB) to the incoming flow. This angle is usually the one of interest. However, since the rays of light emanate from a point, S, the pattern recorded by the film arise from density variation in the neighborhood of the line OP, which projects through OQ onto the film plane as AD. The angle DAB is thus greater than angle CEB for this particular arrangement, and will yield a value of flow Mach number smaller than actual. This trend was evident upon analysis of some of the shadowgraphs obtained during the experiments.

The discrepancy is minimized when inference is made from parts of the film near the point B, or when the shock pattern extends wholly across the tunnel, as is the case for the shock diamond created by the turbulence plate. The location of the shock pattern on the film is subject to similar restrictions in interpretation.

3.4 Microphone and Static Pressure Systems

3.4.1 Microphone System

The fluctuating pressure sensors which were used were Kulite Ultra-miniature microphones Type CPL 070-4. Their head diameter was 0.070 in. and they are manufactured using a monolithic integrated Wheatstone bridge directly formed on a silicon diaphragm. The CPL 070-4 has an input impedance of approximately 750 ohms and may be excited with a 5 volt AC or DC power supply. At a rated pressure of 4 psi they have a sensitivity of 4 millivolts/volt (or 5 mV/psi) and are able to withstand a pressure differential

of 100 psi. During the experiments the reference pressure was held at wind tunnel plenum pressure and the output had a low cut-off of 50 Hz. The natural frequency of the transducer is about 100 kHz, implying a flat dynamic response to about 25 kHz. Higher frequency response behavior is not available, but it will be assumed flat.

A block diagram illustrating the Kulite microphone support electronics is shown in Figure 17. Two microphone channels were used during the turbulence-expansions experiment (see Section 6.0). For the purposes of directly observing the microphone response, the output of the amplified signal was taken to a logarithmic converter, given a DC voltage offset, amplified, and displayed on a digital voltmeter. The offset voltage and amplification were arranged so that the digits displayed on the voltmeter were also the rms level in dB (re: 2×10^{-4} dynes/cm^2) of the pressure fluctuations at the microphone head. The system was found to be linear over the working range and to be stable to within 0.5 dB during any day. It was recalibrated each morning using the calibration procedure described below, an hour being allowed for warm-up of electronics.

Since the expected sound pressure levels were of the order 150-160 dB (Reference 7), a sinusoidal acoustic signal of 160 dB $\pm$ 1 dB at 1 kHz was impressed on the microphone using an acoustic calibrator. The electronics were adjusted so that this figure was read on the digital voltmeter, and that the electrical signal seen by the voltage control oscillator (VCO) unit had an rms level of 1.160 volts. When the acoustic signal was attenuated by 10 dB the voltmeter reading was 150.6 dB, the discrepancy being caused by distortion of the 160 dB signal due to the acoustic calibrator being overdriven. However, the calibration was considered to be accurate enough for the purposes of the experiment. VCO calibration was performed by impressing 2 volt rms and 200 millivolt rms 1 kHz sinusoidal electrical signals on the system; these signals correspond to sound pressure levels of 164.7 dB and 144.7 dB respectively. The calibration signals, two acoustic and two electrical, were recorded at the beginning of each reel of recording tape and were checked before each day's experimenting.

The electrical noise floor (no wind) varied between 116 dB and 126 dB over the duration of the tests, mostly being about 123 dB. This floor, which was rather high, was found to be primarily composed of 60 Hz pickup due to imperfect electrical grounding. The variation was probably caused by changes in the electrical activity of facilities in the neighborhood of the wind tunnel. No shielding of the microphone system has been incorporated into its design. The noise was not considered to be particularly troublesome for two reasons; first, in the spectrum analysis stage it could be easily filtered out, and second, the frequencies which were anticipated to be of interest were around 20 kHz (Reference 7). Response of the microphone system due to mechanical vibrations was considered negligible, since tapping of the instrument head and movement of lead wires resulted in no noticeable increase in noise level.

Caution should be exercised in drawing conclusions from the magnitude of the results of Series D (Section 4.0). During these runs a variable bandpass filter was present in

the circuit, the object being to acquire an on-the-spot estimate of the frequency spectrum of the fluctuations. Upon a calibration check subsequent to the series it was found that the filter, with an input impedance of 600 ohms, was significantly loading the circuit and depressing the reading of the overall sound pressure level. Some tests were performed on the loaded circuit using sinusoidal inputs of varying frequency. It was found that

a) the overall reading was depressed by 5.2 dB from its unloaded value,

b) for a constant input voltage, the output remained constant within 5 percent over the range 400 Hz to 20 kHz. It was decided not to repeat the series of runs in view of these results, and also because trends were being sought rather than accurate measurements. The filter was not in the circuit for the remaining series.

3.4.2 Static Pressure System

Details of the static pressure orifice are given in Figure 10(b) and those of the electrical circuit are shown in Figure 17. The electrical output from a differential pressure transducer referenced to vacuum was amplified so that 1 psi at the orifice caused a 1 volt output, and the digital voltmeter consequently read pressure in psi. The daily stability of this circuit was found to be good, the maximum fluctuations always being less than 0.1 percent.

3.5 Recording and Spectrum Analysis Systems

Two microphone outputs and a voice identification channel had to be recorded at any one time. In the case of all series except Series K (the turbulence-expansion experiments, Section 5.0), the outputs comprised the microphone and static pressure responses from the instrument head. For Series K the upstream and downstream microphone responses were recorded. The readings were simultaneously noted from the digital voltmeter by an observer, and recorded on magnetic tape.

The tape recording system comprised a VCO unit and a CEC VR 3600, 14 channel tape recorder. The following carrier frequencies were used:

Channel 1 : 450 kHz
Channel 2 : 825 kHz
Channel 3 : 1.2 MHz.

Channel 1 was occupied by the instrument head microphone for all series except K, and was the downstream microphone record for Series K. Channel 2 was the upstream microphone response for Series K. Channel 3 contained the static pressure reading for Series B-J (section 4.0).

The recording speed was 120 inches per second, and at least 15 seconds of data were taken for each run. Since the frequencies of interest were well above 1 kHz, this sample length was satisfactory. The tape recording system had a flat frequency response to at least 40 kHz.

In performing the spectral analysis of Channels 1 and 2 the magnetic tape was replayed at 15 inches per second (1/8 speed) through demodulators with center frequencies at 50.25 kHz and 103 kHz. The demodulated signal was passed through a high pass filter (lower cut-off at 20 Hz) and analyzed using a Bruel and Kjaer Type 1612 spectrum analyzer and Type 2305 level recorder. Since the demodulators had a high frequency cut-off at 6.25 kHz, frequencies between 160 Hz and 50 Hz were admitted for analysis, thereby elininating the 60 Hz pickup and microphone effects near its natural frequency.

4.0 DESCRIPTION OF SHOCK-TURBULENCE INTERACTION EXPERIMENTS

The experimental program was divided into a series of tasks, each with a separate objective. A description of the performance of each task, together with any special techniques used, is contained in this Section.

A catalog of the 134 runs making up this experimental program is shown in Table II. In the first column is the run number. The peculiar numbering sequence has its origin in the original program objectives described in Reference 7. However, as the experiments were being performed it was considered advantageous to alter the scheduled runs, and this past adherence to the original sequence led to the present numbering system. The program described in Reference 7 was altered basically in two ways. One was to omit the acoustic-shock interaction study, because it was considered that the effect would not be detectable. Secondly, it was found to be more interesting to use the time available to perform traverses of the flow and acoustic fields (see Figure 1), for the 10-degree wedge at Mach numbers 1.99 and 3.14, than to take representative acoustic levels for various combinations of Mach number and wedge angle.

In Table II each task is labeled "Series A" through "Series K", and the order in which they are listed is, with a few unimportant exceptions, the order in which they were performed. The description of Series K, concerning the expansion-turbulence interaction, will be left to Section 6. Each "X" in the shadowgraph column indicates that a shadowgraph was taken for that run. The "reel" column indicates on which of the six reels of magnetic tape the microphone and static pressure responses are recorded. "dB (o.a.)" and "static (psi)" are the digital voltmeter readings taken by an observer of the overall microphone and static pressure sensors. "Mach No." is the free stream Mach number, and varies depending on the location of the turbulence plate. The derivation of the values in this column is described in Section 5.1.

A task-by-task commentary of the experimental program will now be given.

Series A

The objectives in this series were:

a) To observe the location of the shock diamonds in the flow for each of the upstream and downstream locations of the turbulence plate,

b) To observe the turbulent wake, and

c) To observe if there was any plate oscillation during the run.

It was found that:

a) For the two low Mach number nozzles (marked 1.99 and 2.89) the shock diamond pattern from the leading edge was absent with the plate in the upstream position. In this situation the leading edge is in subsonic flow. In the downstream position shocks were noticed, but these seemed to be weak and appeared, as far as could be judged from the shadowgraph system (see Section 3.3), to be close to the Mach angle. For the Mach number 3.87 nozzle its construction was such that the leading edge of the plate could not be located in subsonic flow, and weak shocks were observed. Symmetry of the shock pattern indicated that the plate was well aligned with the flow.

b) The wake was seen to have a turbulent nature and to remain at approximately the same thickness (0.5 inches) over a distance of at least 6 inches downstream.

c) No plate oscillation was observed during the steady part of the run. Unsteady transients during start-up and close-down did induce plate motion, but this was soon damped.

Series B

For the 2.89 and 3.87 Mach number nozzles, the responses of instrumentation on the instrumentation head were examined as the head was orientated. Orientations were 0-, 3-, and 6-degrees to the free stream, the sensitive face being tilted to intercept the flow. The probe head orientation was arranged using a small inclinometer. The following observations were made:

a) The tunnel r.m.s. pressure fluctuations were recorded as less than 129 dB (re: 2×10^{-4} dynes/cm^2) for the Mach number 2.89 and 3.87 flows, and were relatively unaffected by changing probe head orientation. This level was 3 dB higher than the "air-off" instrument noise (primarily 60 Hz) recorded at that time.

b) From shadowgraphs it was observed that the boundary layer over the sensitive surface of the head was not turbulent. This is in accord with the design parameters of Section 3.2.1.

c) The static pressure readings for 0-degrees orientation fall about 6 percent below those in Table I; this is probably due to pressure in the reservoir not being at 14.7 psi. Further, the static pressure readings for 3- and 6-degrees orientation in each case fall below those calculated by conventional two-dimensional flow deflection methods using the tables of Reference 19. For example, in the Mach 2.89 stream, using a value of 0.440 psi for free

stream static, values of 0.555 psi and 0.678 psi are estimated for 3- and 6-degree deflection readings. However, 0.510 psi and 0.648 psi are actually recorded. The difference is probably due to three-dimensional flow effects over the instrument head, since the static pressure orifice is located 7/8 inch from the leading edge and about 3/8 inch from the side.

Series C

The aims of this series were to obtain an idea of the sound field in the vicinity of the turbulent wake; and also to observe microphone response when the probe head was submerged in turbulence. The microphone location for each run is shown in Figure 18.

The observations made during this test proved to be inconsistent. For example, the runs with the Mach number 2.89 nozzle indicated no difference between the microphone responses inside and outside the turbulence, whereas, with the Mach number 3.87 nozzle, increase of 3 dB and 4 dB were observed in the turbulence. The reason for this inconsistency cannot be found. Minor anomalies may be noted in the static pressure readings, but these are small enough to be attributable to variation of reservoir pressure. Two conclusions may be drawn:

a) The insertion of the plate alters the Mach numbers of flow in the nozzles.

b) Fluctuating pressures outside the turbulence in each case were less than 131 dB.

Series D

The purpose of this series was to observe static and fluctuating pressure profiles across a section of the flow field generated by a wedge, the turbulence being absent. The locations of the Kulite microphone sensing surface, which faces the shock generating wedge, are shown in Figure 19. As with other traverses, the tip of the probe head was adjusted to its position by sighting its profile against a reference placed on the inside wall of the tunnel. This reference was a paper sheet with the probe head locations marked on it, which was positioned relative to fixed markings on the tunnel wall. It is estimated that the positioning procedure is good to within ± 1/32 inch. Simultaneously with this adjustment, the orientation of the instrument head was set using the inclinometer. The static and fluctuating pressure profiles for this series are plotted in Figure 20. It may be seen that there is an appreciable increase, about 13 dB over free stream, in fluctuating pressure at the location of the shock front determined by the static pressure profile. Also the peak is quite wide, having a half width of 0.5 inches. This, and other traverse profiles will be discussed in Section 5.2. Note that Figure 20 is plotted with the corrected readings; i.e., actual readings from Table II plus a 5 dB increment (see Section 3.4.1).

It may be noted that for this profile the sensing surface of the instrument head was kept parallel to the free stream, except for Run 100, in which it was parallel to the estimated local stream. If it were parallel to the local stream throughout the traverse, an expansion would occur over the probe surface with the probe tip located upstream of the shock. This reasoning applies only to the "lower stream" configuration (see Section 2.2.); for the upper stream traverses (Series H, J) the probe surface was kept parallel to the local stream.

Series E

The aim of this series was to observe qualitatively the effects of varying shock generating wedge angle for fixed free stream Mach number and turbulence. For each run, the upper probe surface was held parallel to the local flow, and the probe tip was set at the expected location of the shock front, as shown in Figure 21. Shadowgraphs taken during Runs 111, 113 and 115 are shown in Figure 22. The following conclusions were drawn:

a) At an interaction distance of 1 inch the shock wave loses its coherence. This effect is also indicated by the readings of the static pressure orifice in presence of turbulence being lower than the turbulence free readings. At small interaction distances a significant portion of the mean flow of the wake is subsonic (see Section 2.3.1) so that a pressure step stationary with respect to the laboratory cannot be supported. Larger interaction distances will be required for a proper investigation of shock-turbulence interaction.

b) There is an increase of fluctuating pressure level due to the turbulence being present. The r.m.s. pressure increases with increase in wedge angle. However, the mean flow disturbance is so great that this cannot be regarded as a confirmation of theoretical trends.

c) The 20- and 30-degree wedges are so short in the flow direction that the expansion fan centered on the end of the deflecting surface interacts with the shock a short distance from the wedge. Even for a Mach 1.99 flow the geometry of the flow is not suitable for field traverses with these wedges. For this reason it was decided to devote the remaining runs to investigation with the 10-degree wedge.

Series F

Having observed, in the previous series, that presence of the turbulence system yields a higher fluctuating pressure level at one point in the field, the objective for this series was a traverse of the field pattern. The interaction distance was increased to 2 inches and the nozzle Mach number changed to 2.89. Locations of the microphone and static pressure measurement points are given in Figure 23, and the readings are

plotted in Figure 24. Figure 25 is a shadowgraph of Run 98E where the microphone was just downstream of the fluctuation peak. Although this series will be discussed in greater detail in Section 5.0 some conclusions may be mentioned here:

a) From both shadowgraph and static pressure data, the upstream peak in the fluctuating pressure curve is associated with the position of the shock front. Again the peak has a half width of about 0.5 inches.

b) A second peak which approximately coincides with the head of the expansion fan is observed; there is no evidence of a plateau.

c) The decrease in static pressure level with distance behind the shock wave indicates three-dimensional flow effects around both shock generating wedge and instrument head.

d) From the shadowgraph a slight upstream displacement of the shock due to the interaction with the mean flow of the wake may be noticed.

Series G

In Series F the local flow was impinging supersonically at 10 degrees upon the top of the instrumentation head. The flow adjusts to the deflection through a shock wave attached to the leading edge of the probe. The object of the present series was to find if the fluctuating pressure readings were changed in the same ratio as the static readings. Between runs 99A and 99C, the fluctuating pressure reading decreased 3.4 dB, a ratio of 1.48; static pressures changed by a factor of 1.62. For runs 99A and 99B, the respective ratios are both 1.27. Thus, as a guide the ratio of static pressures at a given location may be taken to be that of the fluctuating pressures.

Series H

This series had as its objective the plotting of pressures along traverse II of Figure 1. The microphone and static pressure locations are shown in Figure 26, and the plots are given in Figure 27. The following effects were noted:

a) There is an increase in observed fluctuating pressure at the location of the Mach line from the edge of the turbulence. At this point the static pressure is on the decrease. The increase in fluctuating pressure is about 10 dB above its value behind the main shock. Shadowgraphs do not reveal any evidence of a shock reflected from the wake (see Figure 28).

b) At the location of the head of the expansion fan there is no sharp dip in static pressure reading. It should be noted in explanation that the pressure sensors are partially shielded by the body of the instrument head from the flows created by the shock generating wedge.

c) Some evidence of non-repeatibility between Runs 117A through M and 117N through R was observed. The latter set of runs show higher static and fluctuating pressure readings. Since shadowgraphs of Runs 117C and 117Q appear identical, the most probable reason for the disagreement is that the reservoir pressure varied; Runs 117A through E and Runs 117N through R were taken on subsequent days and the variation is within the limits of barometric fluctuations.

Series I

The aim of this series was to perform a traverse of the lower stream (Figure 1) for the Mach 1.99 nozzle to see if the features found in Series F are repeated. The pressure sensor locations are given in Figure 19, and the readings are plotted in Figure 30.

The lower Mach number of the present series yields both a larger separation of shock and expansion waves from the wedge and a higher flow density. These effects make measurement easier. Generally the same features were noted for the present series as were observed in Series F. There are, however, changes in the fluctuating and static pressure profiles which do not correlate with barometric variation. These will be discussed in Section 5.2. Figure 31 is the shadowgraph taken during Run 101J.

Series J

This was essentially a repetition of Series H, with the Mach 1.99 nozzle installed. Pressure transducer locations and their responses are given in Figures 32 and 33. Figure 34 is a shadowgraph taken during Run 102C, when a peak in the fluctuating pressure level was noted. The main shock reflection off the wake was seen to be directly over the microphone location. Similar trends to Series H were again noted.

More detailed discussions of the static and fluctuating pressure levels for the traverses (Series D, F, H, I and J) follow in the next Section.

5.0 DISCUSSION OF SHOCK-TURBULENCE INTERACTION RESULTS

The profiles of fluctuating and static pressures measured in Series D, F, H, I and J and plotted in Figures 20, 24, 27, 30 and 33, respectively, are discussed in detail in this section. These profiles comprise the main results of the experiments and were obtained using the 10 degree shock generating wedge and the Mach 1.99 and Mach 2.89 nozzles. From the remarks in the previous section, it is apparent that increases in the fluctuating pressures were observed at appropriate locations in the flow; it remains to be discussed whether these increases were due to acoustic wave generation according to the theories outlined in Section 2.3.2.

The discussion may be divided into three parts: (a) Mean Flow, (b) Fluctuating Pressures, and (c) Spectra; and these will be treated in that order.

5.1 Mean Flow

The nozzles which were used gave flows which had been calibrated at Mach numbers of 1.99 and 2.89. Due to insertion of the turbulence plate with its leading edge upstream of the throat in each case, it was anticipated that the Mach number of the flow would be slightly increased. Calculations of this new Mach number were made from free stream static pressure measurements, and correlating this with shadowgraph and with shock angle from the 10 degree wedge as observed by the static pressure orifice. The results showed that in the case of the Mach 1.99 nozzle the increase in free stream Mach number downstream of the end of the turbulence plate was negligible. In the case of the Mach 2.89 nozzle a flow Mach number of Mach 3.14 yielded the best fit for experimental observations. It may be observed that these findings are consistent with estimates of Mach number based on changing the throat area of the wind tunnel by insertion of the turbulence plate. In passing, it can be noted that insertion of the turbulence plate into the Mach 3.87 nozzle (for example, Series E) had the effect of reducing the flow Mach number. However, in this case it will be remembered that the plate leading edge was downstream of the throat, so that the Mach number of the observed stream could be reduced due to the recompression through the shock diamond waves.

The predicted static pressure profiles were calculated using the tables of Reference 19. Knowing the flow Mach number, the position of the shock arising from a 10 degree wedge may be found, the pressure ratio across it, and also the change in flow Mach number it induces. From the Mach number downstream of the shock, the position of the head of the expansion wave centered on the end of the wedge may be found from the Mach angle. For the upper stream traverses this is sufficient to estimate the static pressure profile. In the case of the lower stream traverses, although the positions of the shock and expansion fronts are found by the above procedure, the flow undergoes another 10 degree deflection, due to the instrument head, before being observed by the pressure sensors. This shock system is treated in the same way as previously, and the predicted static pressure reading is thus calculated.

As seen in Figures 20, 24, 27, 30 and 33 there is a significant discrepancy between predicted and measured profiles. Obviously one of the main contributors to the discrepancy will be the three-dimensional nature of the flow over the wedge, since the width of the wedge is 3 inches and measurements are being taken comparable distances from its surface and behind its leading edge. Also, in the case of the lower stream traverses, an additional three-dimensional flow effect will occur over the instrument head, since again, pressure measurements are being made at a significant distance from the leading edge. Quantitatively, these effects are difficult to estimate, but it may be said that they will tend to give measured static pressure readings below those calculated. This effect is observed in the static pressure profiles lower stream traverses. For upper stream traverses, static pressure above those calculated are observed. However, it must be remembered that for these traverses, the instrument head is located close to the turbulent wake, and it is likely that the pressure variations observed are associated with the interaction between the wake and the shocked flow. Three dimensionality will tend to displace the observed shock front position downstream of its "two-dimensional" position, an effect observed in Figure 20, for the case when no turbulence was present. As observed from the shadowgraphs, the wake from the plate displaces the shock wave to an upstream position, an effect observed in Figures 24 and 30 for static pressure

From Figures 30 and 33 it is seen that, for the Mach 1.99 flow, the wedge shock incident on the wake is partially reflected, whereas in the case of the Mach 3.14 flow, no reflections are observed (Figures 25 and 28). A possible explanation of this effect may be that, in the case of the low Mach number flow, the shock wave locally reduces part of the wake to subsonic flow, hence the shock wave tends to become normal to the mean wake flow. In order to adjust the pressure and flow direction caused by the normal shock to the supersonic stream outside the wake, an auxiliary, or reflected shock, arises. However, for the high Mach number case the wake flow is never subsonic, and the shock angle at each point locally adjusts the flow direction and pressure rise so that no auxiliary, or reflected, shock is necessary.

As discussed in Section 2.3.1, the mean flow field in the region of the wake will be estimated using the measurements reported in Reference 15. The main problem in application of these results is to find a value of $\bar{x}$ which is reasonable in the present case. Fortunately, an approximately correct estimate will suffice. The estimate of $\bar{x}$ involves deciding upon values for x_0 and $(C_D A)^{\frac{1}{2}}$. Suppose that x_0 is arbitrarily chosen to be zero (implying that the self-similar wake originates at the trailing edge of the plate), that C_D has a value of 0.5, and that $A = t^2$ where t is maximum plate thickness (= 0.25 inch). Thus, $\bar{x} \simeq 12$ for an interaction distance of 2 inches. Two reservations about this value may be stated. Since the boundary layer is turbulent as it passes over the end of the plate, it may be surmised that the origin of self-similarity lies upstream of the end of the plate. Also, the estimate of $(C_D A)^{\frac{1}{2}}$ may be considered large, since $t = 0.25$ inch occurs well upstream of the end of the plate, where $t = 0$. For both these reasons, it may be considered that $\bar{x}$ will probably be greater than 12.

An estimate of $\bar{x}$ based on the momentum thickness, θ, is possible. Some wall boundary layer profiles taken in the present wind tunnel are reported in Reference 20. A typical wall boundary layer thickness for Mach 1.99 is $\delta \sim 0.25$ inch. Assuming incompressibility and a linear velocity distribution, from Table 12.1 of Reference 21, it is found that $\theta \sim 0.04$ inch. For both upper and lower boundary layers, $2\theta \sim 0.08$ in. Thus, letting $\bar{x} = x/(2\theta)$, it is found that $\bar{x} \sim 25$, for $x = 2$ inches.

Each of these estimates for $\bar{x}$ may be checked against the shadowgraph investigations by using them to calculate the approximate wake centerline Mach number.

Taking $\bar{x} = 12$, from Figure 2,

$$\frac{u_\infty - u(0)}{u_\infty} = 0.29 \quad \text{i.e.,} \quad \frac{u(0)}{u_\infty} = 0.71,$$

and

$$\frac{T(0) - T_\infty}{T_\infty} = 0.80, \quad \text{i.e.,} \quad \frac{T(0)}{T_\infty} = 1.80$$

However, where a denotes the local speed of sound,

$$\frac{a(0)}{a_\infty} = \sqrt{\frac{T(0)}{T_\infty}} = \sqrt{1.80}$$

so that

$$\frac{M(0)}{M_\infty} = \frac{u(0)}{a(0)} \times \frac{a_\infty}{u_\infty} = 0.53$$

Thus, for $M_\infty = 1.99$, $M(0) = 1.06$; and for $M_\infty = 3.14$, $M(0) = 1.66$. If the condition is now applied that the flow has to undergo a 10-degree deflection, it may be seen from Reference 19 that the shock inclination at the wake axis must be 49 degrees for $M_\infty = 3.14$. For $M_\infty = 1.99$ no shock solution exists to deflect the flow 10 degrees, so that the shock wave tends to become normal to the oncoming flow, and to reduce the flow locally to a subsonic state. This subsonic region is indicated in the Mach 1.99 shadowgraphs both by the orientation of the shock wave at the wake centerline, and by the presence of the reflected shock discussed in an earlier paragraph. The angle of 49 degrees predicted for $M_\infty = 3.14$ compares with the free stream shock angle of 26 degrees; shadowgraphs indicate that the perturbation is not as large as this; i.e., the Mach number defect is not as large as predicted using $\bar{x} = 12$. This reasoning confirms the earlier feeling about the arguments which yielded $\bar{x} = 12$.

Taking $\bar{x} = 25$, $M_\infty = 1.99$, it is found that $M(0) = 1.37$; for $M_\infty = 3.14$, $M(0) = 2.17$. The shock angles are thus found to be 90 degrees (in this case the flow just fails to remain supersonic) and 36 degrees. These values appear more consistent with the shadowgraphs, and will be used in the remainder of the discussion. It may be noted that, within the validity of the comparison with the axisymmetric wake, the value of $\bar{x}$ is quite well defined. For example, the choice of $\bar{x} = 30$ yields supersonic flow throughout for $M_\infty = 1.99$.

5.2 Fluctuating Pressures

5.2.1 Predictions

As a first step in the discussion of the fluctuating pressure profiles which were observed, it will be useful to estimate the levels predicted by the results of References 5 and 17. It will be assumed that the acoustic waves arise from the interaction of the area of the shock wave intercepting the wake flow between the upper and lower wake edges; from Figure 4 of Reference 16, this region is seen to include most of the turbulence. From Reference 16, the wake edge is located about 3L from the axis. For $\bar{x} \sim 25$, $L \sim 0.70$; i.e., the turbulence enters the shock along a strip of 0.168 inch ($= 2 \times 3 \times 0.7 \times 0.04$ inch) width. This value is seen to be characteristic of the shock front distortion observed in the shadowgraph. Over this strip it will be assumed that the turbulence intensity has its axial value at $\bar{x} = 25$, or, from Figure 3,

$$\frac{\Delta u(0)}{u_\infty - u(0)} = 0.53$$

From Figure 2(a),

$$\frac{\Delta u(0)}{u(0)} = \frac{\Delta u(0)}{u_\infty} \times \frac{u_\infty}{u(0)}$$

$$= \frac{(0.16 \times 0.53)}{0.84} = 0.101$$

i.e., a turbulence level of 10 percent. (For $\bar{x} = 12$, the turbulence level would be 23 percent.)

The acoustic pressure predictions based on Figure 4 will now be made. It will be assumed that the shock strength and orientation will be defined by the mean flow conditions on the wake axis at $\bar{x} = 25$, as discussed in Section 5.1. For $M_\infty = 1.99$, M_n, the flow Mach number normal to the shock wave, equals 1.37. Thus, from Figure 4,

$$p_{rms} = 0.101 \times 0.35 \times q \qquad \text{Far-field}$$

$$0.101 \times 2.65 \times q \qquad \text{Near-field}$$

Using $q = \frac{1}{2} \gamma p_\infty M^2(0)$, = 2.96 psi in the present case,

$$p_{rms} = 0.105 \text{ psi} = 151.2 \text{ dB} \qquad \text{Far field}$$

$$= 0.791 \text{ psi} = 168.7 \text{ dB} \qquad \text{Near field}$$

dB is referred to 2×10^{-4} dynes/cm^2.

For $M_\infty = 3.14$, $M_n = 2.17 \sin 36^\circ = 1.28$ (see Section 5.1). It is found that

$$p_{rms} = 0.016 \text{ psi} = 134.0 \text{ dB} \qquad \text{Far field}$$

$$= 0.111 \text{ psi} = 151.7 \text{ dB} \qquad \text{Near field}$$

The method which yields the above predictions assumes an infinite shock and isotropic turbulence environment in comparison to the distance between the shock front and point of observation. This situation is obviously not fulfilled in the present set of experiments. A better model is to regard the shock-turbulence interaction region as a line of acoustic sources across the flow. The acoustic power generated by these sources may be calculated using Ribner's results (see Figure 5, and Reference 17). If the acoustic energy is then assumed to be radiated uniformly between the shock and acoustic lines, the root mean square pressure fluctuations may be calculated. Although it will be seen that this method requires a number of assumptions in the present instance, with a consequent accumulated uncertainty in the predictions, it is nevertheless considered to be more reliable than the previous one.

The turbulent energy flux into the shock front per unit length of interaction strip is given by

$$J_t = \frac{5}{2} \rho(0) \cdot u^3(0) \left(\frac{\Delta u(0)}{u(0)} \right)^2 \cdot t$$

where t is the strip thickness over which the turbulence is assumed isotropic. As discussed previously, t is taken as 0.168 inch (= 0.427 cm) for $\bar{x} = 25$. For $M_\infty = 1.99$, $J_t = 1.40 \times 10^8$ erg/cm/sec, and for $M_\infty = 3.14$, $J_t = 8.33 \times 10^7$ erg/cm/sec.

From Figure 5, J_a, the acoustic energy generated per second per unit length of interaction strip may be calculated knowing the Mach number of the flow normal to the shock on the wake axis. The normal Mach numbers are 1.370 and 1.276 for M_∞ = 1.99 and 3.14, respectively, giving efficiencies, from Figure 5, of 0.34 and 0.25 percent, respectively. Thus, the acoustic energy generated over each centimeter of interaction strip, J_a, is 4.73×10^5 and 2.08×10^5 erg/sec for M_∞ = 1.99 and 3.14, respectively.

The reasoning described in Section 2.3.2 may now be used to yield a value of p_{rms}. Taking as an example the location of the microphone for Run 101 T, where the observation point is 7.3 cm from the interaction region, M_∞ = 1.99, lower stream and $\theta = 10^\circ$, it is found that p_{rms} = 593 dynes/cm^2, equivalent to 129.5 dB. For Run 102 H where the microphone is located 2.3 cm distant, $\theta = 39^\circ$, p_{rms} = 1239 dynes/cm^2, equivalent to 135.5 dB. Choosing the microphone locations for Runs 98 B and 117 G as typical field points for lower and upper streams, respectively, in the M_∞ = 3.14 flows, the results are: Run 98 B, p_{rms} = 213 dynes/cm^2, equivalent to 120.5 dB; Run 117 G, p_{rms} = 571 dynes/cm^2, equivalent to 129 dB. These results are summarized in Table III.

5.2.2 Comparison with Experiment

The overall pressure fluctuation profiles which have been made from the traverses may be examined by investigating both their general shape and their magnitude.

The most obvious features about the shape of the profiles in the lower stream (Figures 24 and 30) are the two peaks. The peaks which lie in the upstream direction are obviously associated with the main shock wave from the wedge. This is borne out by the similarity of the peaks with that of Series D (Figure 20) when no turbulence was present, and also by the coincidence of these peaks with the increase in static pressure. The magnitude and width of the peaks is determined by the interaction of the shock wave with both the turbulence and with the laminar boundary layer covering the surface of the probe. The downstream peaks appear to arise from the turbulent stream impinging upon the upper probe surface. It is not believed that they occur because of the reflection of the shock wave from the leading edge of the probe off the wake, since shadowgraphs show no reflection to occur in the case of M_∞ = 3.14. It may be noted that the upstream and downstream peaks completely dominate the profiles, and no region of the profiles can be obviously said to be primarily due to shock-turbulence effects.

However, the profiles taken in the upper stream seem less dominated by these effects. As is seen from Figures 27 and 33, there is an increase in the sound pressure level at the location of the Mach line from the edge of the turbulence. The peak which is

reached has a much greater width than the shock induced peaks seen in the lower stream traverses, and hence does not seem to be characteristic of shock interaction. Nevertheless, it is known that, at least in the case of $M_\infty = 1.99$, the main shock wave has a reflection off the wake which closely coincides with the position of the Mach line (see Section 5.1). Although investigation of the spectra of the signals (see Section 5.3) does not reveal any positive identification of the nature of the disturbances, it will be assumed, for comparison with the calculations of Section 5.2.1, that they are acoustic.

The predictions of References 5 and 17 are compared in Table III with measurements for specific instances of microphone location and flow Mach number. In each case the probe head was adjusted parallel to the local stream, and no correction will be made for impinging flows. The lower stream fluctuation levels quoted in the table are less than those of the profiles because of the difference in orientation. It is seen from the table that the agreement between theory and experiment is not good. Although the trend of the results is better indicated by the predictions of Reference 17, the magnitudes estimated are too low by 6–11 dB. In the case of Reference 5 predictions, these vary between 13 dB higher and 6 dB lower than measured.

It is clear that the results of Reference 5, summarized in Figure 4, are not applicable to the present situation. The discrepancy arises because the experimental conditions do not closely approximate to the theoretical model, which assumes isotropic turbulence entering an infinite plane shock front. This situation would be better simulated in the present experiment if the observation point were located on the wake axis within, say, 1/10 inch of the shock front. In the calculations no account of observation position was taken.

On the other hand, the predictions based on Reference 17 take account of the variation in position of the observation point. The discrepancy between these estimates and those which were measured could arise in two ways. The first is that the turbulence could be stronger than estimated. For example, if the turbulence was taken to be 20 percent, the value of p_{rms} would be twice that calculated (equivalent to an increase of 6 dB). Although it is felt that the value $\bar{x} = 12$, which yields an estimated turbulence of 23 percent, is too low, the error of the predictions may be compounded by errors in the estimates $\rho(0)$, $M(0)$, etc. The second possibility is that the anticorrelated entropy mode (Reference 16) is yielding a substantial additive influence. As was pointed out in Section 1.0, numerical information on shock interaction with coexisting modes has yet to be obtained, but it seems that the effect could be significant. It may be observed that the fluctuating pressures which were observed were much lower than those predicted in Reference 7. Those estimates were based upon Reference 5, and also assumed shock strength and flow conditions based upon the free stream, rather than in the wake where the interaction in fact takes place.

5.3 Spectra

In this section, the spectral shapes obtained upon analysis of some of the signals will be described. Conclusions must be cautiously drawn, however, since not too much is known about the detailed response and noise floor characteristics of the Kulite microphone and associated circuitry.

Before describing the spectra of the responses of some of the traverse features, it is interesting to calculate the fraction of the range of frequencies of the turbulence covered by the present microphone system. It was seen (Section 2.3.1) that the major part of the velocity fluctuation spectrum falls within $n_s \leq 0.1$. Taking $\Lambda_s \sim L \sim 0.028$ in., and $u = u(0)$, it is found that $f = 57.6$ kHz and 73.8 kHz for $M_\infty = 1.99$ and 3.14, respectively. The microphone system is believed to be uniformly responsive to at least 40 kHz. It may be noted that the longitudinal wavelength of velocity fluctuation which will give rise to a 40 kHz acoustic signal at the fixed microphone is about 1 inch for each of the Mach numbers.

The shape of the spectrum of the microphone response will be determined by a number of factors. The predominant influence will be the turbulence spectrum entering the shock wave, but distortion may occur due to wake effects such as refraction by shear and density fields.

The description of the observed spectra may be divided as follows:

Series D

The spectra obtained from some of the runs in this series are shown in Figure 35. There is a slight peaking of the spectrum at about 15 kHz for responses obtained at the shock front position. For downstream observation points this is not apparent.

Series F

The spectra obtained for the responses which determined the forward (i.e., upstream) and rear (i.e., downstream) peaks (see Figure 24) are given in Figure 36(a) and (b), respectively. It is seen that the spectra for the forward peak have a maximum around 7 kHz, and that amplification of about 20 dB occurs fairly uniformly for frequencies below about 20 kHz. At the convection velocity behind the main shock wave this corresponds to wavelengths longer than about 2 inches, a length about 100 times greater than the longitudinal autocorrelation macroscale. These spectra, and others associated with measurements in the neighborhood of shock waves, are probably determined both by the spectrum of turbulence upon which the shock impinges and by the unsteady aerodynamics of the shock interaction with the boundary layer over the surface of the instrument head.

It is seen that there is a distinct difference in the spectral shapes from both forward and rear peaks. This supports the belief (see Section 5.2.2) that the rear peak is due to the turbulence intercepting the instrument head.

Series H

The spectra for the upper stream traverse with $M_\infty = 3.14$ are shown in Figure 37. The data corresponding to the peak location in Figure 27 are plotted using the higher values of Runs 117 N-R, but inspection of the spectra of Runs 117 A-D reveal identical features. It may be seen that the spectra of the large amplitude signals peak at about 2 kHz, considerably lower than for the shock induced signals. As the microphone is moved further downstream it is seen that the signal contains decreasing proportion of low frequency fluctuations. This would appear to indicate that the pressure do not arise from jet-like noise sources (Reference 22) where low frequency shear noise is generally observed closer to the axis. However, it cannot be said that the spectral features provide any indication that the fluctuations are of an acoustic nature, or that they are characteristic of the type of interaction which is being sought.

Series I

The spectra for the forward and rear peaks are shown in Figure 38. A maximum is indicated about 12 kHz for both peaks, although the rear peak does not show as much high frequency content. The similarity between the two sets of spectra was not obvious in the $M_\infty = 3.14$ case. Further, it appears that the spectrum shape is relatively constant throughout any one peak, unlike the previous instances where low frequencies dominated the more intense fluctuations. The apparent increase in the high frequency content of the $M_\infty = 1.99$ signals may appear to be in contradiction to the lower convection velocity of the flow. However, as was described in Section 5.1, the aerodynamic situation in the interaction region appears to be different from the $M_\infty = 3.14$ case, so that the same mechanism may not be responsible for the signals in each case. Further, the flow Reynolds numbers are different, and it is possible that the turbulence structures at the interaction point will not be the same. Whether either or both of these mechanisms is responsible has not been determined in the present work.

Series J

Figure 39 presents the spectra for this series, and these may be compared with the spectra of Figure 37 for $M_\infty = 3.14$. The spectral shapes appear very similar, except that, in the present case, the maximum occurs near 10 kHz instead of 2 kHz, as seen in Figure 37. Again this feature runs contrary to what might be expected on the basis of convection velocity, and again the possible explanations are mean flow or Reynolds number effects.

By way of conclusion it may be stated that no indication of the nature of the fluctuations could be gained from an inspection of their spectra. The most noteworthy observation is that the lower Mach number, but higher Reynolds number, flow apparently causes a move to higher frequencies of the maximum point in the spectrum. The origin of this effect is undecided.

6.0 DESCRIPTION OF EXPANSION-TURBULENCE INTERACTION EXPERIMENT

The objective of this experiment was to check the predictions made in Reference 8 concerning the possibility of having high fluctuating pressure levels arising from the passage of turbulence over an expansion shoulder.

The basis for the calculations is that the pressure variations may be determined by the rotation of the expansion fan around its apex. Figure 6 of Reference 8 gives, for various expansion angles, estimated peak-to-peak pressure fluctuations as a function of Mach number when the flow has a constant total head of 2,500 psf and an amplitude velocity variation of 10 percent. If it is assumed that the fluctuations in the present case are approximately sinusoidal then, for a 10-degree expansion corner and atmospheric reservoir conditions, rms pressure fluctuations of about 141 dB and 130 dB may be expected downstream of the corner for $M_\infty = 1.99$ and 3.14, respectively. For an expansion of 20 degrees, the corresponding predicted fluctuating pressure levels are 141 dB and 128 dB.

In the experiments, which were carried out at the end of the shock-turbulence series, three expansion angles of 10, 20 and 30 degrees were used. The construction of these wedges and mounting of the microphones are shown in Figure 12. The purpose of the upstream transducer was to observe the magnitude of pressure fluctuations before the interaction took place. The turbulence was again the wake of the flat plate used in the shock-turbulence experiments. Figure 40 shows the location of the microphones for the present experiment, Series K (Runs 145 A - 150 C). The wedges were run in two configurations; one with the rear surface parallel to the tunnel centerline, and the other with the front surface in the parallel position. In the first configuration the wake experienced a flow deflection before encountering the corner. This has the effect of slightly decreasing the flow Mach number approaching the corner, and increasing the expected fluctuating pressures (see Reference 8).

The readings which were observed are noted in Table II. In the first configuration it is seen that the upstream transducer, which ideally should have a very low reading, is actually sensing pressure fluctuations which are several dB higher than the expected effect. Also it is noted that the response of the downstream transducer is less than that of the upstream one. For the second configuration, it is seen that the upstream microphone response is again greater than the downstream reading, although the upstream pressure fluctuations have been reduced considerably over the first configuration. The spectra of the responses from the upstream microphone appear quite flat up to the high frequency limit of the system. The spectra of the downstream transducer show that the reduction of overall level across the corner occurs as a reduction of the frequency components mainly below about 20 kHz.

From the measurements it is therefore concluded that the expected increase of fluctuating pressure level was not observed. The main reason is probably that the relationship that the turbulence scale be greater than the distance of the downstream observation point from the corner is not attained. In fact, from the arguments put forward in Section 5.1, the reverse is probably true. Since the effects of expansion fan rotation are confined to the characteristic eddy size, the mechanism proposed in Reference 8 is not observed in the present experiment.

7.0 CONCLUSIONS AND RECOMMENDATIONS

7.1 Conclusions

From the experiments which were carried out on the shock-turbulence interaction, the following main conclusions can be drawn:

- Traverses of the flow fields by the microphone indicated increases in the fluctuating pressure level both at the location of the interacting oblique shock wave, and at the location of the Mach line from the edge of the turbulent wake.

  The peak fluctuating pressures at the shock wave locations were 154 dB (re: 2×10^{-4} dynes/cm^2) and 145 dB for the Mach number 1.99 and 3.14 flows, respectively. The shape of these peaks was found to be characteristic of that which was observed when the Mach number 2.89 flowfield was traversed when no turbulence was present. Thus, these peaks are characteristic of the shock wave interaction with the probing instrument head rather than of the shock-turbulence interaction.

  Peak fluctuating pressures of about 145 dB were observed at the location of the Mach line for both Mach number 1.99 and 3.14 flows. The shape of these peaks was not characteristic of the shock interaction with the instrument head, although, in the case of the Mach number 1.99 flow, a shock was observed by shadowgraph at this location. Inspection of the spectra of the microphone responses at these locations revealed no clear indication of the source of the fluctuating pressures.

- For typical field points, the measured overall fluctuating pressures were compared with the predictions made by Lowson's calculations (Reference 5) and with those made by Ribner (Reference 17). Agreement between theory and experiment is not good.

  In the case of Reference 5, the predictions vary between 13 dB higher and 6 dB lower than measured, and no account is taken of variation in position of the microphone. The disagreement is hardly surprising since the theoretical model assumes the interaction to be taking place between isotropic turbulence and an infinitely plane shock wave, conditions which are not met experimentally.

  Although the condition of isotropic turbulence is not fulfilled for comparison with the predictions of Reference 17, some account is taken of the finite extent of the acoustic source. Predictions are

between 6 dB and 11 dB too low, but show the correct trend with change in microphone position and nozzle Mach number. Assuming that the fluctuations which were observed are of an acoustic nature, the discrepancy could arise either from an incorrect estimate of turbulence intensity, or from neglect of entropy spottiness strongly anticorrelated with the velocity fluctuations.

Some other conclusions, which are incidental to the main theme, may be stated:

- As far as can be judged by the shadowgraphs of the positions of the shocks in the mean flow, the application of Demetriades' results (Reference 15) for an axisymmetric wake to the present case of a flat plate wake appeared reasonable. The major assumption involved basing the transverse length scale on the momentum thickness of the turbulent boundary layer on the plate, and supposing that the turbulence appeared to originate at the trailing edge of the flat plate. The shadowgraphs indicated that in certain cases, predicted by Demetriades' results, the centerline wake flow was reduced by the shock wave to a subsonic state.

- Inspection of the spectra revealed that spectra taken at the location of the Mach lines had maxima at a higher frequency for the Mach number 1.99 flow than for the Mach number 3.14 flow. The mechanism causing this result was not identified.

Finally, the experiment to observe the production of fluctuating pressures by the interaction between large scale turbulence and a centered expansion fan, failed in its objectives. The reason was that the large ratio, required in the theoretical model, of a typical eddy scale to the distance of the microphone from the corner was not met in the experiment.

7.2 Recommendations

It is useful to note here some recommendations which may prove beneficial to the design of subsequent experiments on the interaction between turbulence and shock waves. Two of the most important are stated below:

- Since the fluctuations observed by the microphone may arise from many different sources, it would be advantageous to design the experiment so that the acoustic nature of the fluctuations could be established. This may be achieved by performing spectral correlations on the responses from two microphones located at different positions in the field. The convection velocity deduced by this procedure would then equal the sum of free stream and sound propagation velocities if the fluctuations were acoustic.

- It would also be advantageous to have a more detailed knowledge of the frequency response of the microphone system. It is suggested that the results of a subsidiary experiment to give this information would provide increased confidence in the spectral analysis of the signals.

Some other significant but less important points may be made in this respect:

- The nature of the turbulence entering the shock wave could be measured, yielding more pertinent values for $\bar{x}$ and $(C_D A)^{\frac{1}{2}}$ than used here. Undoubtedly, this would necessitate an extensive and careful series of measurements. However, it is not listed with the more important recommendations since it was felt that the application of Demetriades' results to the present conditions was satisfactory, considering the objectives of the experiment, and the verification supplied by the mean flow observations.

- Regarding experimental technique, the experiment could be performed in a larger wind tunnel, so that larger models could be used. It would be a distinct advantage to have the instrument head continuously and remotely adjustable. Also, a parallel shadowgraph system would yield quantitative flow information.

REFERENCES

1. H. S. Ribner, "Convection of a Pattern of Vorticity Through a Shock Wave," NACA Report No. 1164 (1954).

2. H. S. Ribner, "Shock-Turbulence Interaction and the Generation of Noise," NACA Report No. 1233 (1955).

3. F. K. Moore, "Unsteady Oblique Interaction of a Shock Wave with a Plane Disturbance," NACA Report No. 1154 (1954).

4. C. T. Chang, "On the Interaction of Weak Disturbances and a Plane Shock of Arbitrary Strength in a Perfect Gas," Ph.D. Thesis, Johns Hopkins University (1955).

5. M. V. Lowson, "The Fluctuating Pressures Due to Shock Interactions with Turbulence and Sound," Wyle Laboratories Research Staff Report WR 66-35, (1966); also "Pressure Fluctuations Resulting from Shock Interactions," J. Sound Vibration, 7, 380 (1968).

6. E. Cuadra, "Interactions of a Shock Wave with an Entropy Discontinuity," Wyle Laboratories Research Staff Report WR 67-17 (1967).

7. S. W. Radcliffe, "An Experimental Program for the Investigation of Shock-Turbulence Interaction Phenomena," Wyle Laboratories Research Staff Technical Memorandum 68-5 (1968).

8. S. W. Radcliffe, "Pressure Fluctuations Generated in the Interaction of Large Scale Turbulence with a Centered Expansion Fan," Wyle Laboratories Research Staff Technical Memorandum 67-9 (1967).

9. L. S. G. Kovasznay, "Turbulence in Supersonic Flow," J. Aero. Sciences, 20, 657 (1953).

10. L. S. G. Kovasznay, "Interaction of a Shock Wave and Turbulence," Proc. Heat Transfer and Fluid Mechanics Inst., I-1 (1955).

11. M. A. Hollingsworth and E. J. Richards, "A Schlieren Study of the Interaction Between a Vortex and a Shock Wave in a Shock Tube," Aeronautical Research Council Report 17985, Fluid Motion Sub-Committee 2323 (1955).

12. D. S. Dosanjh and T. M. Weeks, "Interaction of a Starting Vortex as well as a Vortex Street with a Traveling Shock Wave," AIAA Journal, 3, 216 (1965).

13. J. E. Werner, "Shock Wave-Turbulence Interaction, Investigations in a Shock Tube," AFOSR TN-59-46 (1959).

14. D. S. Dosanjh and R. P. Hamernick, "Interaction of an Advancing Shock Front with a Concentrated Heat (Entropy) Source," Proc. 6th International Shock Tube Symposium, Freiburg im Breisgau, p. 299 (1967).

15. A. Demetriades, "Mean Flow Measurements in an Axisymmetric Compressible Turbulent Wake," AIAA Journal, 6, 432 (1968).

16. A. Demetriades, "Turbulence Measurements in an Axisymmetric Compressible Wake," Physics of Fluids, 11, 1841 (1968).

17. H. S. Ribner, "Acoustic Energy Flux from Shock-Turbulence Interaction," J. Fluid Mechanics, 35, Part 2, 299 (1969).

18. L. L. Beranek, "Acoustic Measurements," John Wiley and Sons, New York (1967).

19. Ames Research Staff, "Equations, Tables and Charts for Compressible Flow," NACA Report No. 1135 (1953).

20. M. G. Butler and C. W. Simmons, "Boundary Layer Calibration of the 7 in. by 7 in. Bi-Sonic Wind Tunnel," Wind Tunnel Note 107 (1964).

21. H. Schlichting, "Boundary Layer Theory," McGraw-Hill Book Company, New York (1960).

22. H. S. Ribner, "The Generation of Sound by Turbulent Jets," Advances in Applied Mechanics, 8, 104 (1964).

TABLE I

AERODYNAMIC CONSTANTS FOR 7 IN. BY 7 IN SUPERSONIC WIND TUNNEL

Mach No.	1.99	2.89	3.14*	3.87
Dynamic Pressure (psi)	5.29	2.76	2.24	1.21
Static Pressure (psi)	1.91	0.471	0.325	0.115
Reynolds No./in.	305,185	198,000	174,000	118,000
Throat Area (sq in.)	30.28	11.14	9.36	4.90

Atmospheric conditions: $P = 14.^{-}$ psia, $T = 90^{\circ}F$, $\rho = 0.0722$ lb/ft^3 .

*M 2.89 nozzle with turbulence plate in upstream position.

TABLE II

RUN CATALOG

Run	Shadow-graph	Reel	dB (o.a)	Static psi	Mach No.	Comments
A. To Investigate Shock Waves from Plate						
49	X	-	-	-	1.89	Downstream position
50		-	-	-	2.07	But see Run 147B. Upstream position
51	X	-	-	-	2.73	Downstream position
52	X	-	-	-	3.14	Upstream position
53	X	-	-	-	3.23	Upstream position. See 76 for downstream
B. To Investigate Instrument Head Behavior						
4	X	1	126.4	0.440	2.89	0° Orientation
5		1	126.1	0.510		3° Orientation
6	X	1	126.3	0.648		6° Orientation
7	X	1	128.5	0.106	3.87	0° Orientation
8	X	1	128.5	0.136		3° Orientation
9	X	1	128.7	0.156		6° Orientation
						Orientation is such that probe surface is exposed to upstream
C. To Investigate Environment of Plate						
70		2	128.8	0.396	3.14	For locations see Figure 18
71		2	130.4	0.363		
72		2	131.5	0.385		
73A		2	130.2	0.343		
74		2	126.8	0.328		0° Orientation in each case
75		2	130.9	0.307		
76	X	1	129.7	0.099	3.41	
77	X	1	130.7	0.105		
79	X	1	134.2	0.094		
80	X	1	133.4	0.113		

TABLE II (Continued)

Run	Shadow-graph	Reel	dB (o.a)	Static psi	Mach No.	Comments
D. To Investigate Field of Shock Generating Wedge (10°)						
						For locations see Figure 19
100	X	3	125.1	0.881	2.89	Head at 0° to local stream
100A			127.3	0.531		
100B			123.8	0.471		
100C			133.4	0.715		
100D			138.6	1.564		
100E			131.6	1.450		
100F			136.5	1.540		
100G			130.1	0.700		Head at 0° to upstream flow
100H			127.3	1.385		Static pressure on 100G was unsteady
100I			126.3	1.427		
100J			126.0	1.391		
100K			125.7	1.290		
100L			123.8	0.969		
E. To Investigate Effects of Varying Shock-Generating Wedge Angle						
						For locations see Figure 21
111	X	1	137.2	0.217	3.41	10° wedge; turbulence, 1 in. interaction distance
112	X		127.1	0.297		As 111; no turbulence
113	X		142.6	0.161		20° wedge; turbulence, 1 in. interaction distance
114	X		127.0	0.275		As 113; no turbulence
114B			127.8	-		Free stream measurement
115	X		144.0	0.111		30° wedge; turbulence, 1 in. interaction distance
116	X		125.7	-		As 115; no turbulence

TABLE II (Continued)

Run	Shadow-graph	Reel	dB (o.a)	Static psi	Mach No.	Comments
F. Lower Stream Traverse in Mach 3.14 Flow (10° Wedge)						
						For locations see Figure 23
91	X	2	139.2	0.742	3.14	Interaction distance = 2 in.
98	X		134.5	0.373		Interaction distance = 4 in.
98A			126.3	0.367		Interaction distance = 4 in.
98B	X		129.7	0.572		Interaction distance = 2 in., head at 0° to local flow
98C	X		133.5	1.124		
98D			136.7	1.156		
98E	X		138.3	1.165		
98F			144.7	1.157		
98G	X		138.5	0.870		
98G		3	134.5	0.586		
98G			134.2	0.630		
98H			128.0	0.380		Traversal of shock-turbulence environment on side of turbulence away from wedge (lower side). 0° orientation of probe head to free stream. Interaction distance = 2 in.
98I			133.0	0.488		
98J			143.5	1.188		
98K			144.8	1.180		
98L			137.6	1.112		
98M			135.7	1.044		
98N			134.4	1.092		
98O			132.9	1.026		
98P			134.3	1.008		
98Q			135.5	0.945		
98R			135.0	0.830		
98S	X		132.0	0.604		
98T			131.3	0.494		

TABLE II (Continued)

Run	Shadow-graph	Reel	dB (o.a)	Static psi	Mach No.	Comments
G. To Investigate Effects of Probe Head Orientation in Fluctuating Field						
						Kulite located at 98M (See Figure 23)
99A		3	136.3	1.005	3.14	Orientation at -3° to free stream
99B		↓	134.2	0.793	↓	Orientation at -6° to free stream
99C	X	↓	132.9	0.617	↓	Orientation at - 10° to free stream
H. Upper Stream Traverse in Mach 3.14 Flow (10° Wedge)						
117A	X	4	134.1	0.760	3.14	For locations see Figure 26
117B		↓	135.7	0.754	↓	
117C	X		136.9	0.697		
117D			139.3	0.630		
117E			138.3	0.573		
117E			139.0	0.567		
117F			142.0	0.631		
117G			140.3	0.567		
117H			139.0	0.552		Traversal of shock-turbulence environment on side of turbulence towards wedge (upper side) 0° orientation of probe head to local stream. Interaction distance = 2.5 in.
117I			137.4	0.540		
117J			137.7	0.551		
117K			138.1	0.575		
117L			137.8	0.621		
117M			137.1	0.635		
117N			135.1	0.858		
117O			136.4	0.835		
117P			137.5	0.842		
117Q	X		143.0	0.787		
117R		↓	145.0	0.710	↓	

TABLE II (Continued)

Run	Shadow-graph	Reel	dB (o.a)	Static psi	Mach No.	Comments
I. Lower Stream Traverse in Mach 1.99 Flow (10° Wedge)						
101A	X	4	138.6	2.360	1.99	For locations see Figure 29
101B			152.8	5.036		
101C			146.8	4.700		
101D	X		143.7	4.490		
101E			142.2	4.220		
101G		↓	139.0	3.740		
101H	X	5	137.2	3.950		
101I			144.2	4.060		
101J			144.4	3.890		Traversal of shock-turbulence environment on lower side. 0° orientation of probe head to free stream. Interaction distance = 2 in.
101J	X		145.2	3.870		
101K			146.0	3.540		
101L			148.4	3.360		
101M	X		148.8	2.950		
101N		↓	140.2	2.488		
101O		4	134.2	2.247		
101P			147.9	2.720		
101Q		↓	154.1	4.950		
101R		5	142.7	2.755		
101S			137.0	2.052		
101T	X	↓	137.8	2.860	↓	Head oriented at 0° to local stream of 101L

TABLE II (Continued)

Run	Shadow-graph	Reel	dB (o.a)	Static psi	Mach No.	Comments
J. Upper Stream Traverse in Mach 1.99 Flow (10° Wedge)						
102A	X	5	135.8	3.667	1.99	For locations see Figure 32
102B			138.0	3.655		
102C	X		144.6	3.660		
102D			143.6	3.276		
102E			142.9	3.180		
102F			143.7	3.093		Traverse of shock-turbulence environment on upper side. 0° orientation of probe head to local stream. Interaction distance = 2 in.
102G			142.4	3.168		
102H			141.0	3.210		
102I	X		139.4	3.275		
102J			138.0	3.240		
102K			136.4	3.151		
102L			135.5	3.040		
102M	X		139.2	3.920		

TABLE II (Continued)

Run	Shadow-graph	Reel	Up-stream dB (o.a)	Down-stream dB (o.a)	Mach No.	Comments
K. Turbulence - Expansion Experiments						
154A	X	6	149.3	134.2	1.99	For locations see Figure 40
145B	X		136.4	130.2		
146A	X		138.2	139.2		
146B	X		140.4	139.2		
147A	X		146.4	144.6		Rear surface of wedge kept parallel to free stream. Wedge corner located in similar position for each wedge.
147B	X		146.0	143.8		
148A	X		142.0	138.3	3.14	
148B	X		142.0	138.4		
149A	X		137.2	131.9		
149B	X		137.3	132.4		
150A	X		133.1	128.5		10° wedge with front surface parallel to free stream.
150B	X		133.0	128.3		
150C			130.0	124.4		

TABLE III

COMPARISON OF PREDICTED AND MEASURED FLUCTUATING PRESSURES

Run Number	Measured	Predicted	
		Reference 5	Reference 17
101 T	137.8	151.2	126.5
102 H	141.0	151.2	132.5
98 B	129.7	134.0	117.5
117 G	140.3	134.0	126.0

Pressure Levels are in dB re: 2×10^{-4} dynes/cm^2

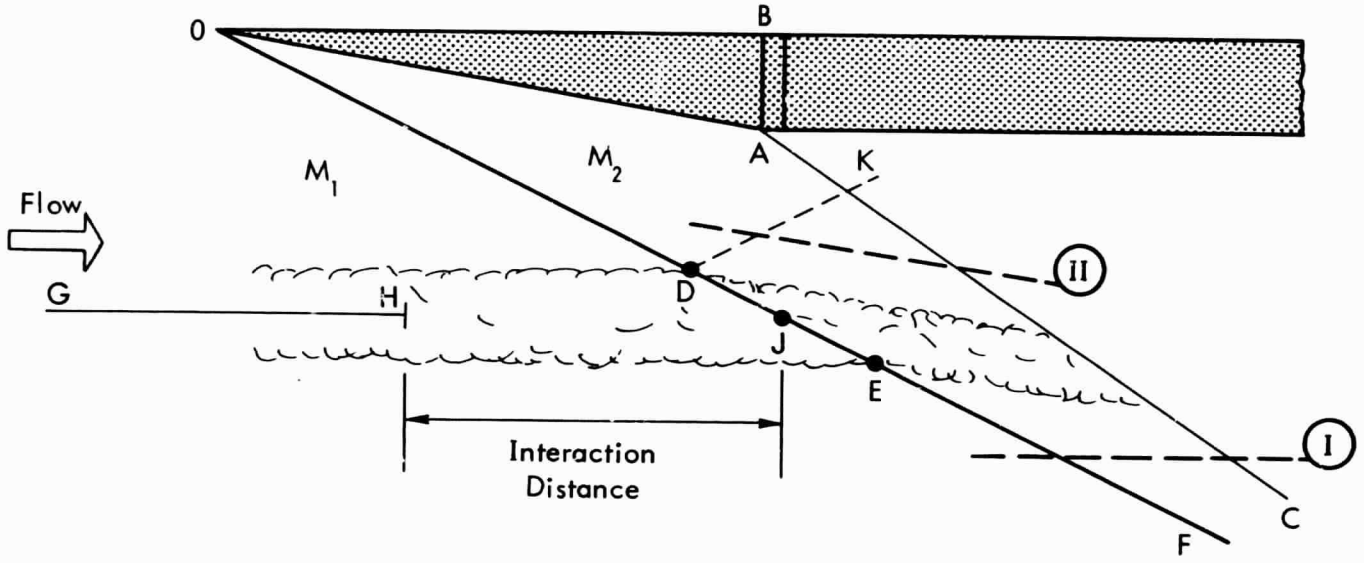

Figure 1. General Arrangement for Shock-Turbulence Experiments

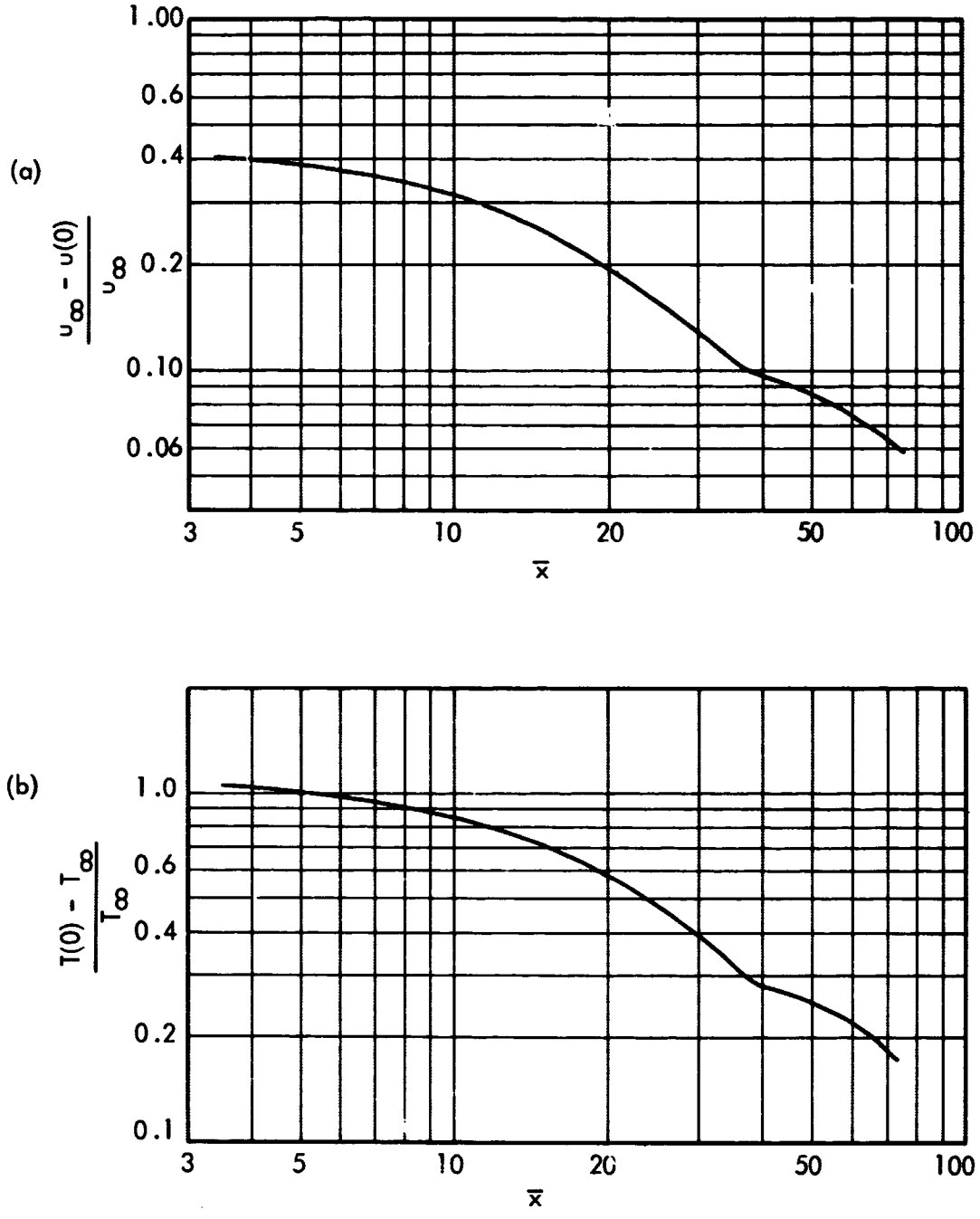

Figure 2. (a) Axial Variation of Velocity, u(0)
(b) Axial Variation of Temperature, T(0)
(After Demetriades, Reference 15)

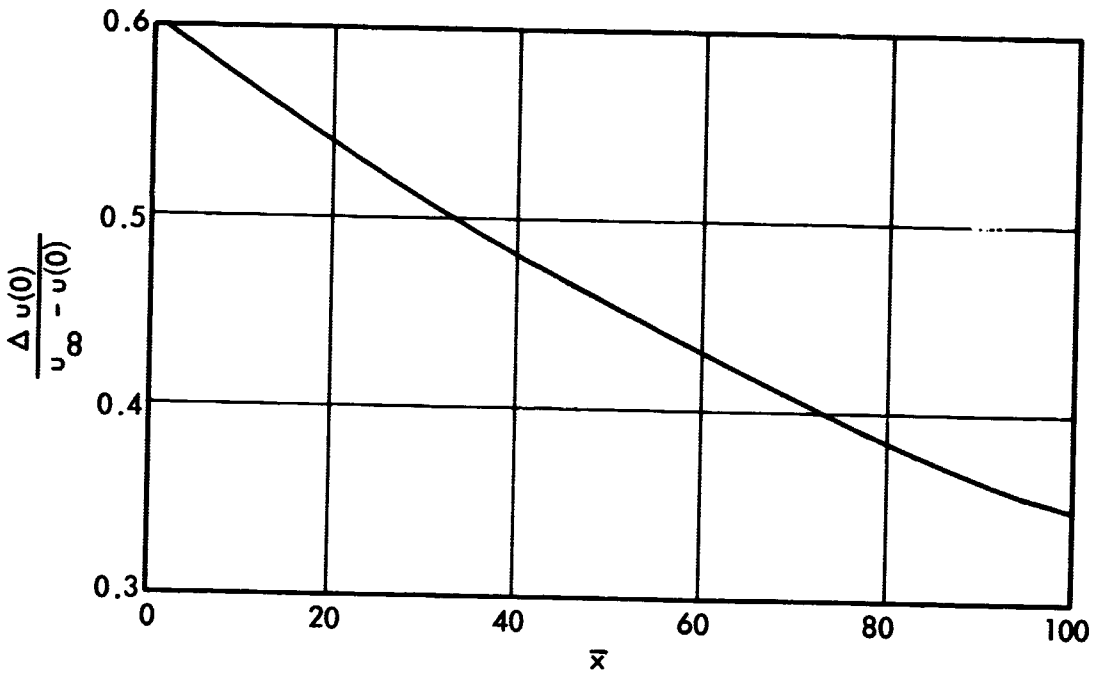

Figure 3. Axial Variation of Velocity Fluctuations
(After Demetriades, Reference 16)

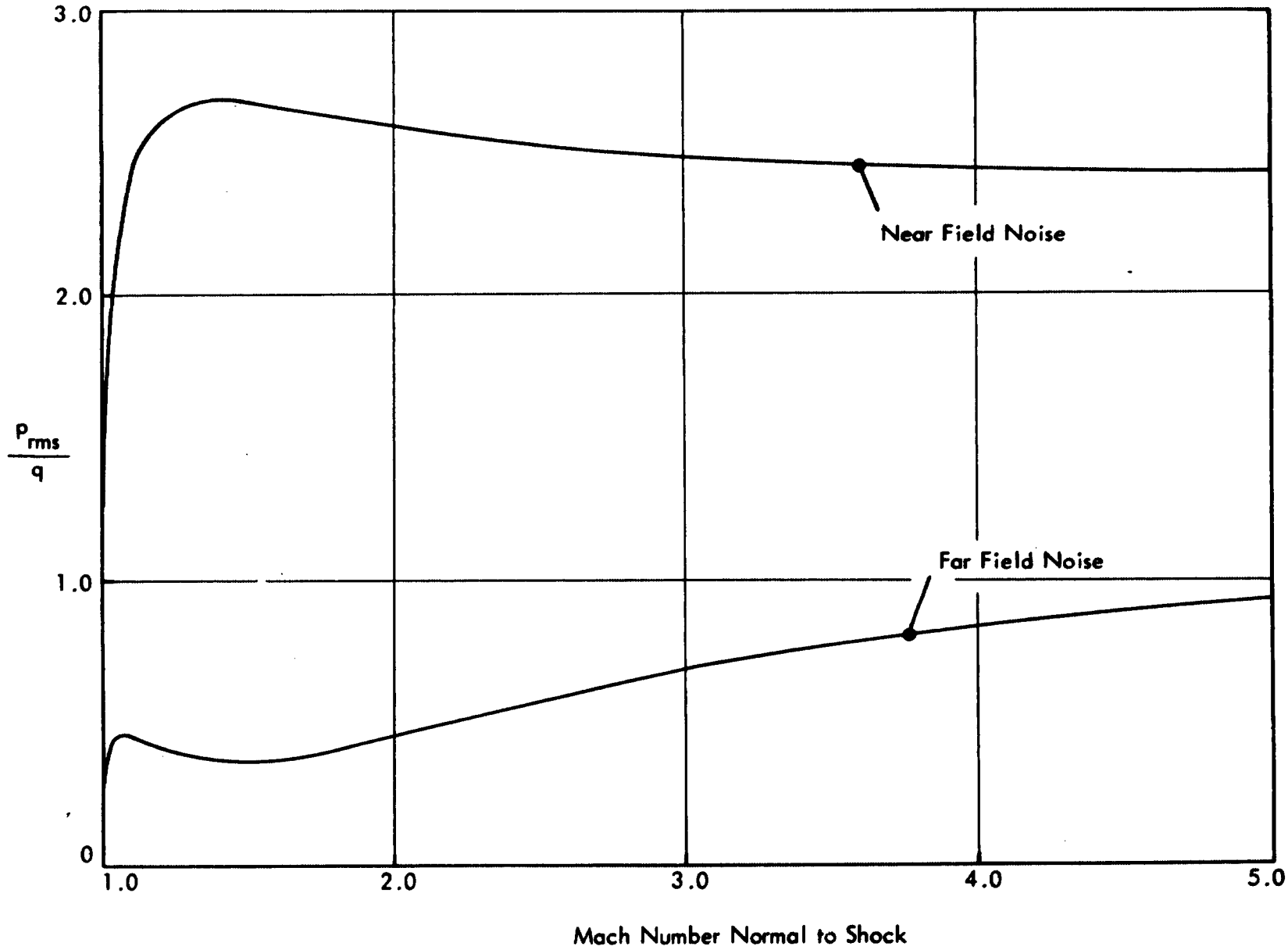

Figure 4. Near and Far Field Sound Level for Shock Interaction With Unit Isotropic Turbulence (After Lowson, Reference 5)

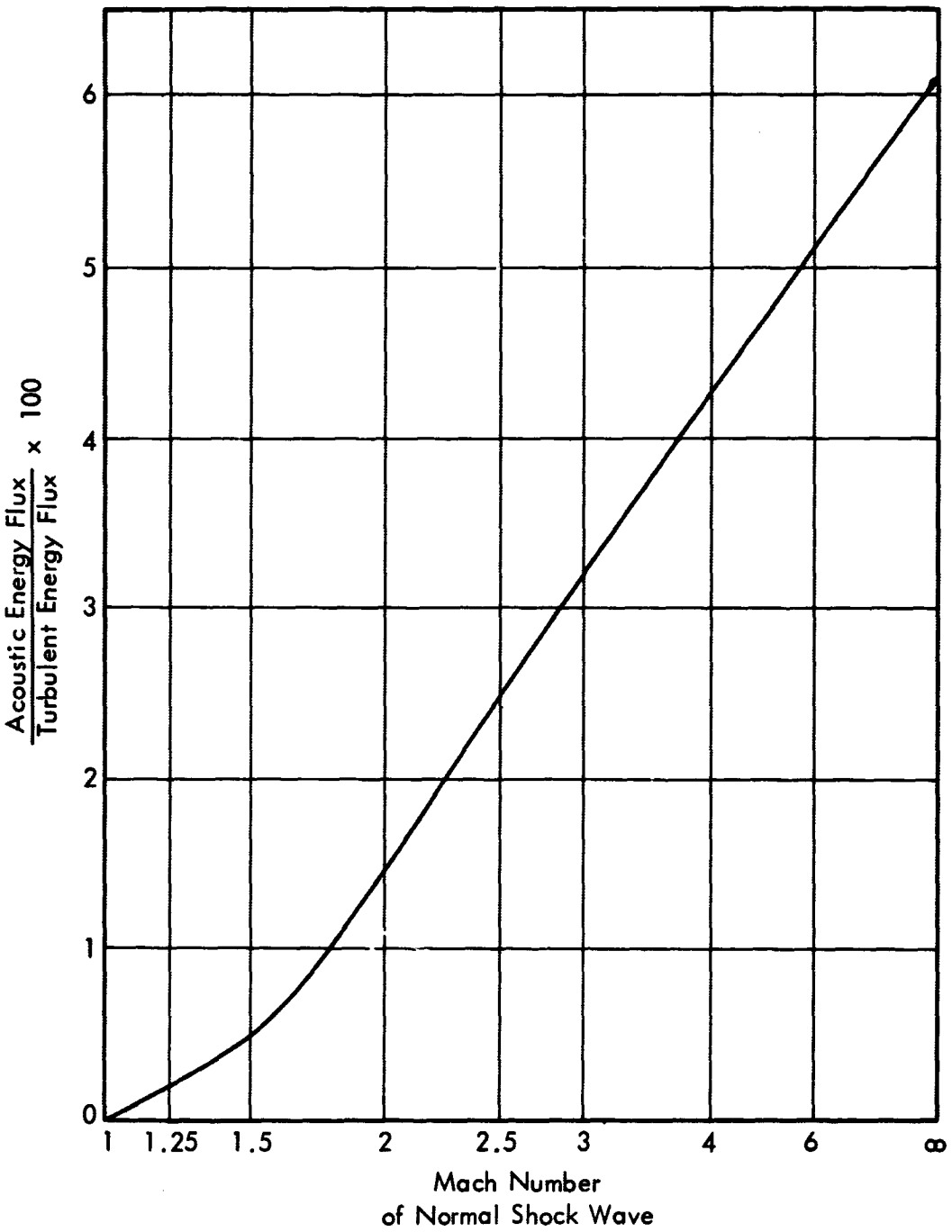

Figure 5. Percentage of Turbulent Energy Converted to Acoustic Energy (After Ribner, Reference 17)

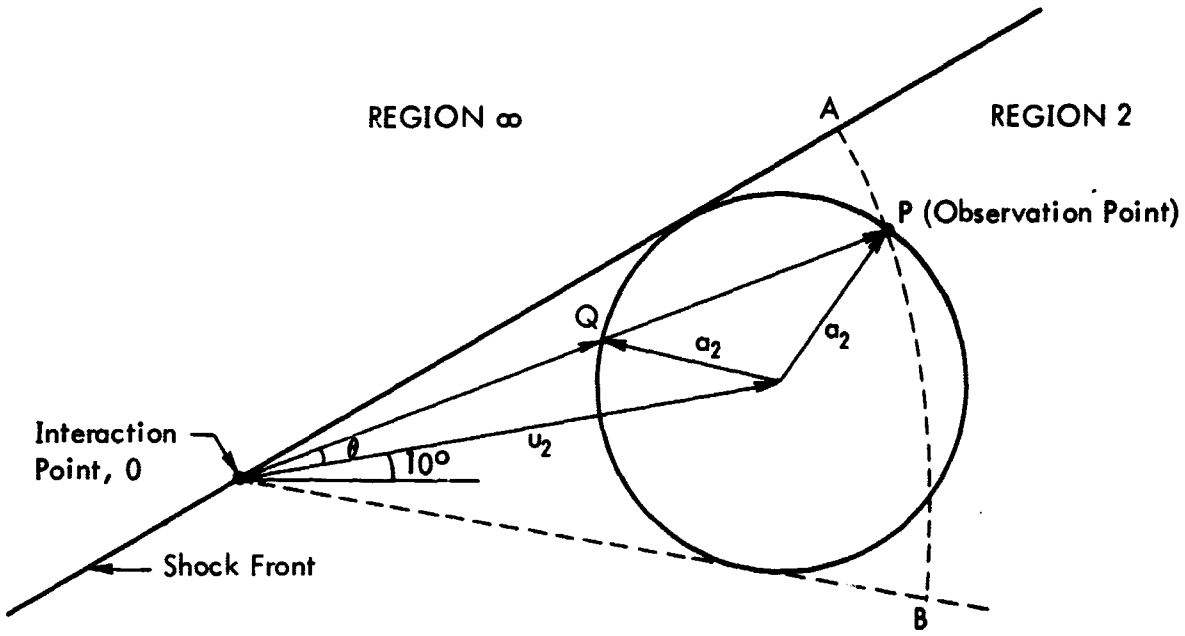

Figure 6. Velocity Diagram for Sound Propagation

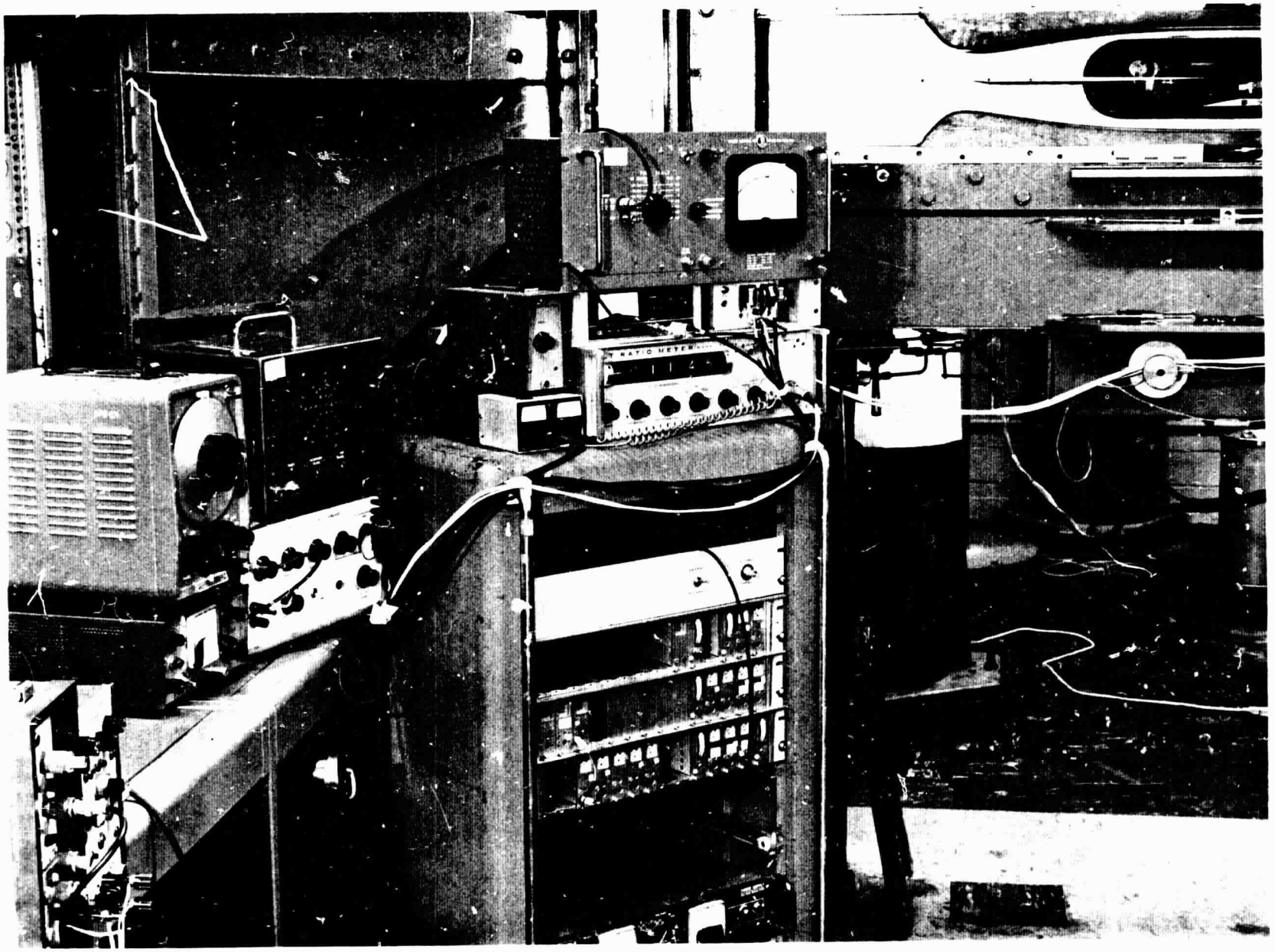

Figure 7. General View of Instrumentation and Wind Tunnel

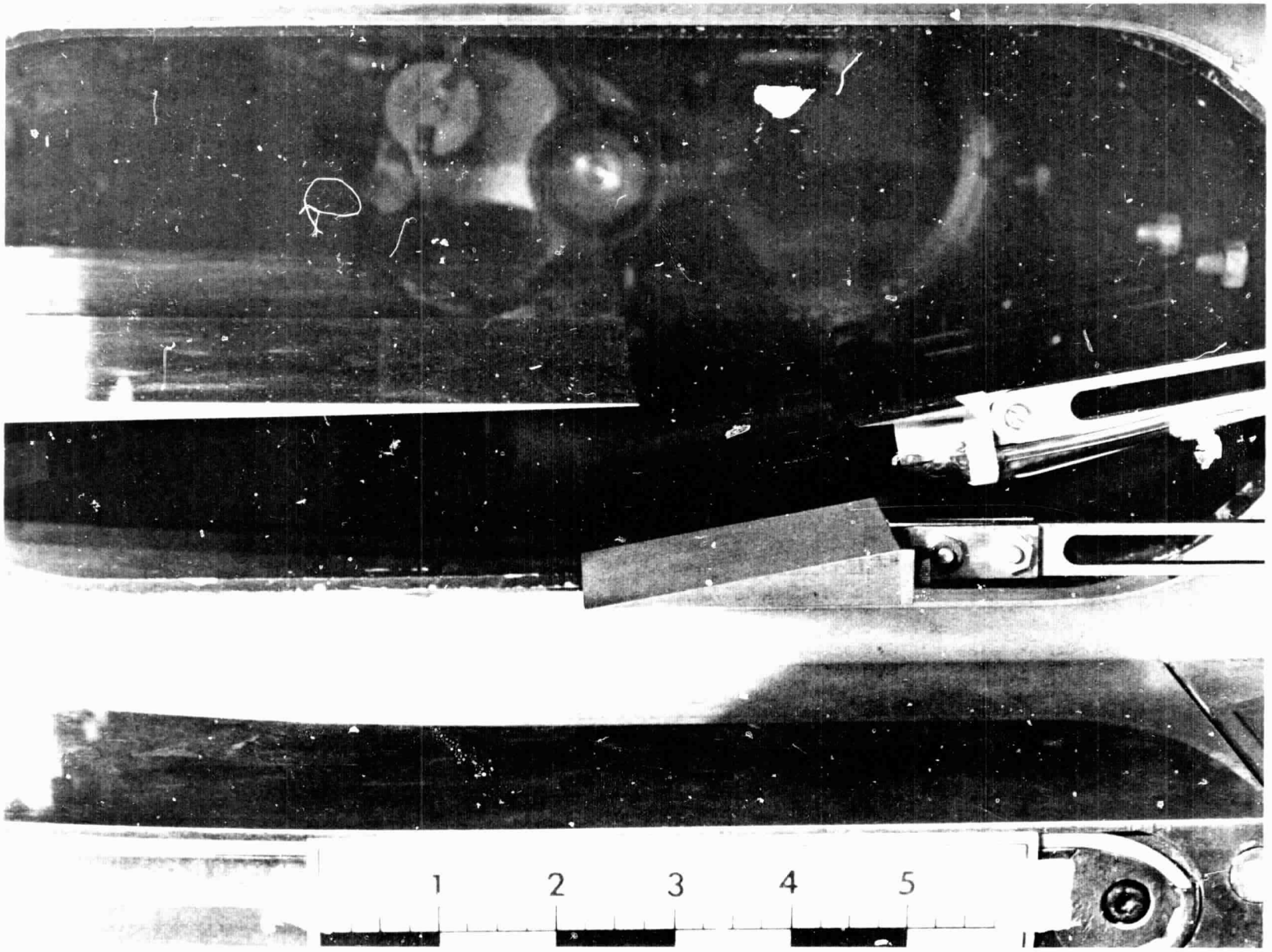

Figure 8. Typical Model Locations in Wind Tunnel

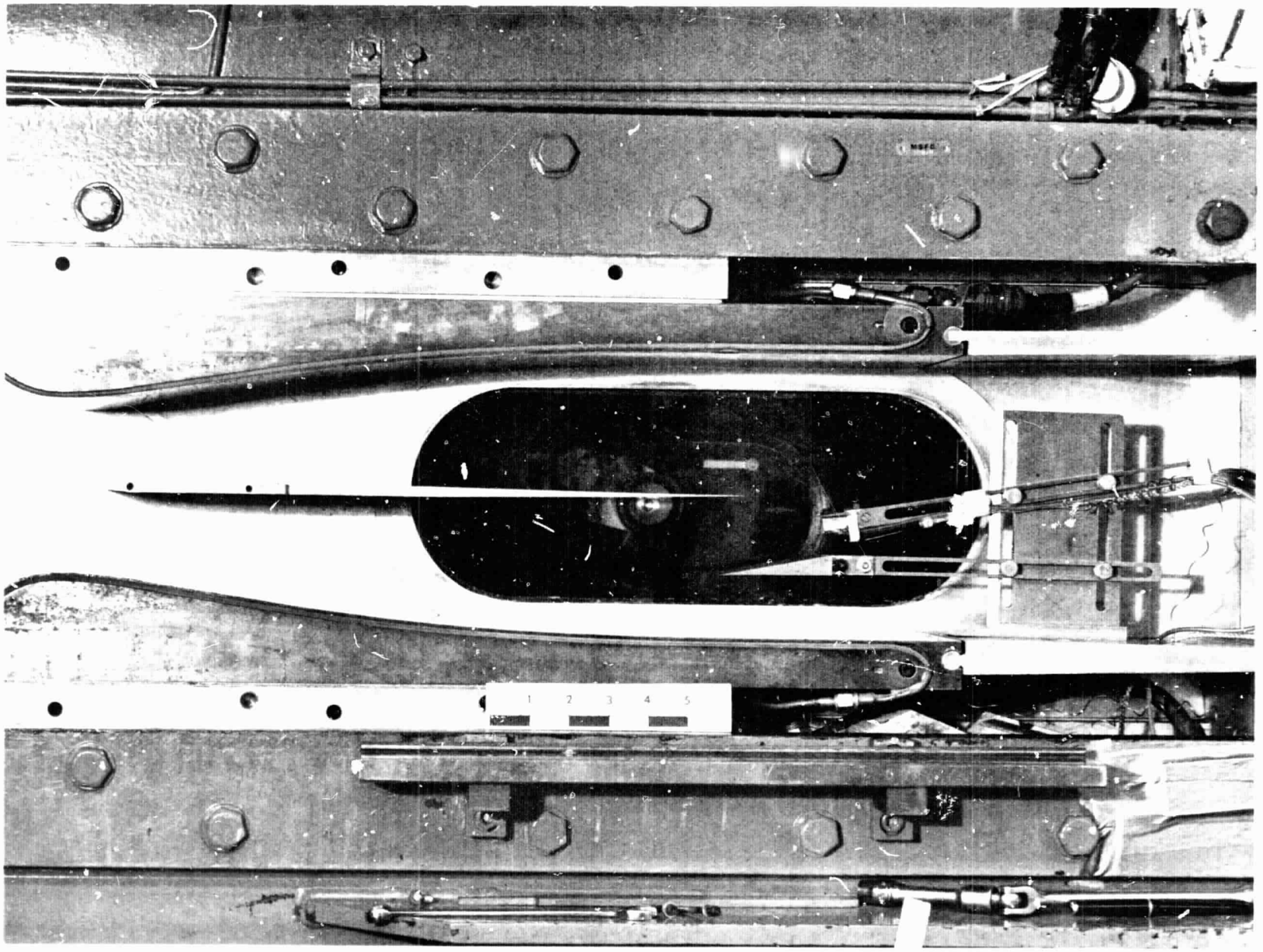

Figure 9. View of Model Assembly

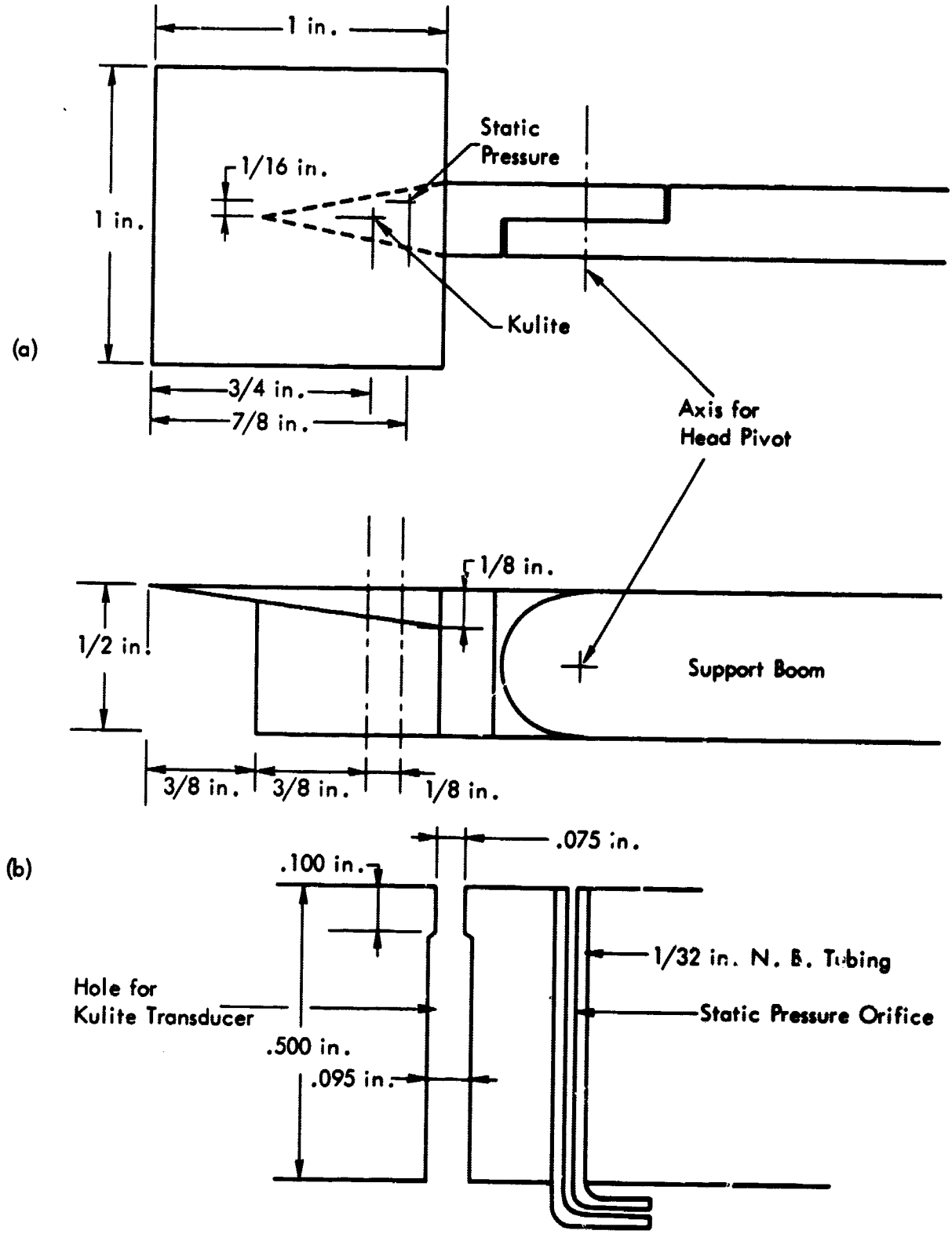

Figure 10. (a) Dimensions of Instrument Head
(b) Details of Static Pressure Orifice and Hole for Kulite Transducer

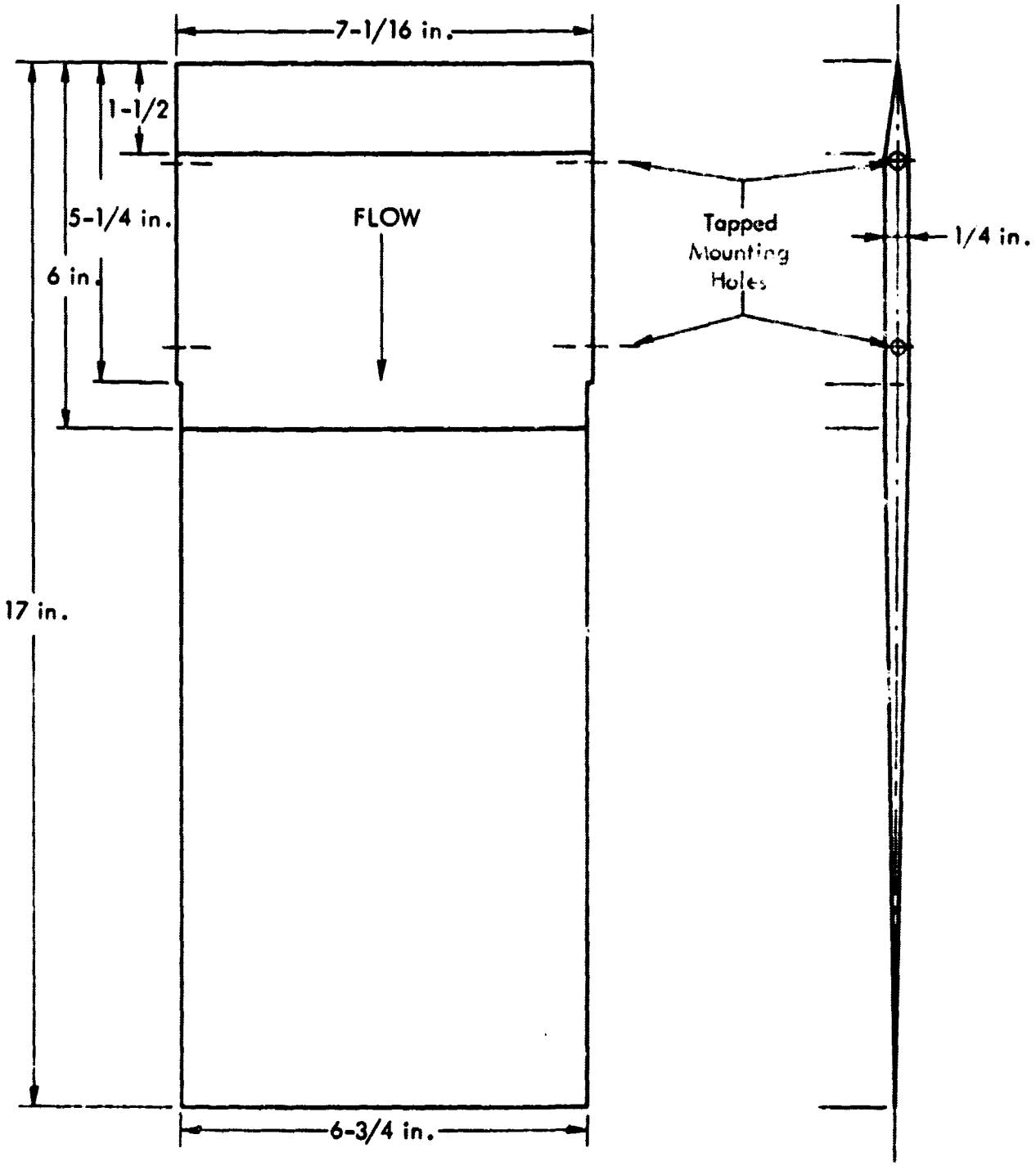

Figure 11. Turbulence Generating Plate

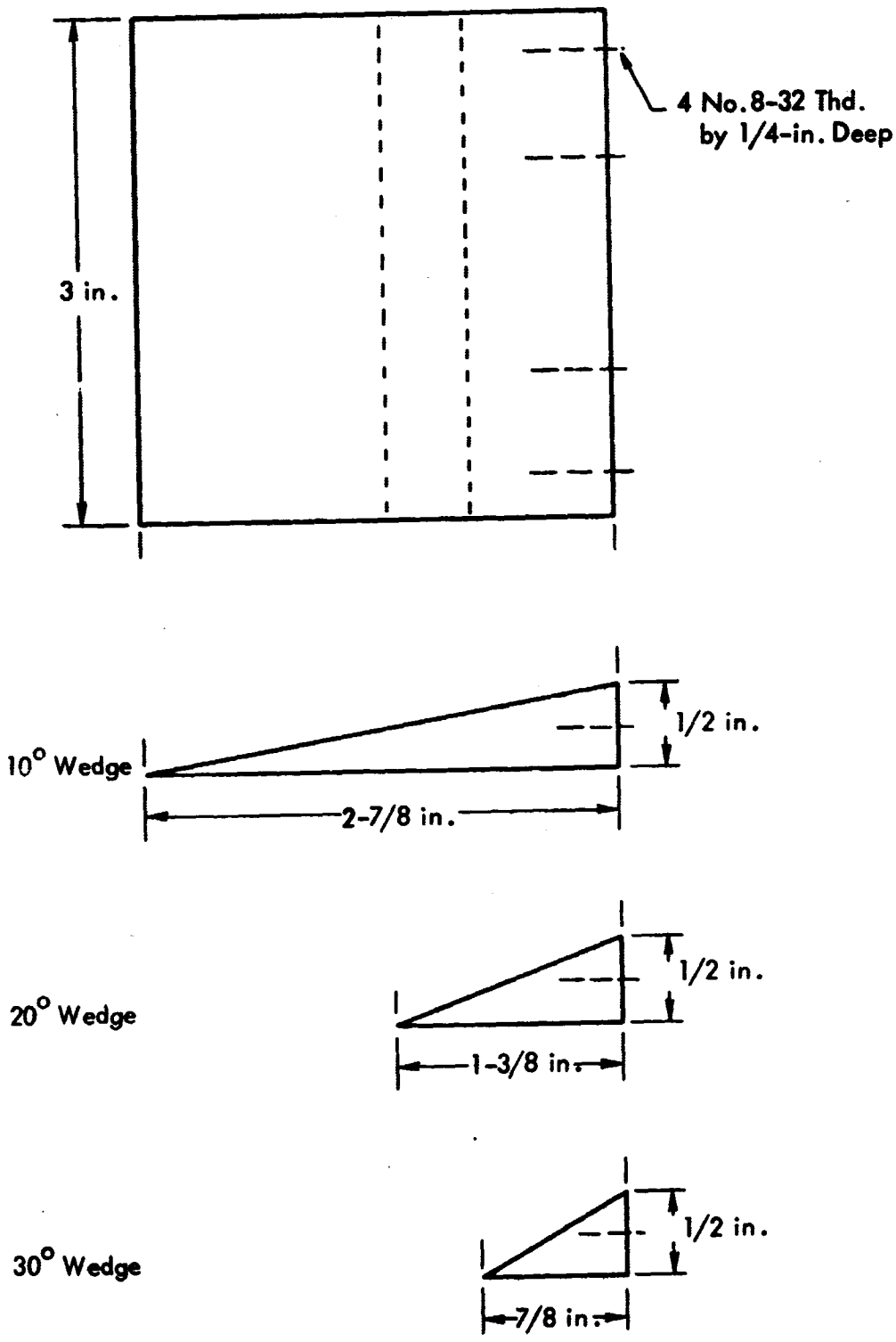

Figure 12. Shock Generating Wedges

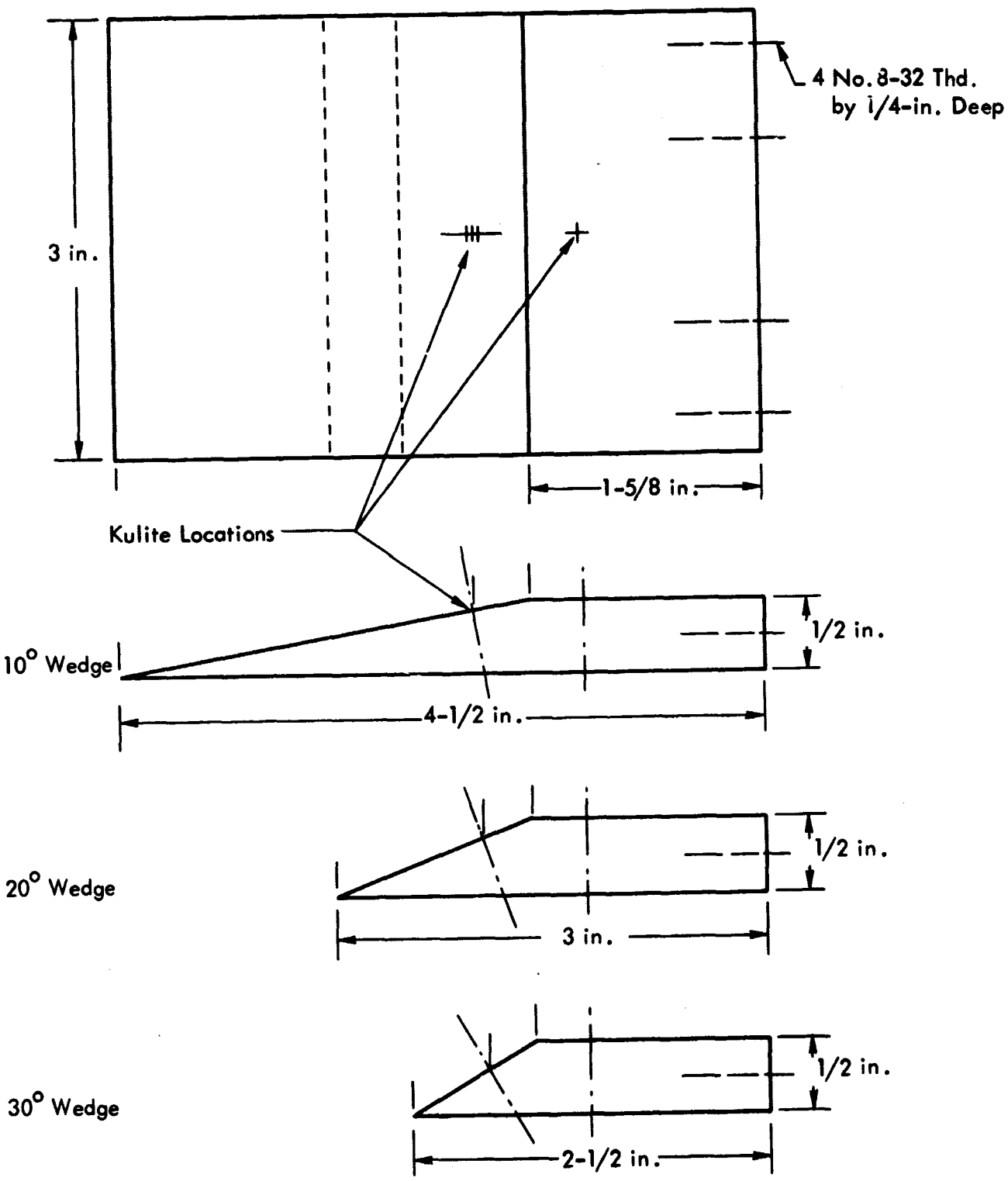

Figure 13. Turbulence-Expansion Wedges

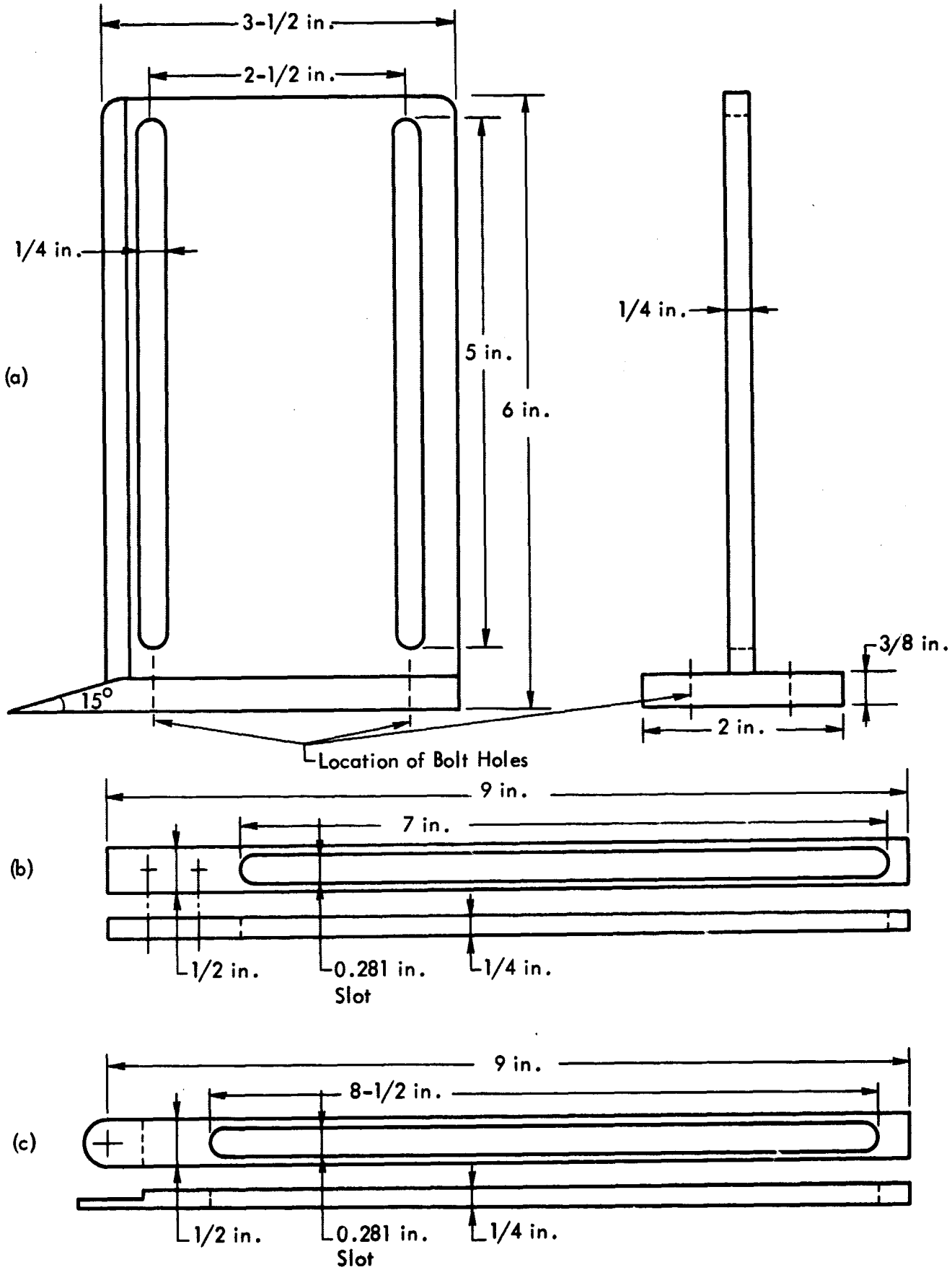

Figure 14 . (a) Support Strut (b) Support Boom for Wedges
(c) Support Boom for Instrument Head

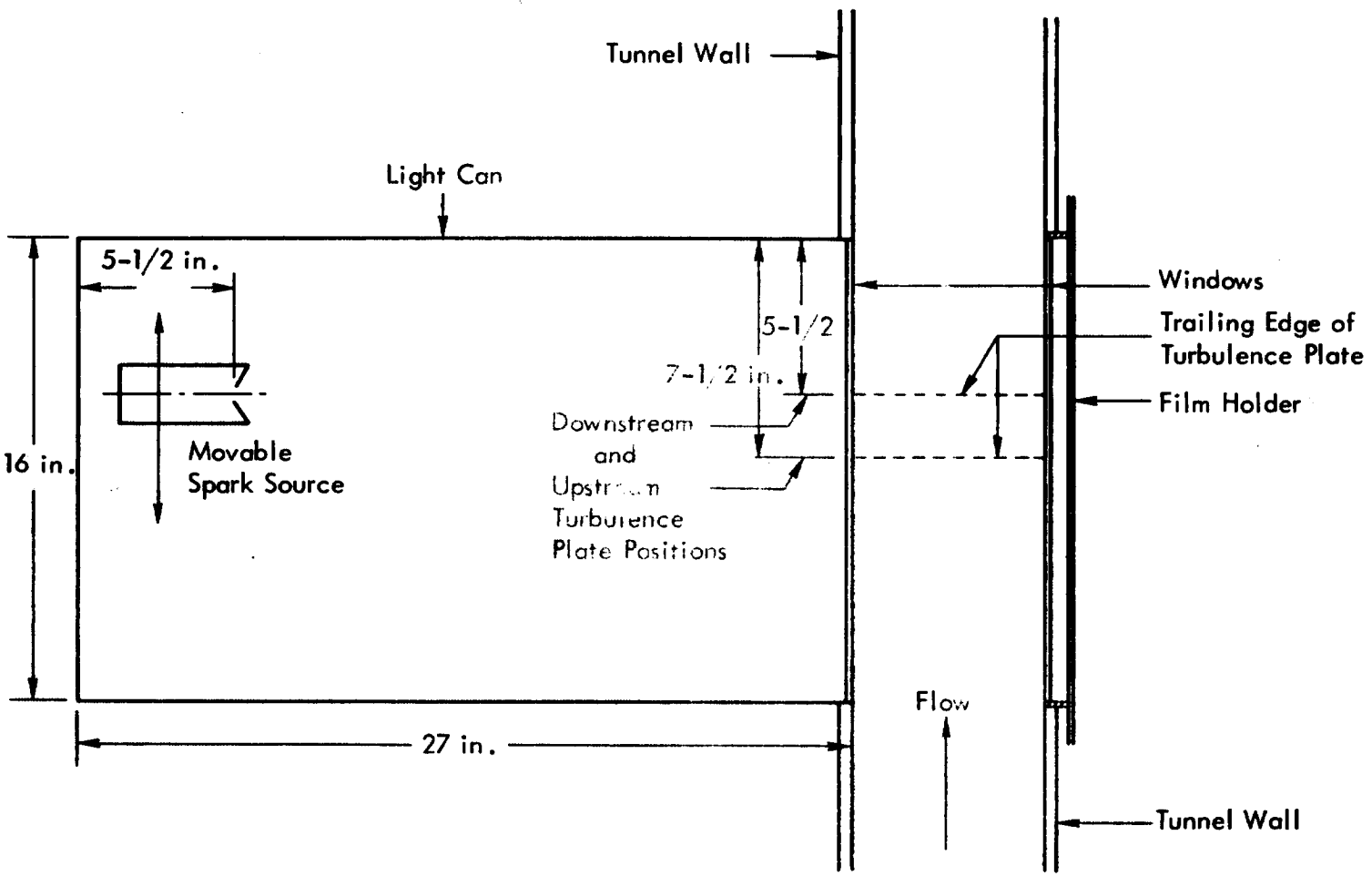

Figure 15. Layout of Direct Shadowgraph System

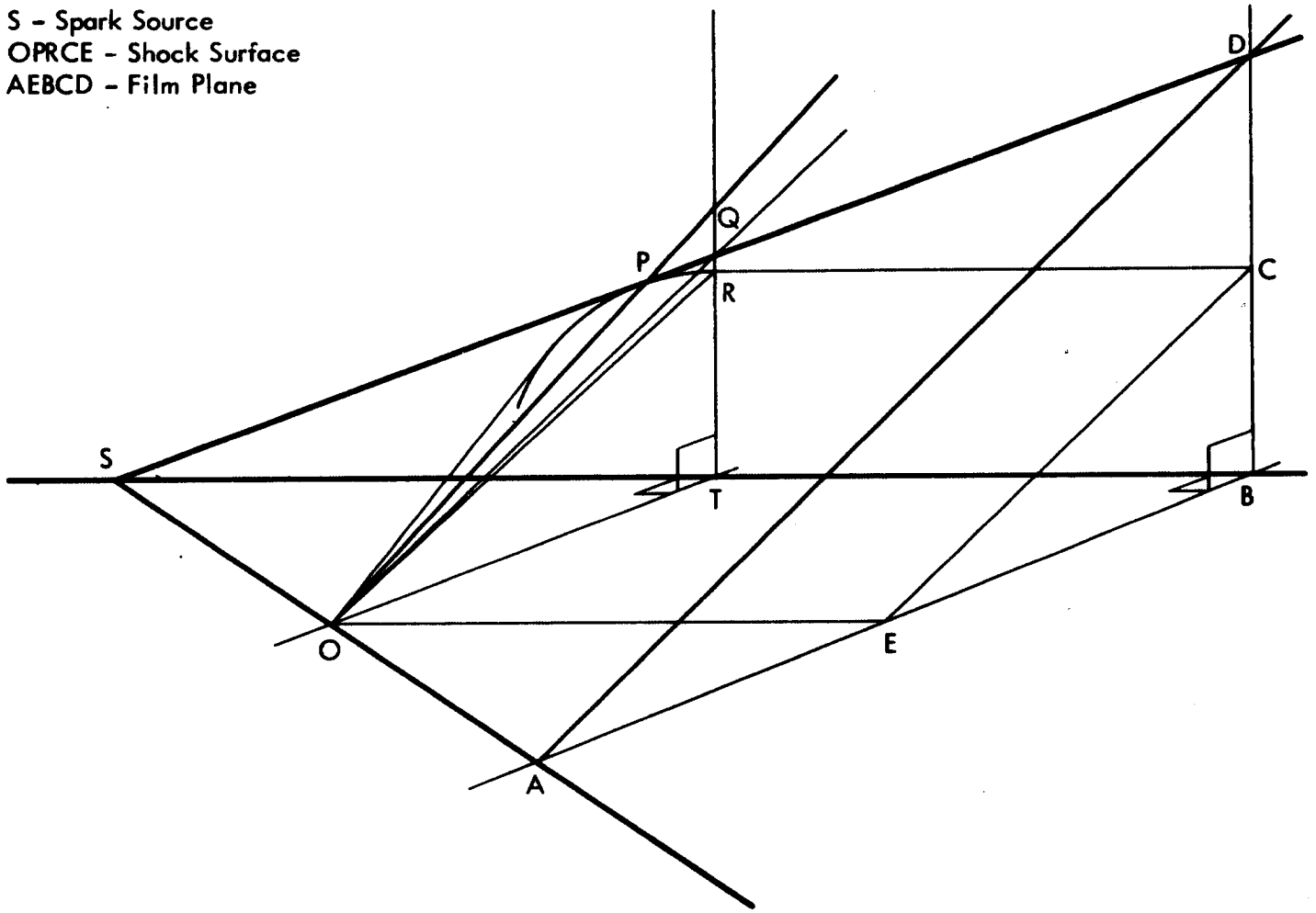

Figure 16. Diagram of Shadowgraph Image Formation.

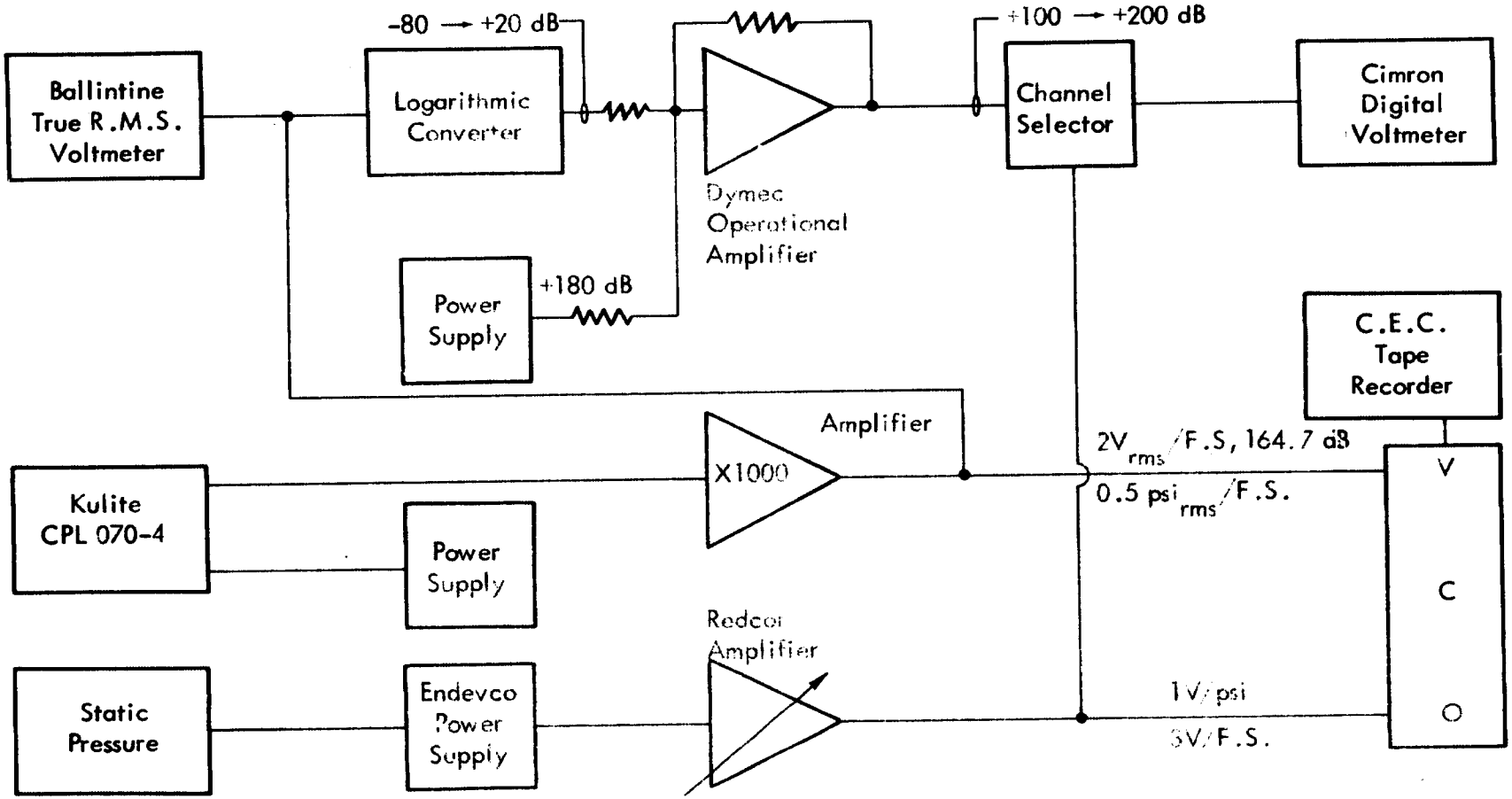

Figure 17. Diagram of Microphone and Static Pressure Circuits.

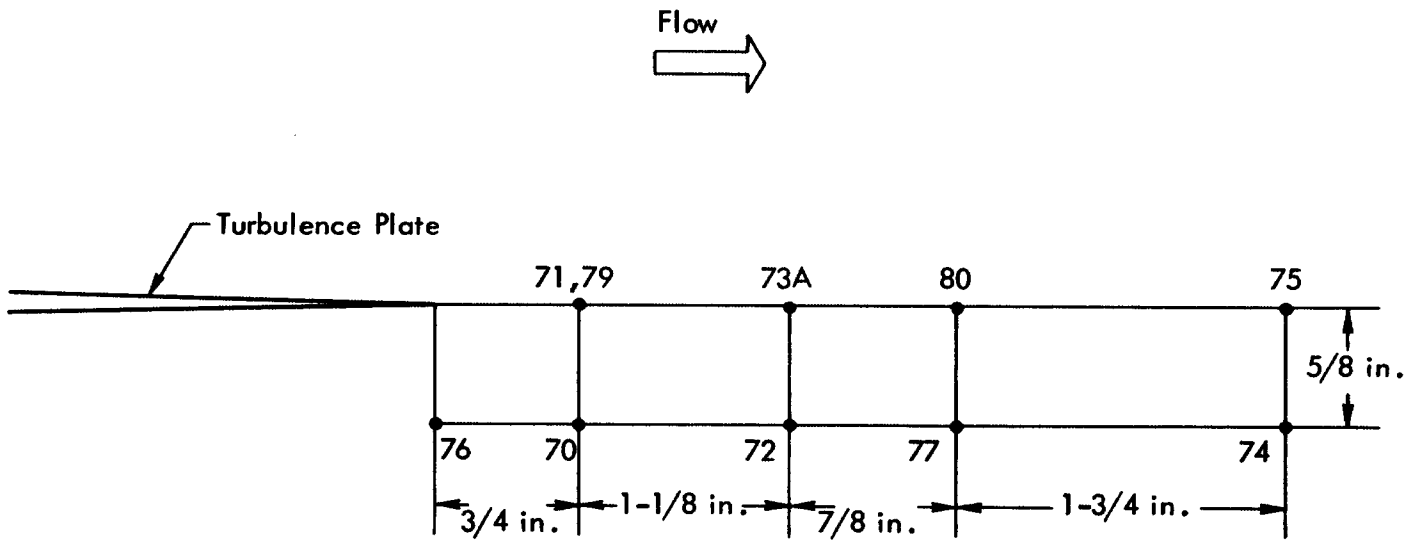

NOTE: Static Pressure Orifice Located 1/8 in. Downstream in Each Case.

Figure 18. Location of Microphone for Series C (Runs 70-80)

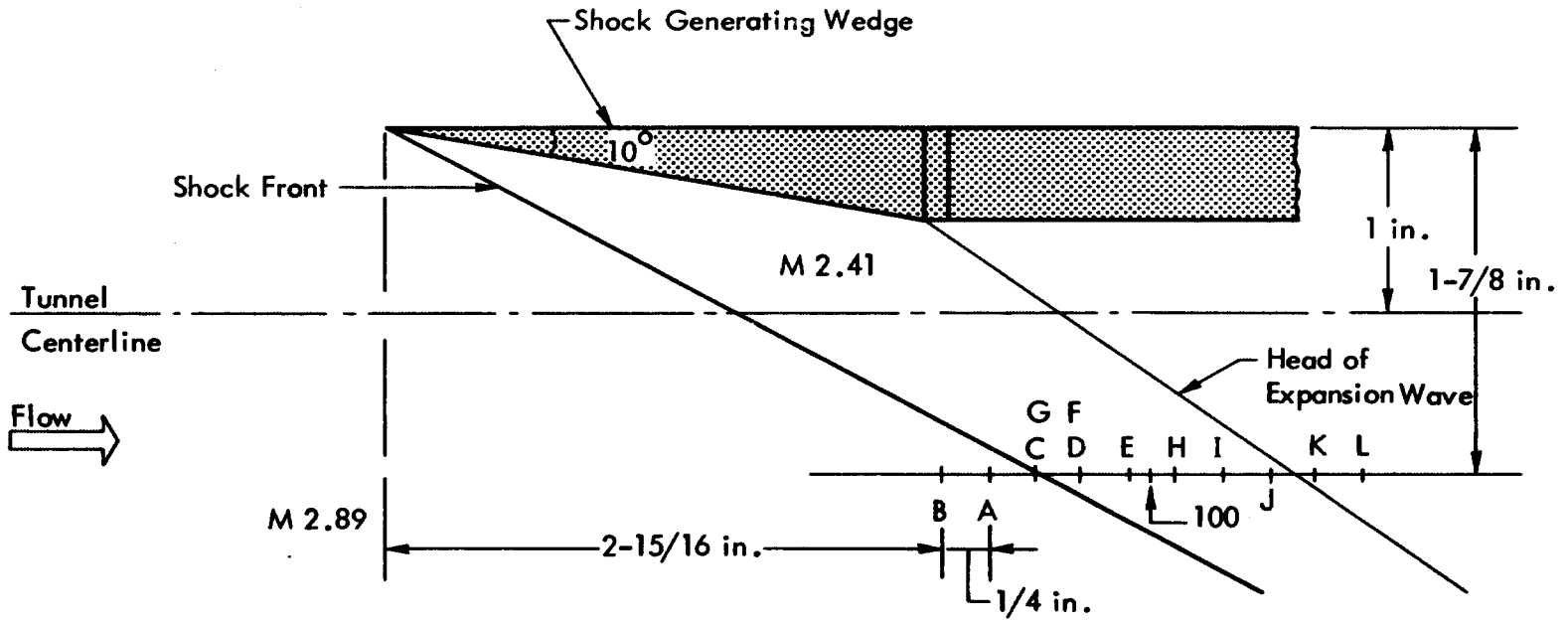

NOTE: Static Pressure Orifice Located 1/8 in. Downstream in Each Case.

Figure 19. Location of Microphone for Series D (Runs 100-100L)

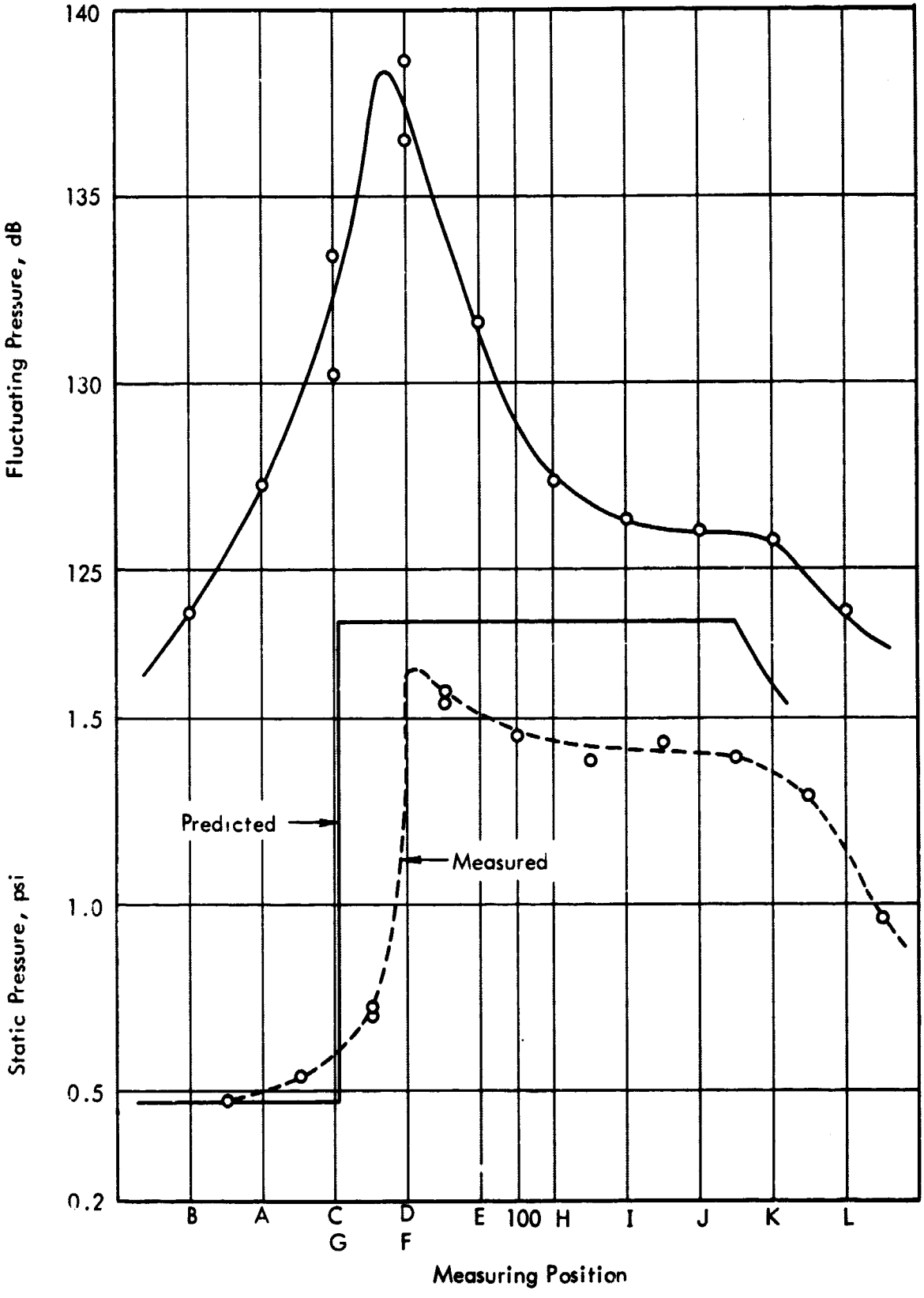

Figure 20. Static and Fluctuating Pressures for Series D.

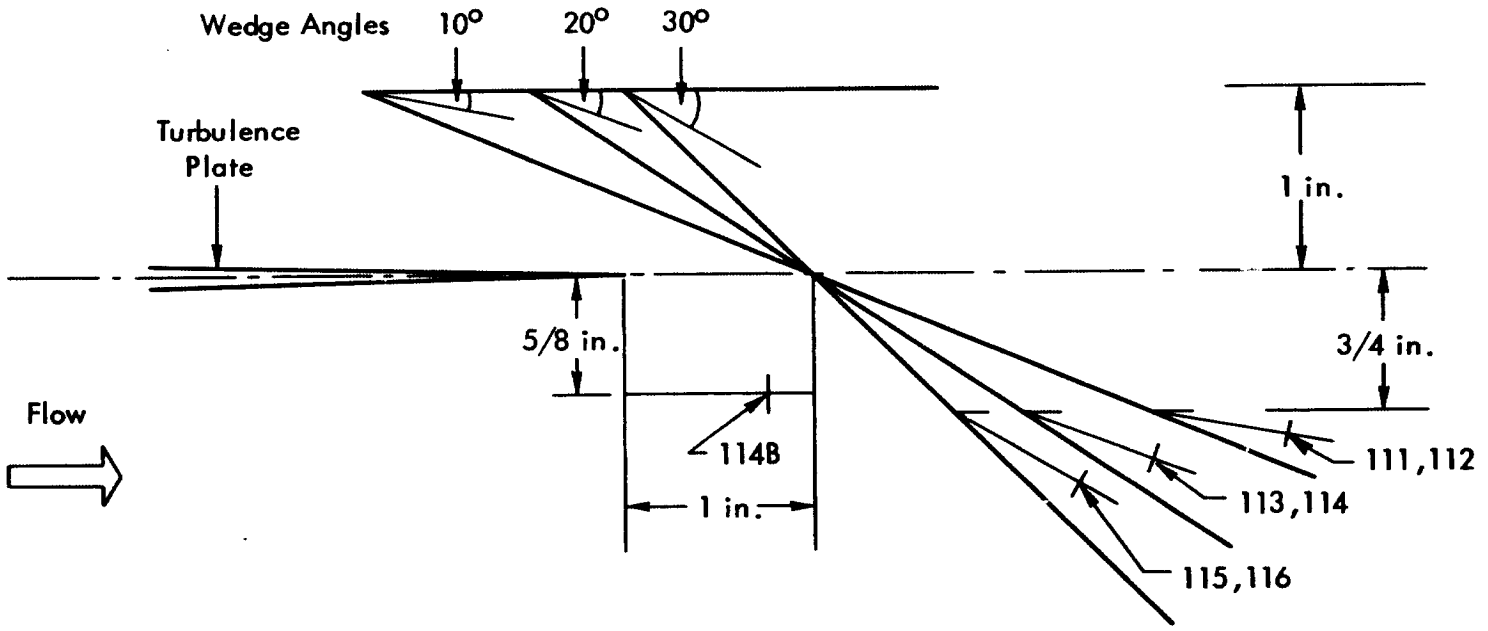

NOTE: Static Pressure Orifice Located 1/8 in. Downstream in Each Case

Figure 21. Location of Microphone for Series E (Runs 111-116)

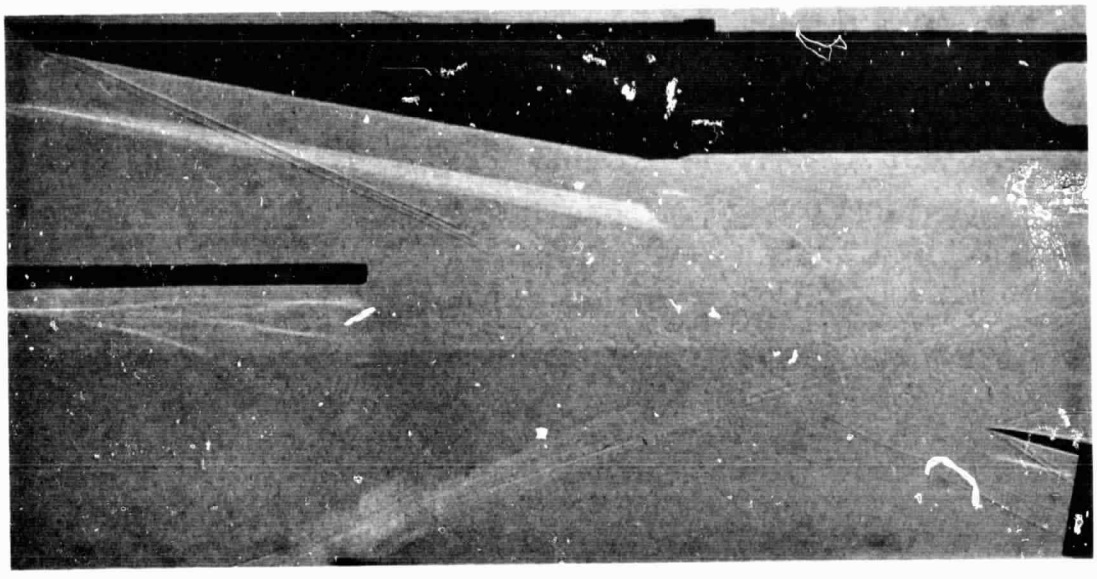

Run 111

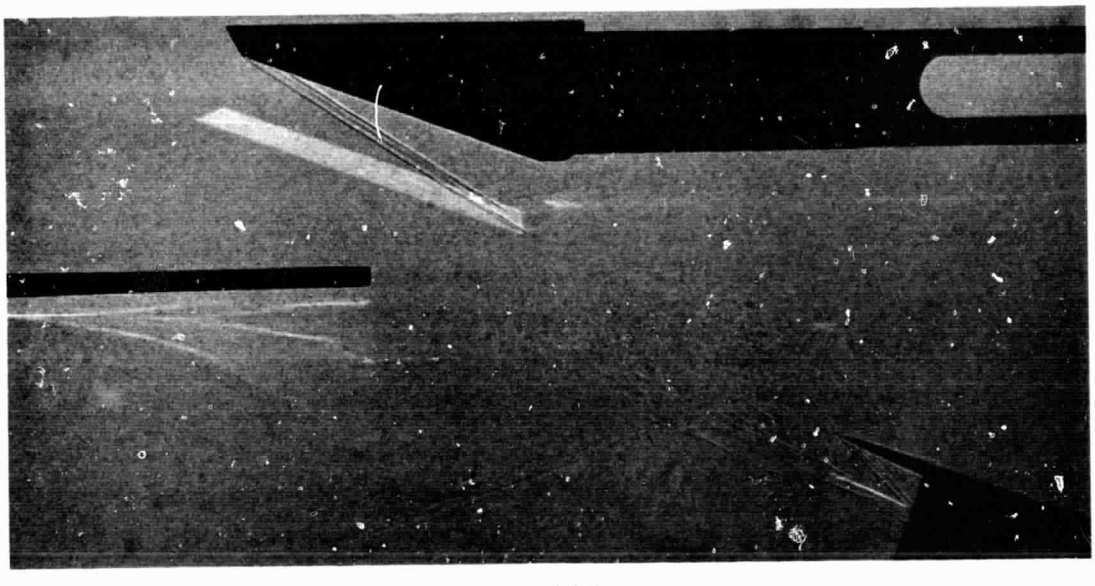

Run 113

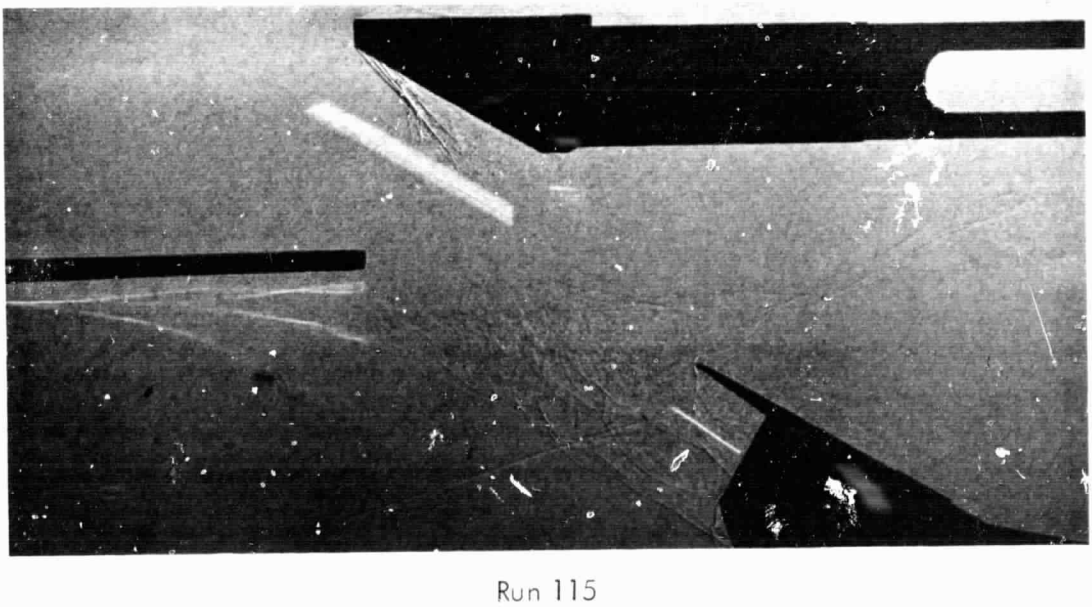

Run 115

Figure 22. Shadowgraphs of Runs 111, 113 and 115

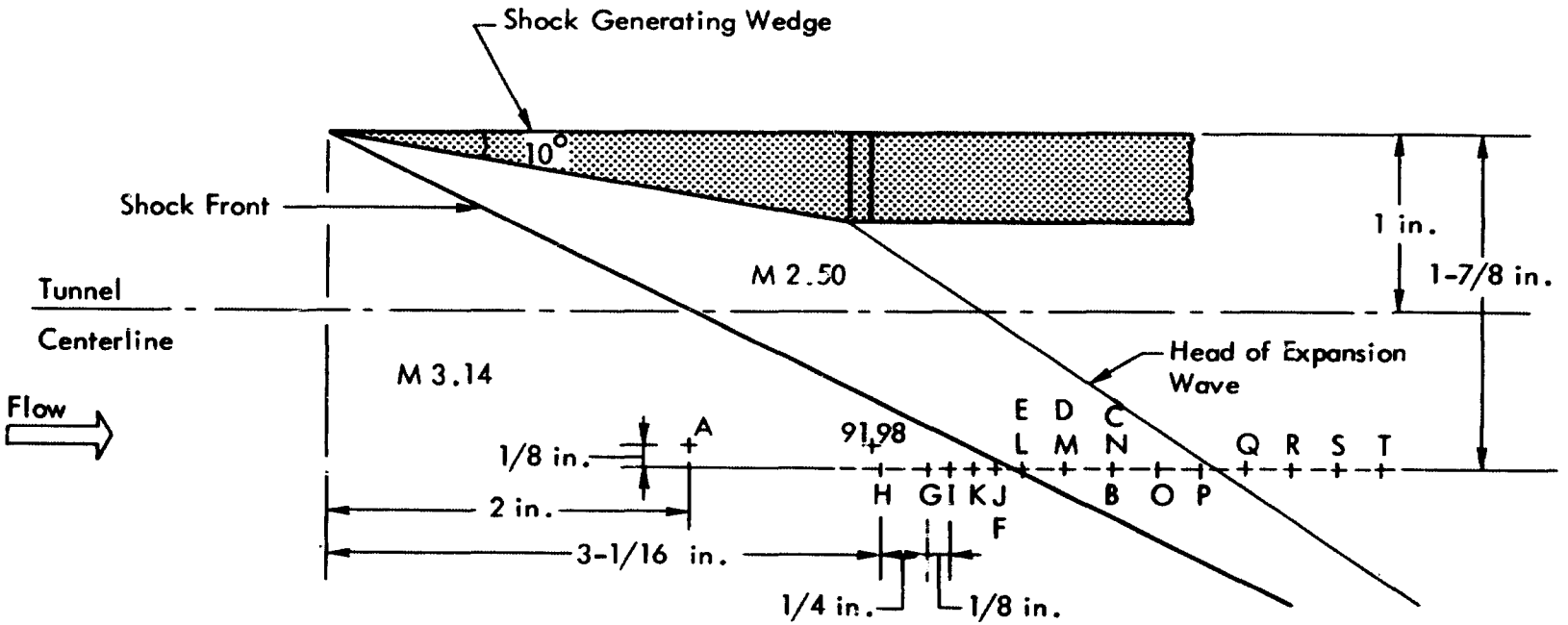

NOTE: Static Pressure Orifice Located 1/8 in. Downstream in Each Case.

Figure 23. Location of Microphone for Series F (Runs 91, 98-98T)

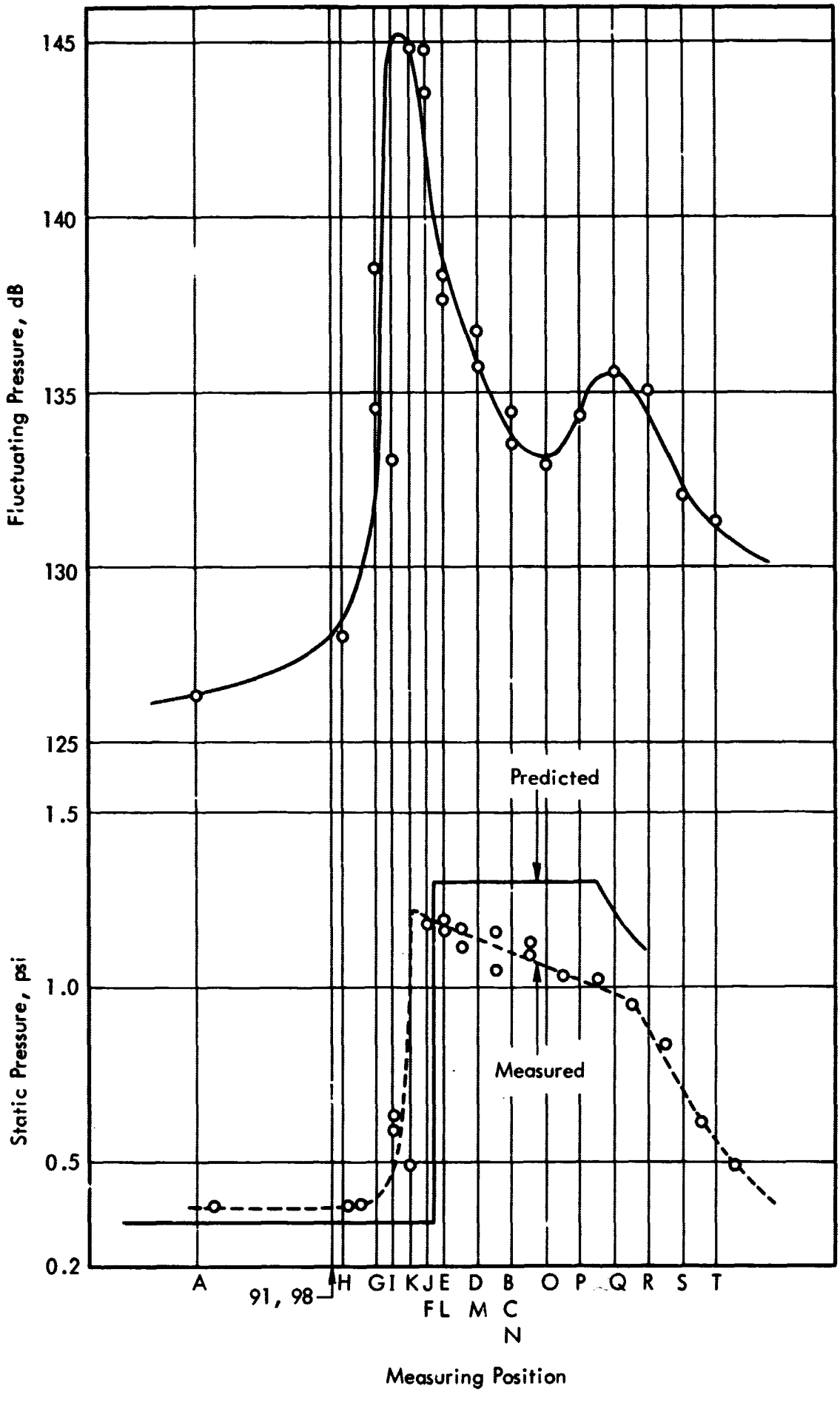

Figure 24. Static and Fluctuating Pressures for Series F.

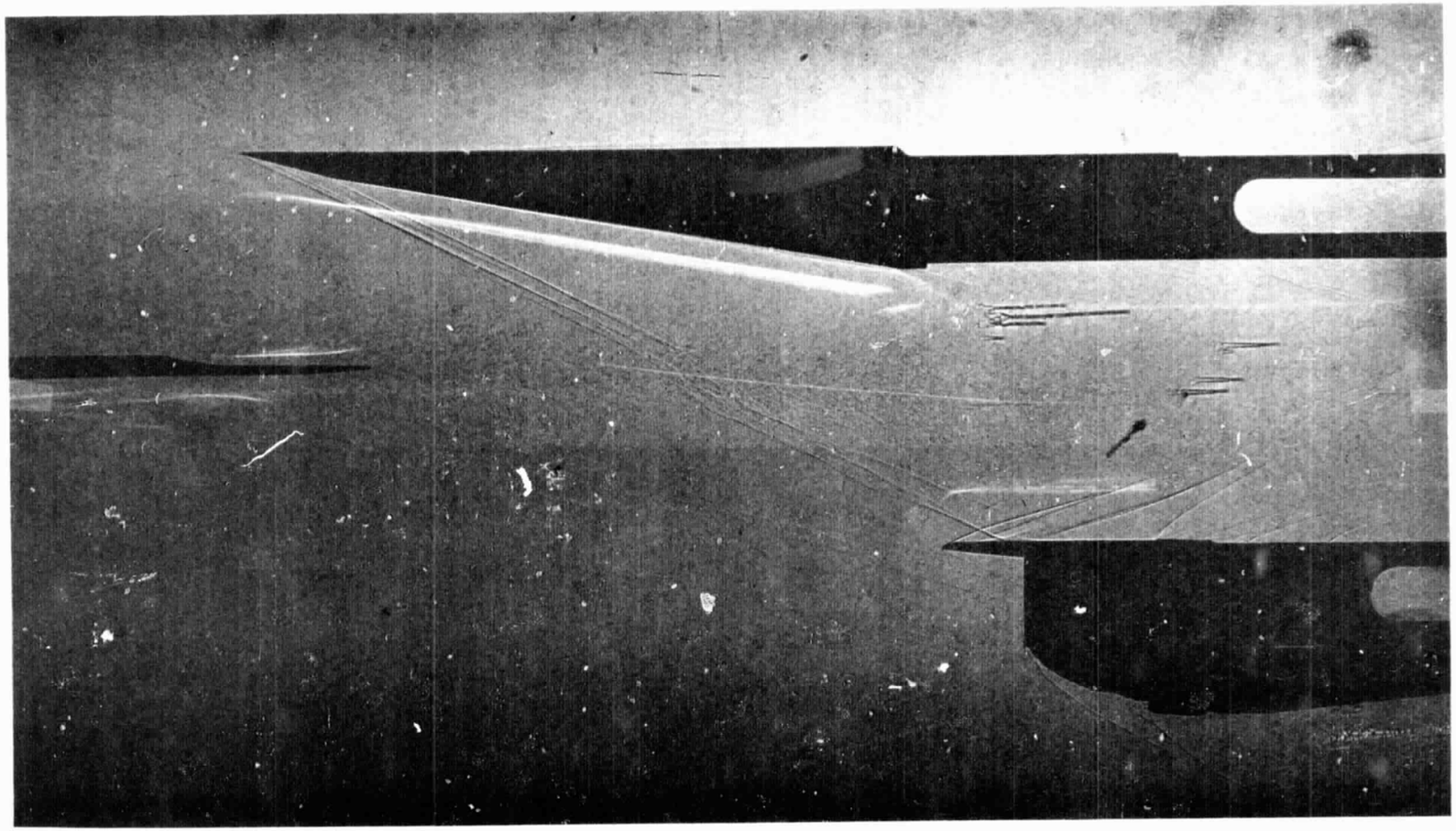

Figure 25. Shadowgraph of Run 98E

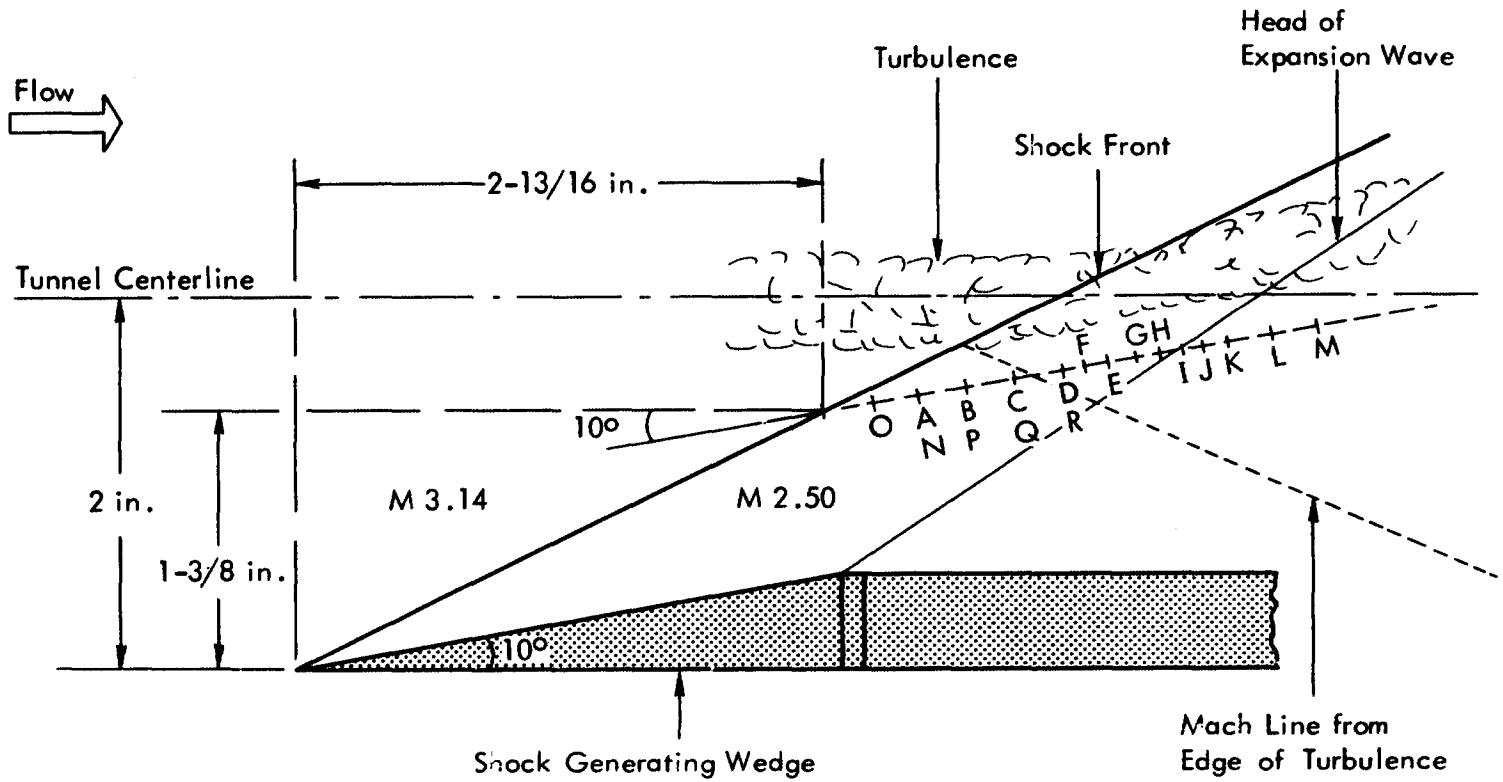

NOTE: Static Pressure Orifice Located 1/8 in. Downstream in Each Case.

Figure 26. Location of Microphone for Series H (Runs 117A-117R)

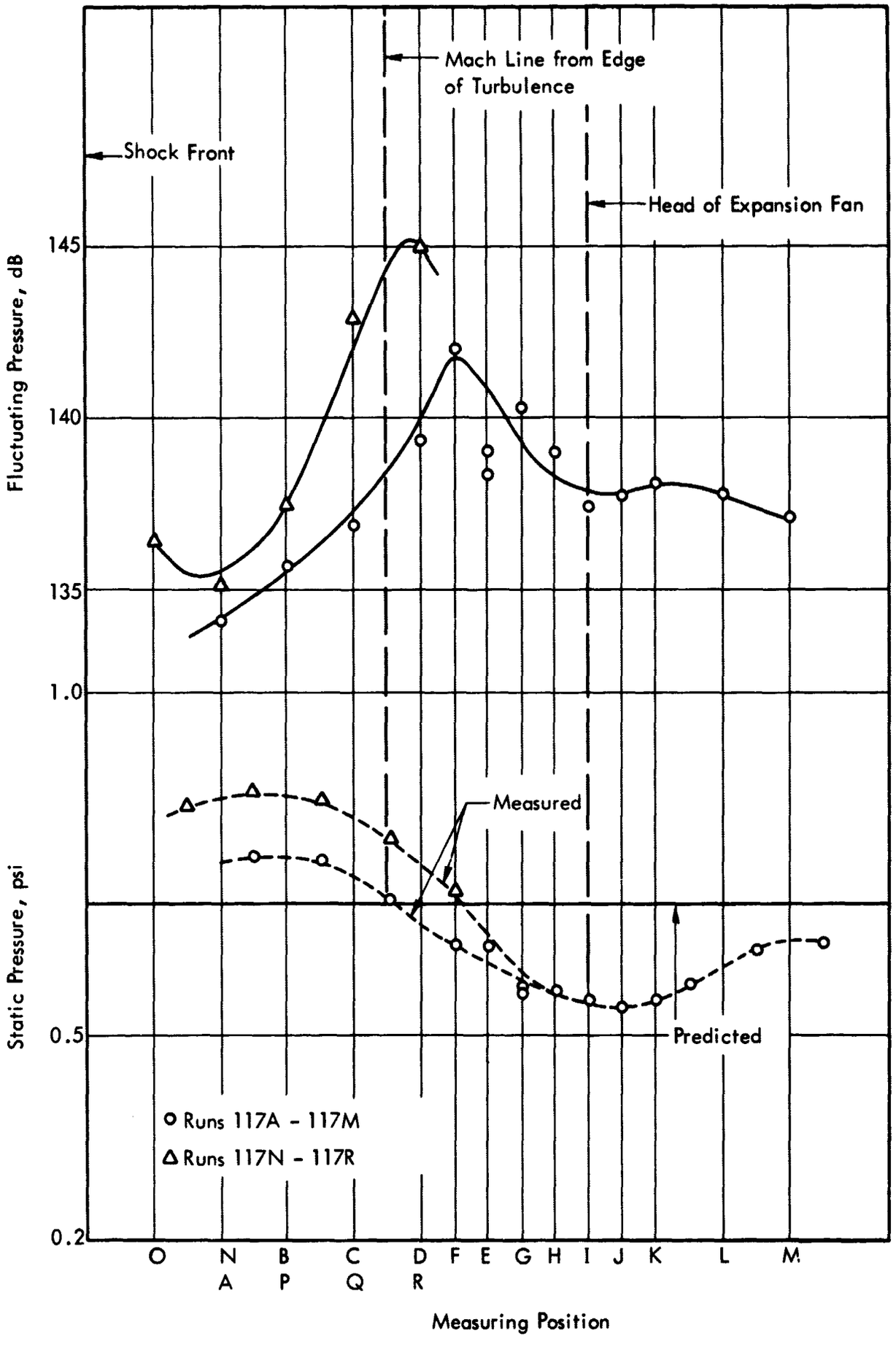

Figure 27. Static and Fluctuating Pressures for Series H.

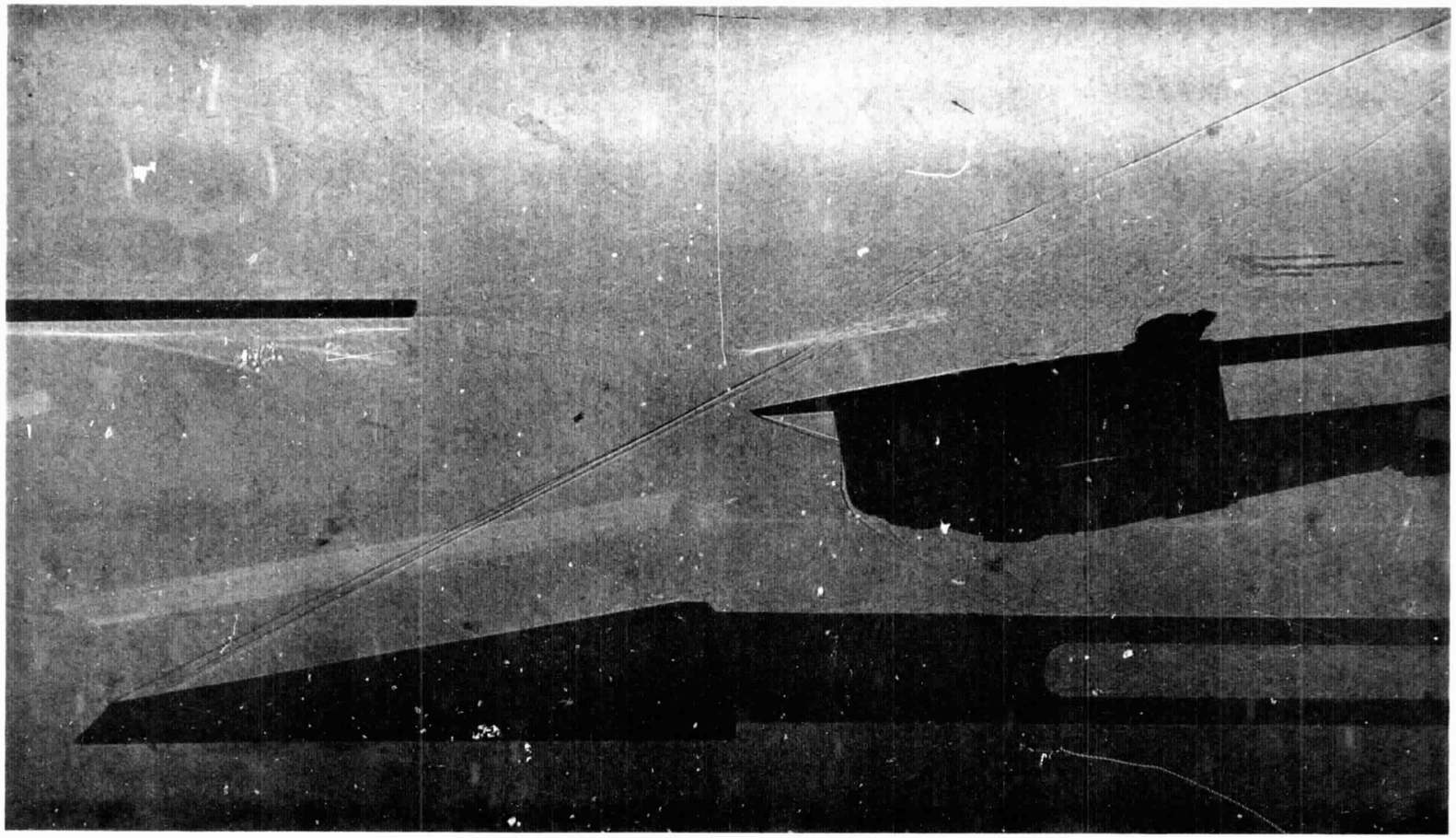

Figure 28. Shadowgraph of Run 117Q

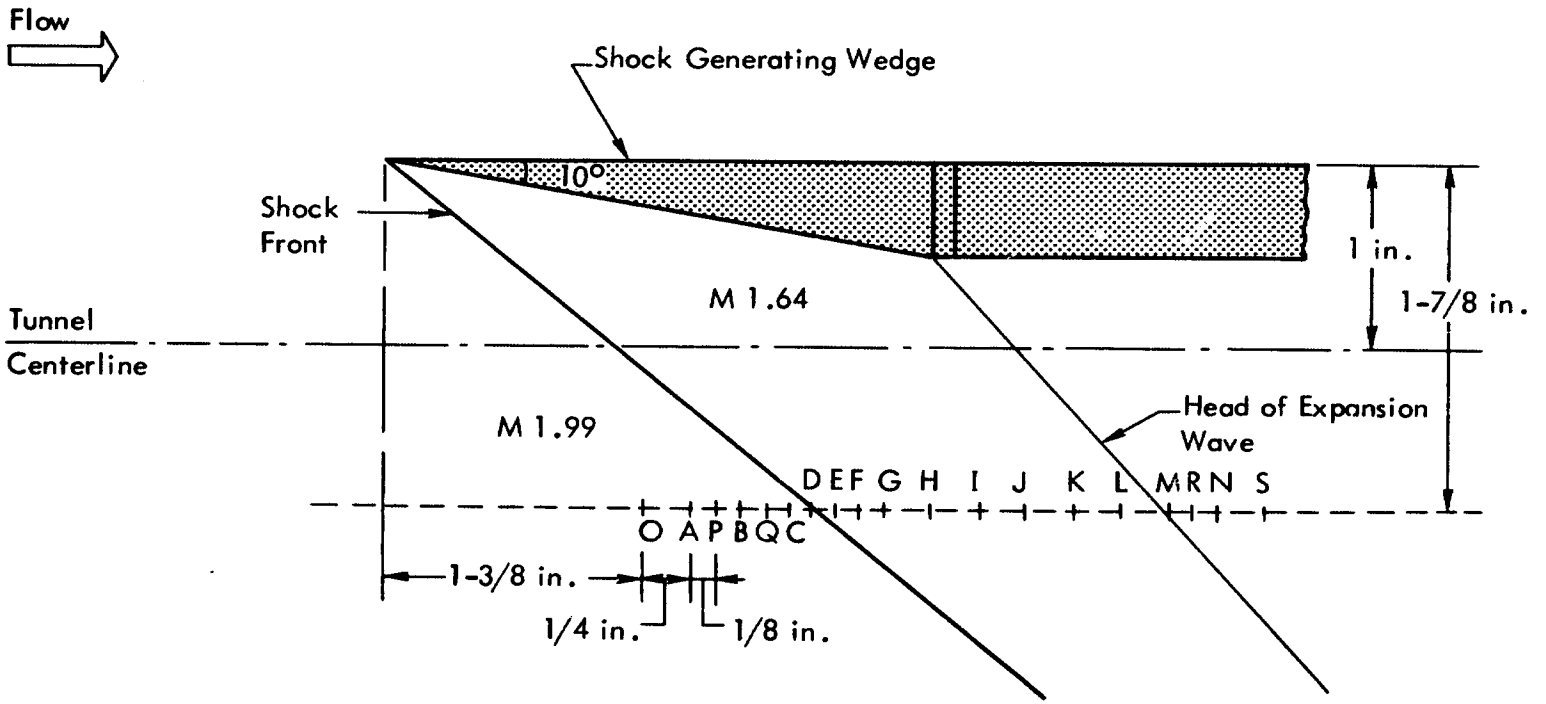

NOTE: Static Pressure Orifice Located 1/8 in. Downstream in Each Case.

Figure 29. Location of Microphone for Series I (Runs 101A-101T)

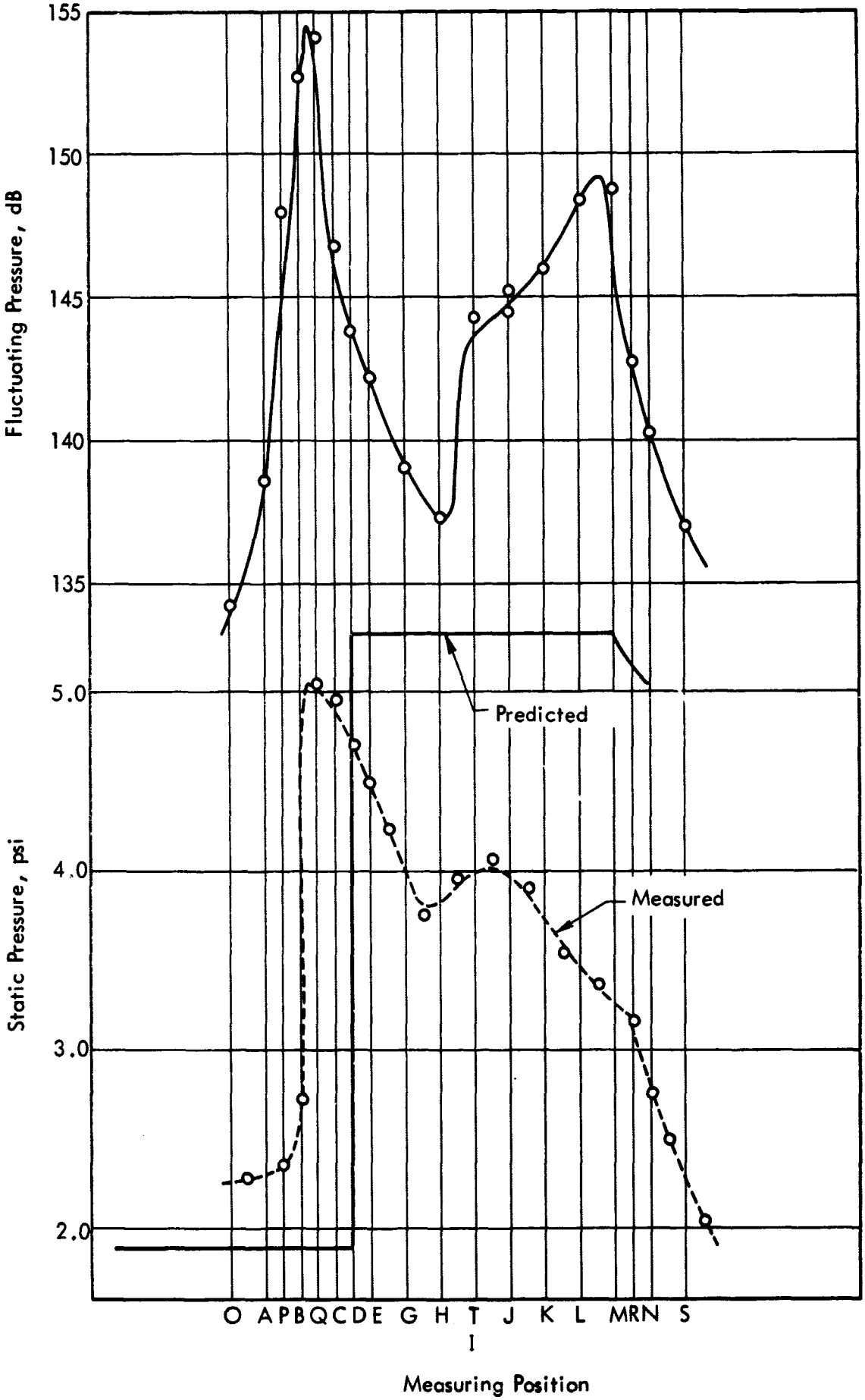

Figure 30. Static and Fluctuating Pressures for Series I.

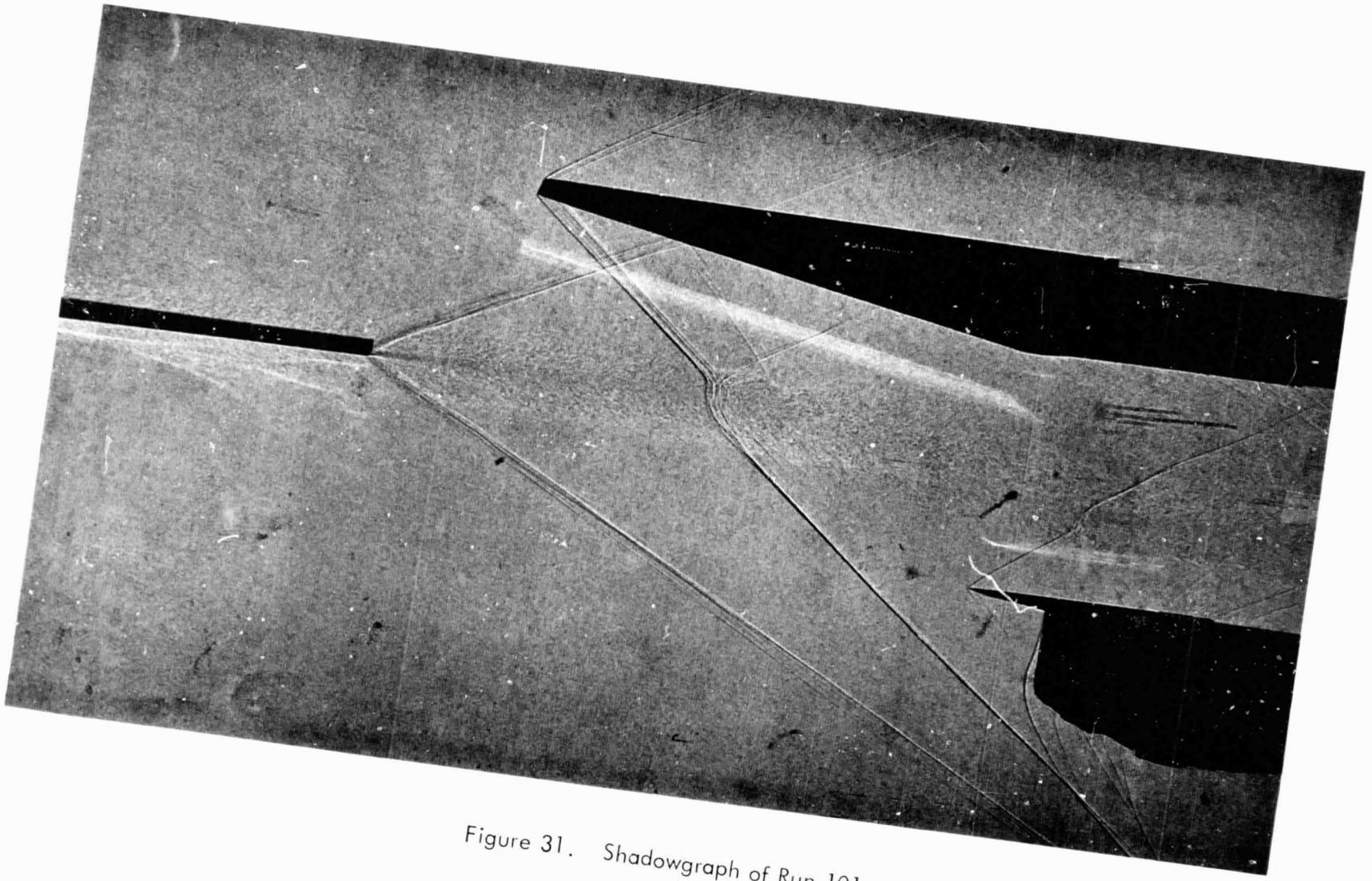

Figure 31. Shadowgraph of Run 101 J

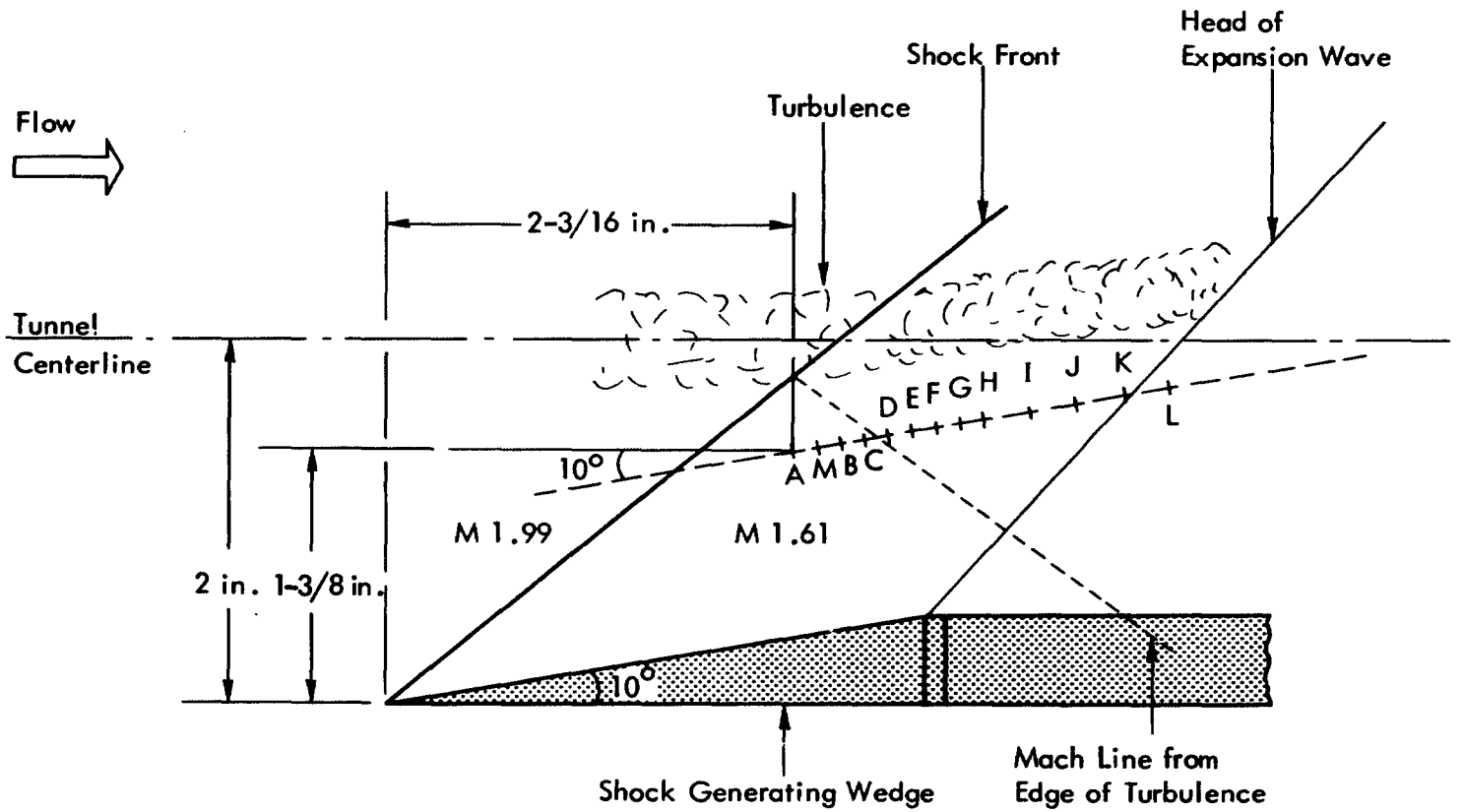

NOTE: Static Pressure Orifice Located 1/8 in. Downstream in Each Case.

Figure 32. Location of Microphone for Series J (Runs 102A-102M)

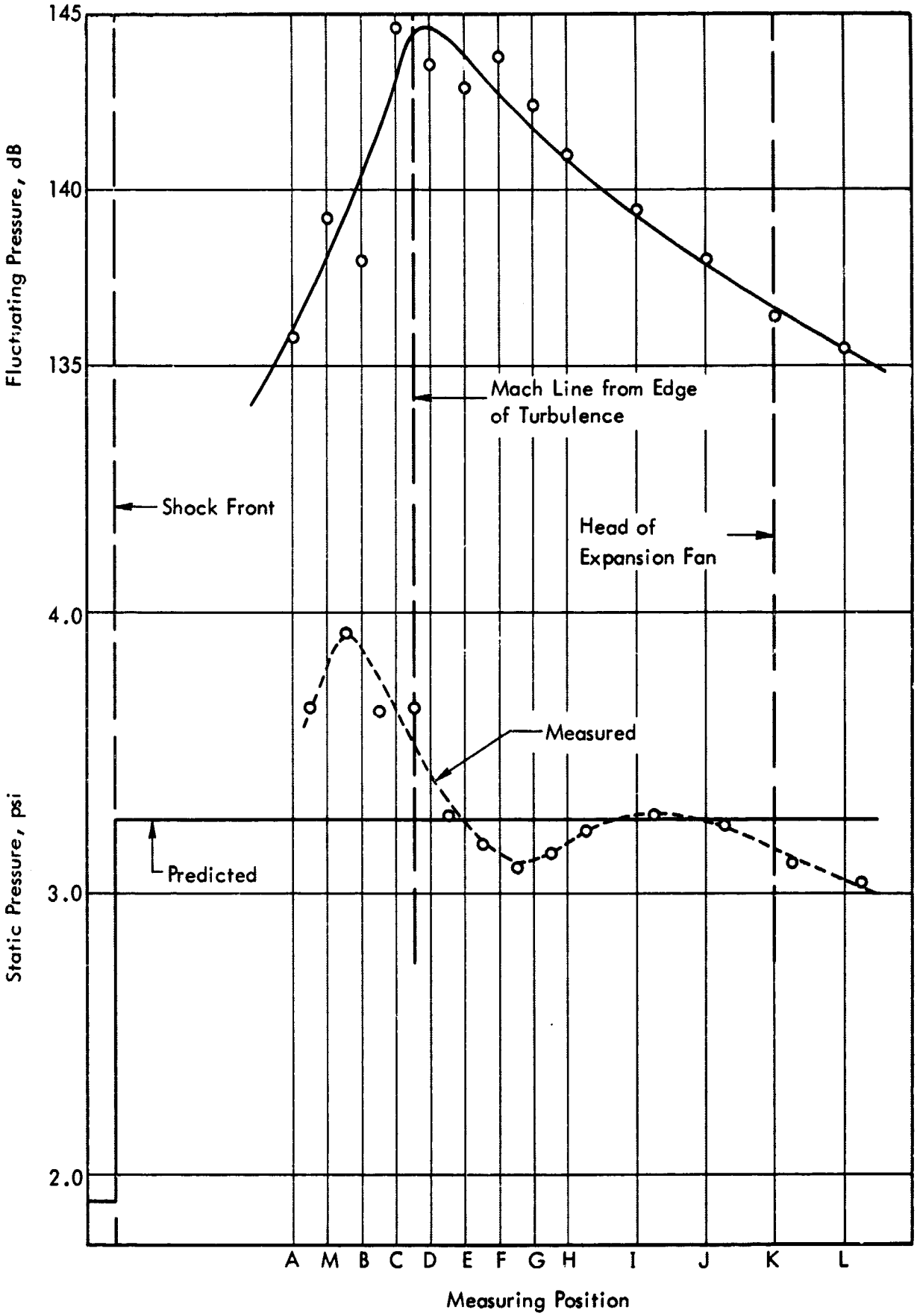

Figure 33. Static and Fluctuating Pressures for Series J.

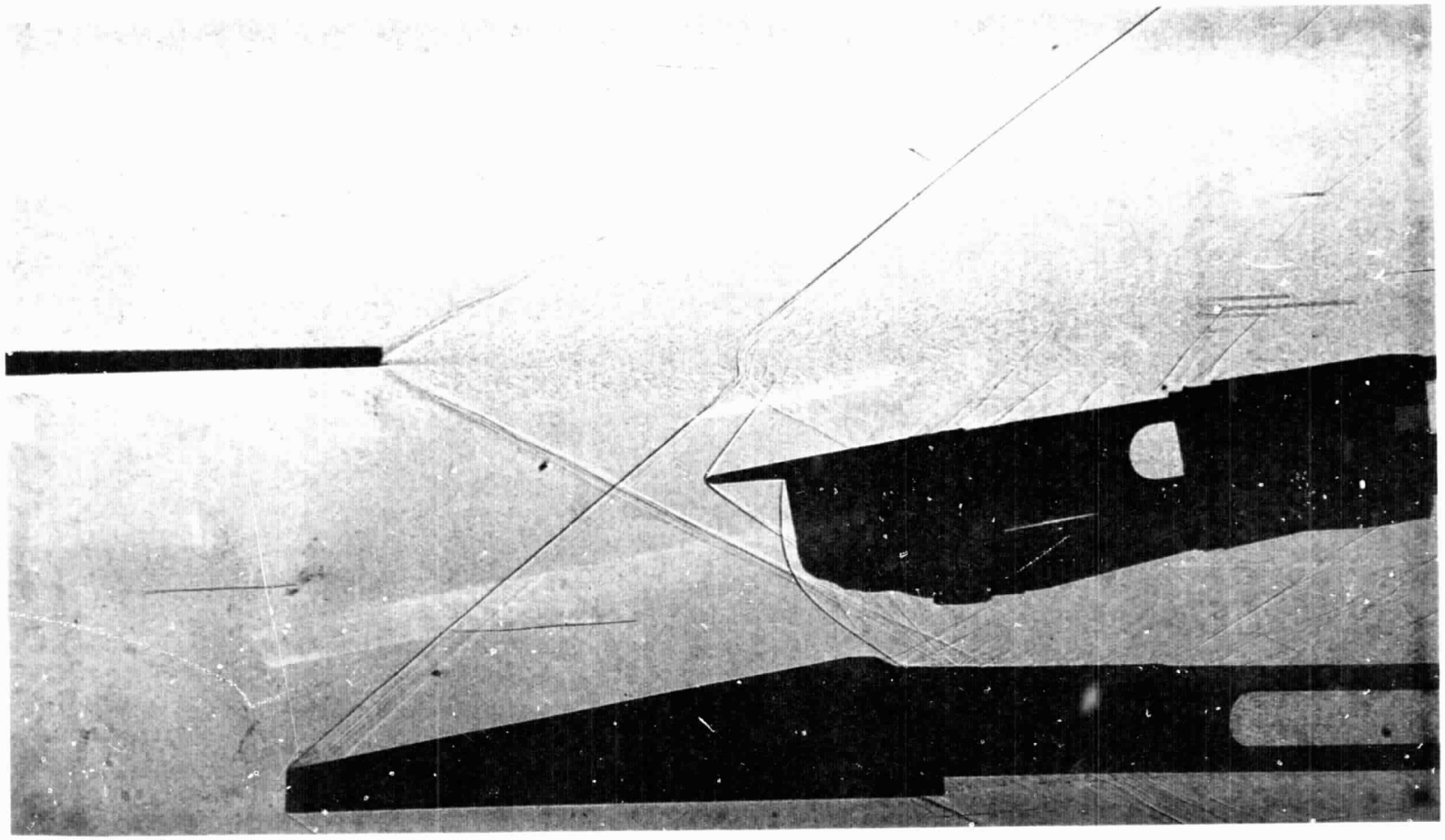

Figure 34. Shadowgraph of Run 102C

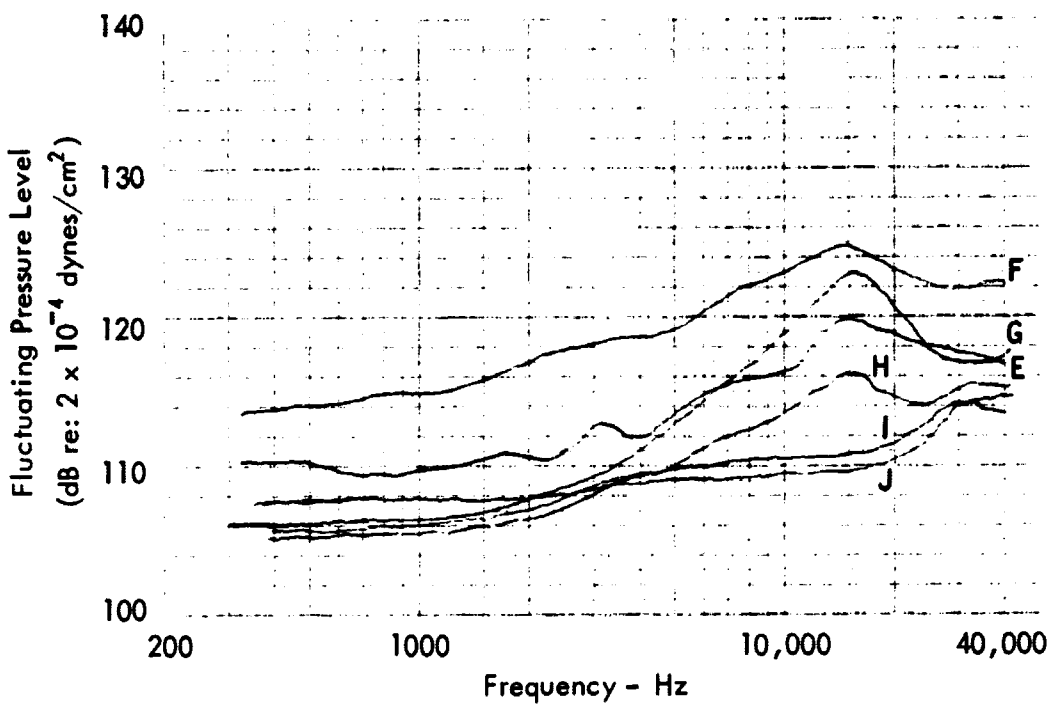

Figure 35. Spectra of Responses Taken During Series D
(Runs 100 E-J)

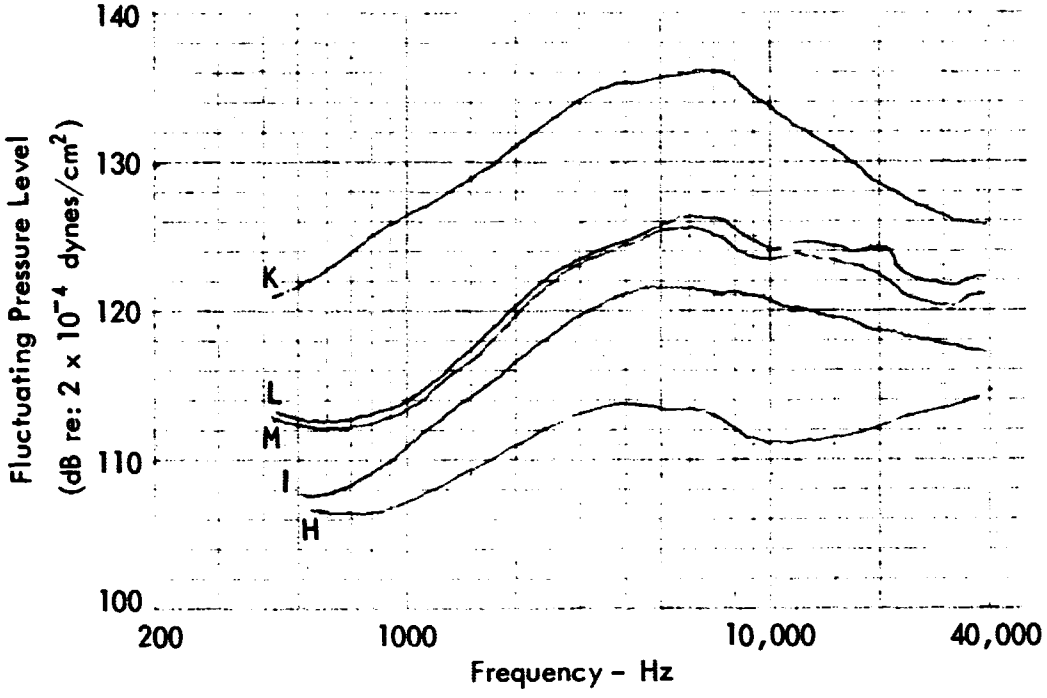

(a) Forward Peak

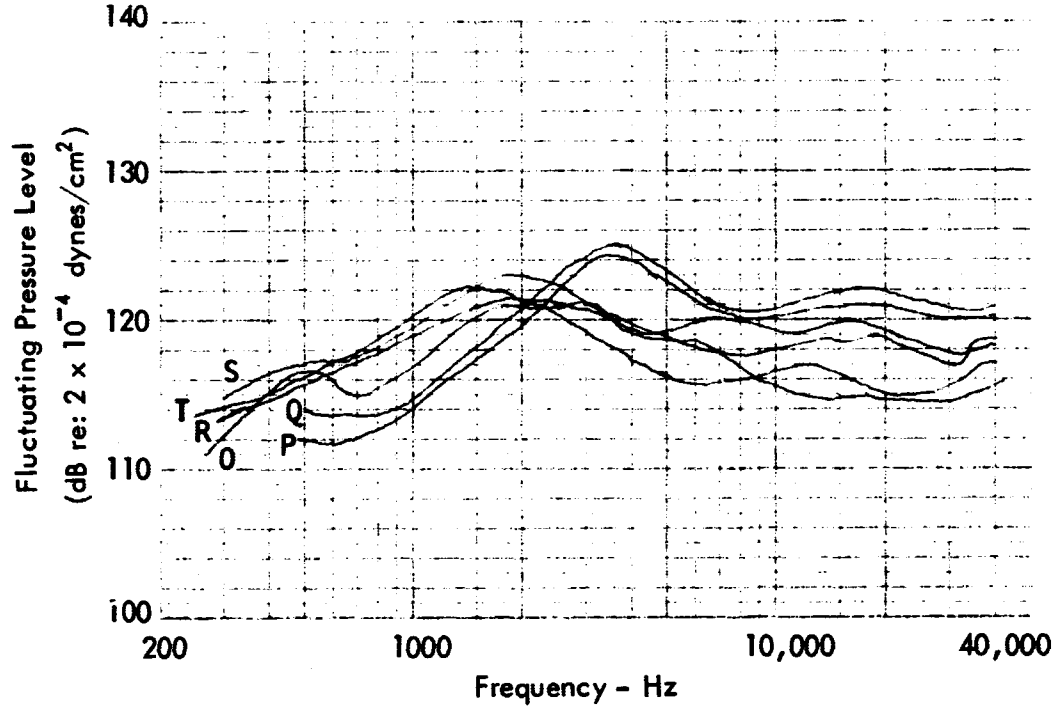

(b) Rear Peak

Figure 36. Spectra of Responses Taken During Series F
(Runs 98 K-M, P-T)

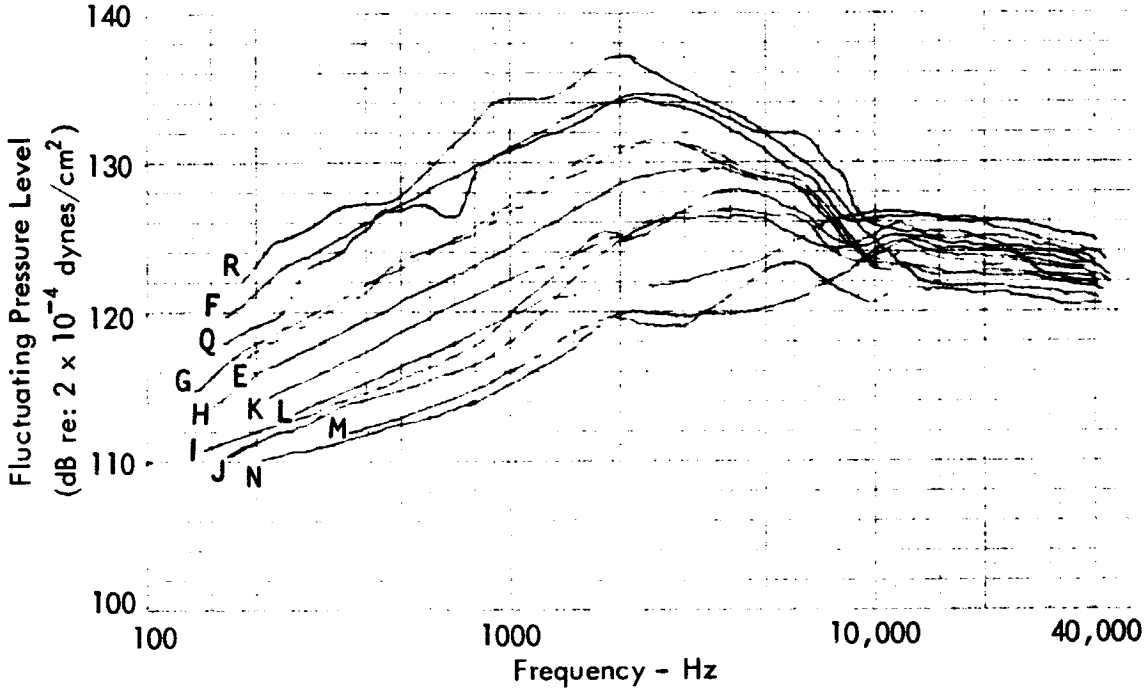

Figure 37. Spectra of Responses Taken During Series H
(Runs 117 E-N, Q, R)

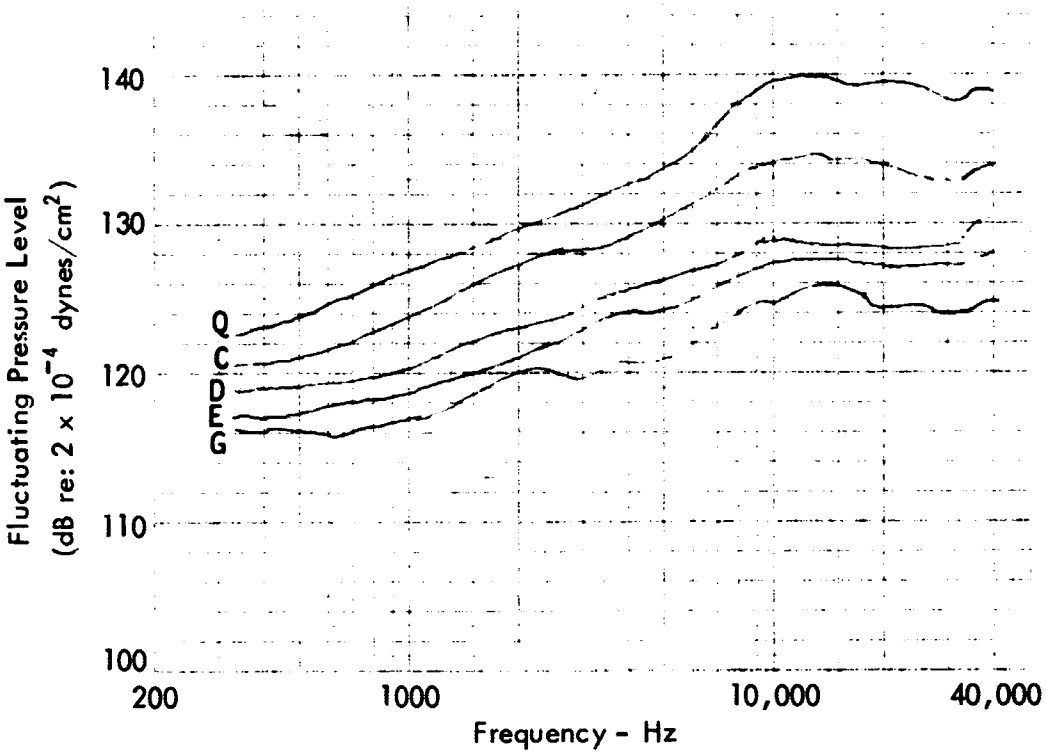

(a) Forward Peak

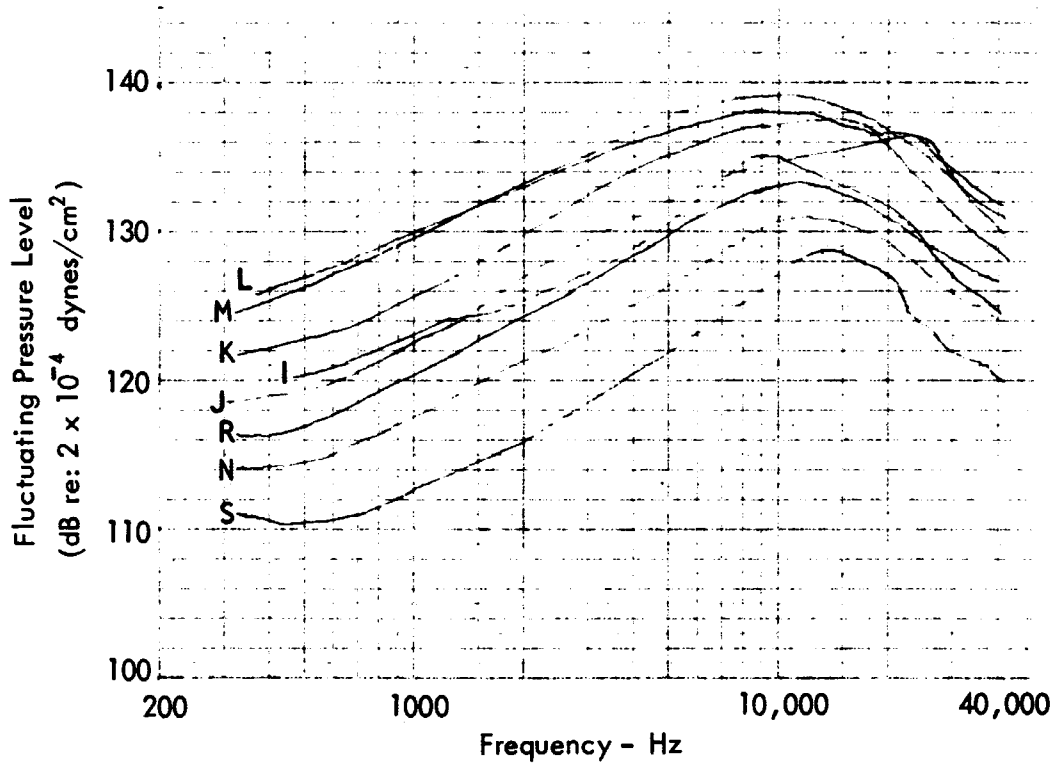

(b) Rear Peak

Figure 38. Spectra of Responses Taken During Series I
(Runs 101 C-E, G, I-S)

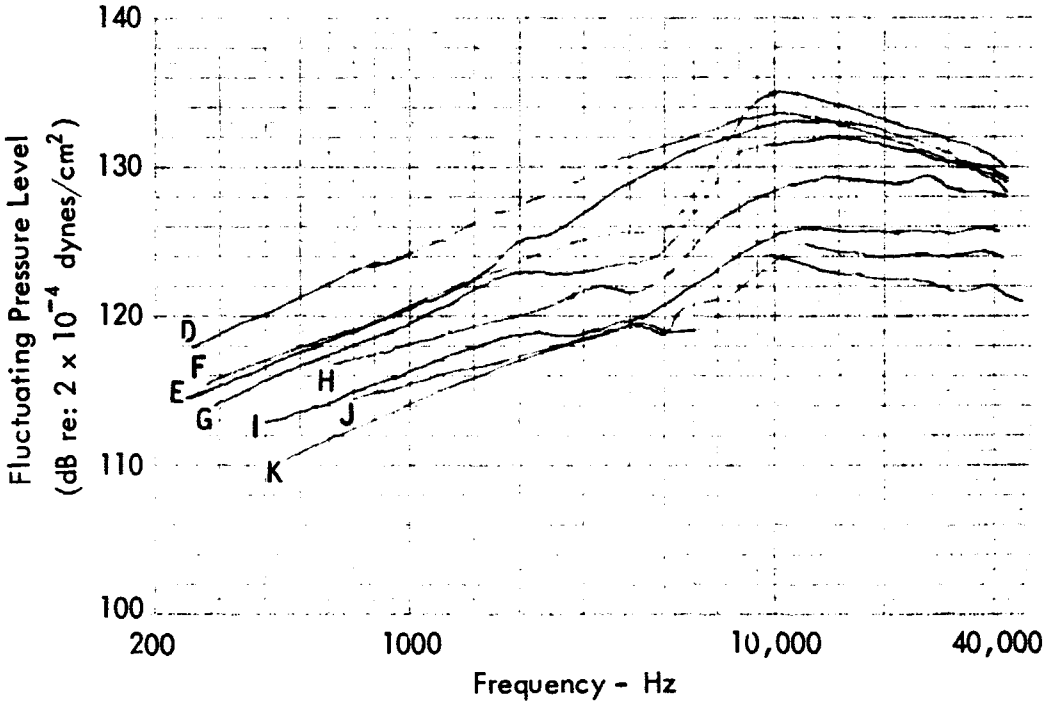

Figure 39. Spectra of Responses Taken During Series J
(Runs 102 D-K)

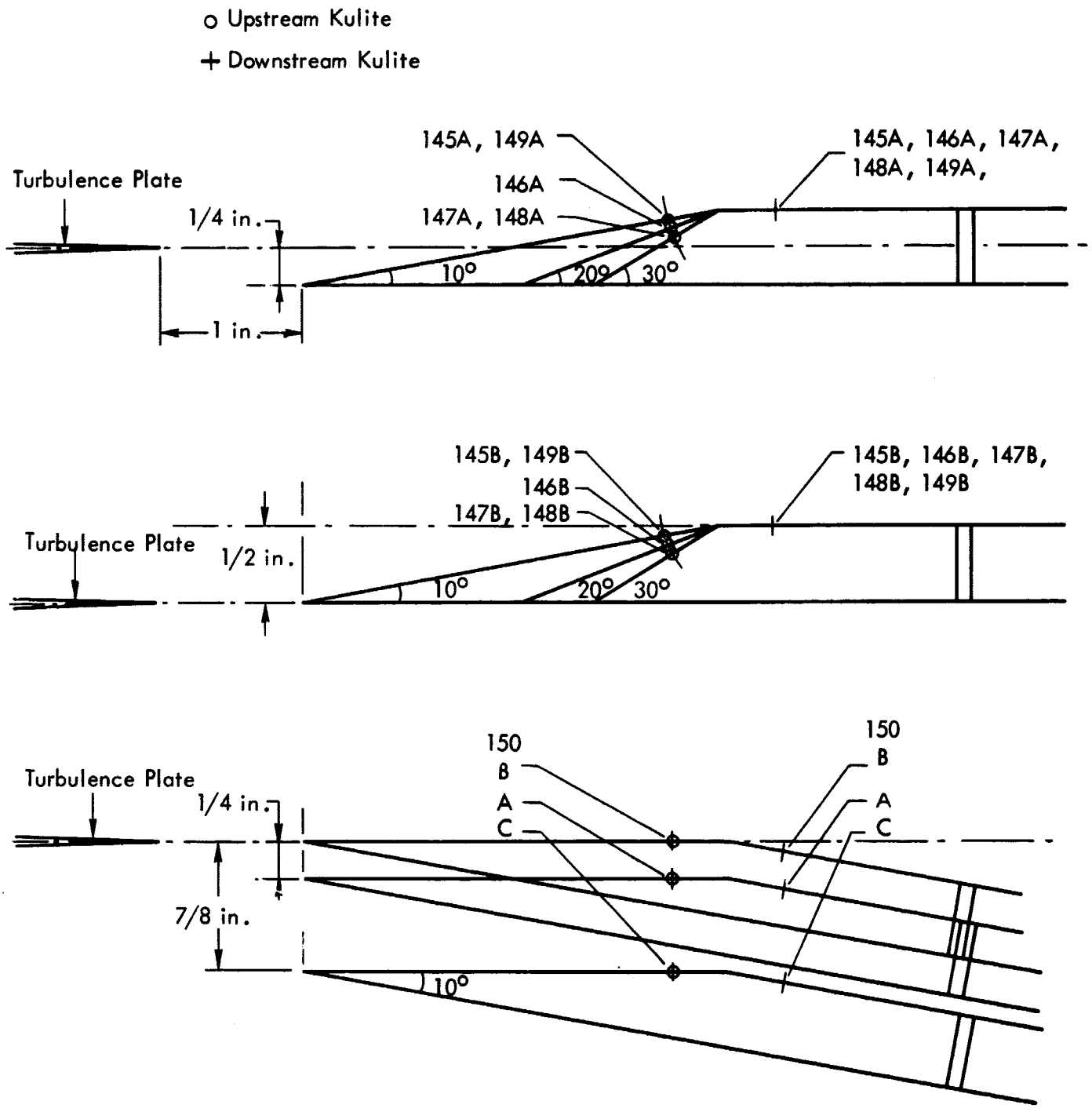

Figure 40. Location of Microphones for Series K (Runs 145A-150C)